Heat Transfer Enhancement Using Nanofluids for Thermal Energy Applications

By

Shomaz Ul Haq

NUST-2014-63503-MCES-64114-F

Session 2014-16

Supervised by

Assistant Professor Dr. Majid Ali

A Thesis submitted to the U.S.-Pakistan Center for Advanced Studies in Energy in partial fulfillment of the requirements for the degree of

MASTERS of SCIENCE in

ENERGY SYSTEMS ENGINEERING

U.S.-Pakistan Center for Advanced Studies in Energy

(USPCAS-E)

National University of Sciences and Technology (NUST)

H-12, Islamabad 44000, Pakistan

November 2017

Heat Transfer Enhancement Using Nanofluids for Thermal Energy Applications

By

Shomaz Ul Haq

NUST-2014-63503-MCES-64114-F

Session 2014-16

Supervised by

Assistant Professor Dr. Majid Ali

A Thesis submitted to the U.S.-Pakistan Center for Advanced Studies in Energy in partial fulfillment of the requirements for the degree of

MASTERS of SCIENCE in

ENERGY SYSTEMS ENGINEERING

U.S.-Pakistan Center for Advanced Studies in Energy

(USPCAS-E)

National University of Sciences and Technology (NUST)

H-12, Islamabad 44000, Pakistan

November 2017

THESIS ACCEPTANCE CERTIFICATE

Certified that final copy of MS/MPhil thesis written by Mr. Shomaz Ul Haq, (Registration No. NUST-2014-63503-MCES-64114-F), of U.S.-Pakistan Center for Advanced Studies in Energy has been vetted by undersigned, found complete in all respects as per NUST Statues/Regulations, is free of plagiarism, errors, and mistakes and is accepted as partial fulfillment for award of MS/MPhil degree. It is further certified that necessary amendments as pointed out by GEC members of the scholar have also been incorporated in the said thesis.

Signature: _____

Name of Supervisor: Dr. Majid Ali_____

Date: -11-2017_____

Signature (HoD): _____

Date: -11-2017_____

Signature (Dean/Principal): _____

Date: -11-2017_____

Certificate

This is to certify that work in this thesis has been carried out by **Mr. Shomaz Ul Haq** and completed under my supervision in thermal energy laboratory, U.S.-Pakistan Center for Advanced Studies in Energy, National University of Sciences and Technology, H-12, Islamabad, Pakistan.

Supervisor: _____

Dr. Majid Ali
U.S.-Pakistan Centre for Advanced Studies in Energy
NUST, Islamabad

GEC member # 1: _____

Dr. M. Bilal Khan
U.S.-Pakistan Center for Advanced Studies in Energy
NUST, Islamabad

GEC member # 2: _____

Dr. Muhammad Zubair
U.S.-Pakistan Center for Advanced Studies in Energy
NUST, Islamabad

GEC member # 3: _____

Dr. Emad Ud Din
U.S.-Pakistan Center for Advanced Studies in Energy
NUST, Islamabad

HoD-USPCAS-E _____

Dr. Zuhair S. Khan
U.S.-Pakistan Center for Advanced Studies in Energy
NUST, Islamabad

Dean/Principal _____

Dr. M. Bilal Khan
U.S.-Pakistan Center for Advanced Studies in Energy
NUST, Islamabad

Dedication

I dedicate my thesis to my beloved parents, siblings, and friends for their affection and support during my studies. Especially to my mother for always believing in me, praying for me, and giving me courage.

Abstract

Heat transfer is basic need for energy production for many energy applications. This is accomplished by thermal fluids that exchange heat with a heat source or another fluid for either thermal energy or electrical energy production. The use of conventional thermal fluids faces problems of low convective heat transfer and thermal conductivity. Nanofluids are a kind thermal fluid with the potential of revolutionizing heat transfer in energy systems. Having increased convective heat transfer and thermal conductivity than conventional fluids, they offer environmental benefits together with low energy costs. There is a strong applicability of nanofluids in commercial and domestic applications such as automotive, energy production like solar and nuclear energy.

A nanofluid is a dispersion of nanometer sized particles in a conventional fluid (base fluid) such as water. Because of their sub microscopic nature, they easily mix with the fluid simultaneously increasing thermal conductivity of the fluid due to their metallic nature. Thus, they offer advantages of higher thermal conductivity of solids and rapid flow of fluids. This has led to increased research in this area and many theoretical, experimental, and simulation models have arised complicating an accurate assessment of heat transfer involved. First an extensive and detailed literature review of both experimental along with simulation study highlighting the differences and similarities of approaches as well as results. The analysis revealed the domination of forced convection in applications and thus formed the basis of this study. A full three dimensional (3D) CFD analysis for forced hydrodynamically and thermally developing laminar nanofluid flow in pipes is applied in CFD code ANSYS CFX using different comparison criteria. Effects of concentration and diameter of nanoparticle, heat flux, inlet temperature, Re number, as well as the type of nanofluid itself (based on type of nanoparticle and base fluid) on heat transfer is investigated. Understanding of the results revealed that concentration is the dominant factor for enhancing heat transfer. A concentration of 1%-5% increased the convective heat transfer by more than 5% for nanofluids like alumina (Al_2O_3-water). This is found to be extremely beneficial in pipes whose wall temperature decrease requiring less heat to cool them. Based on the differences in heat transfer for temperature dependent and independent models, it is found that the application determines the type of thermophysical and convective models to be used.

Table of Contents

List of Figures

List of Tables

List of Publications

1. Shomaz Ul Haq, Sara Sultan, Hamza Ahmad Raza, Ibadullah Safdar, Sufyan Naeem, and Majid Ali “Effect of characteristic parameters on nanofluid thermal energy performance” under review in Journal “International Journal of Sustainable Energy”

2. Shomaz Ul Haq, Hamza Ahmad Raza, Ibadullah Safdar, Sara Sultan, Sufyan Naeem, and Majid Ali “Comparative numerical investigation on effect of characteristic parameters on thermal energy enhancement by alumina-water and cupric-oxide-water nanofluids” accepted in Conference “International Conference on Energy Conservation and Efficiency 2017”

3. Shomaz Ul Haq, Ibadullah Safdar, Hamza Ahmad Raza, Sara Sultan, Sufyan Naeem, and Majid Ali “Numerical analysis of heat transfer and fluid friction on entropy generation in nanofluids” accepted and presented at Conference “International Conference on Impact of Nano-Science on Energy Technologies 2017”

Chapter 1: Introduction

1.1 Energy

Energy of any country is vital for the economic, educational, social, and infrastructure development as well as the improvement in lifestyle and standard of living. Energy crisis is not new to a country like Pakistan where most of the plants are thermal based on fluids such as oil or gas and thus research and development in heat transfer is crucial. At the end of the first decade and start of second decade 2010-2011, it is predicted annual energy shortfall would exceed 8000 MW by the end of the current year 2017 and shoot above 13000 MW at the end of the current second decade [1].

Any thermal reaction in a power plant or system generates heat which needs to be removed for utilization of energy and conversion of steam or work. Thermal energy addition, removal, and transport remains a crucial problem in the commercial, residential, and industrial sectors. Efficient heat transfer is one way to promote clean and sustainable energy. The efficiency of a thermal power plant depends on heat transfer fluid (HTF) or working fluid. Fluid is circulated by a pump and using a good HTF can increasing efficiency and reduce pumping requirements.

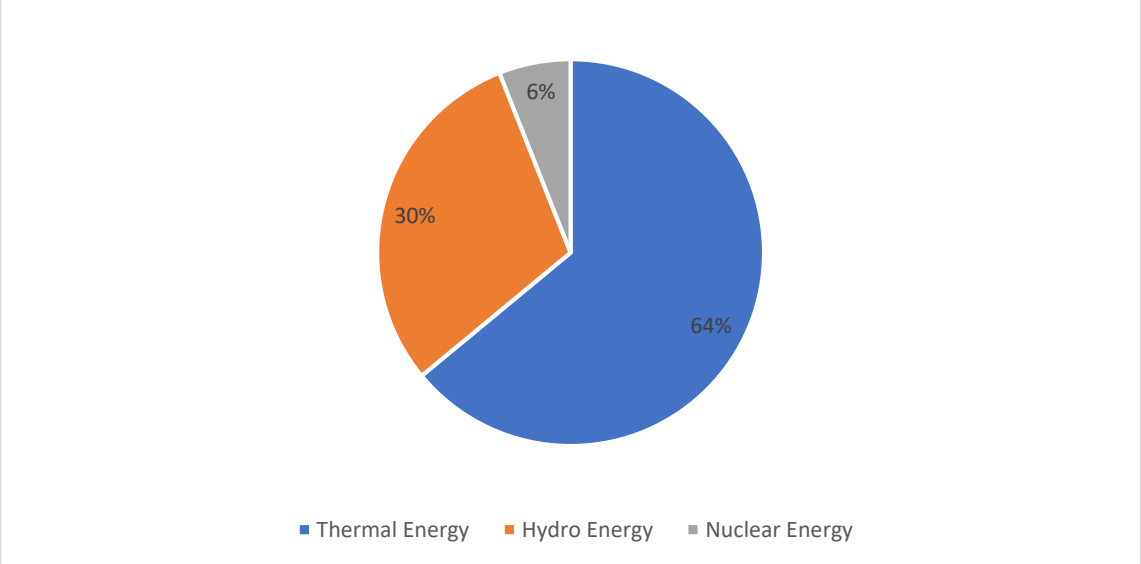

Figure 1.1 Electricity generation by energy source in Pakistan for fiscal year 2017 [2]

1.2 Heat Transfer Fluid

An HTF is a fluid that flows around or through a device to transfer heat created by device to other apparatus which utilize or dissipate it. They play a crucial role in the efficient use of energy. A variety of HTFs like air, water, hydrocarbons (HCs), molten salts, refrigerants, phase change liquids, and silcones exist or have been developed to meet operating needs of diverse applications like natural gas compressors, geothermal energy, refrigeration and solar energy. Due to its vast applications learning properties of HTFs is crucial and a number of criteria must be examined before choosing an HTF for a specific application.

- Chemical compatibility with common metals-stainless steels (to avoid corrosion)
- Easily pumpable
- High heat capacity or thermal conductivity
- High or long-term stability (low decomposition rate etc.)
- High thermal cycling tolerance
- Low cost, environmental impact, freezing point, and viscosity
- Low viscosity (to decrease parasitic losses at low and nominal temperatures)
- Non-toxic
- Possibility to operate continuously at higher temperatures
- Possibility to be combined with heat storage systems

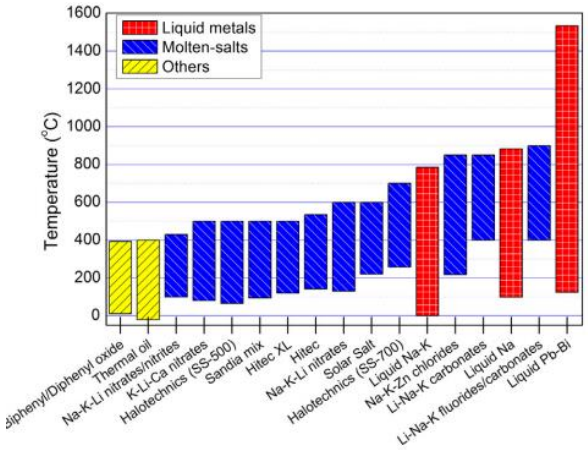

Figure 1.2 Comparison of operating temperatures of different heat transfer fluids [3]

1.3 Enhancement of Heat Transfer

Heat transfer enhancement play a role in increasing thermal power by the use of external heat pumps, sources or vibrators, vortex generators [4], micro-channels, miniaturized heat exchangers, fuel cells, surface treatment [5], and additives (solid particles, gas bubbles, and liquid droplets for fluids) in various applications [6]. Additives remain a viable option for improving heat transfer without expensive added costs and environmental concerns.

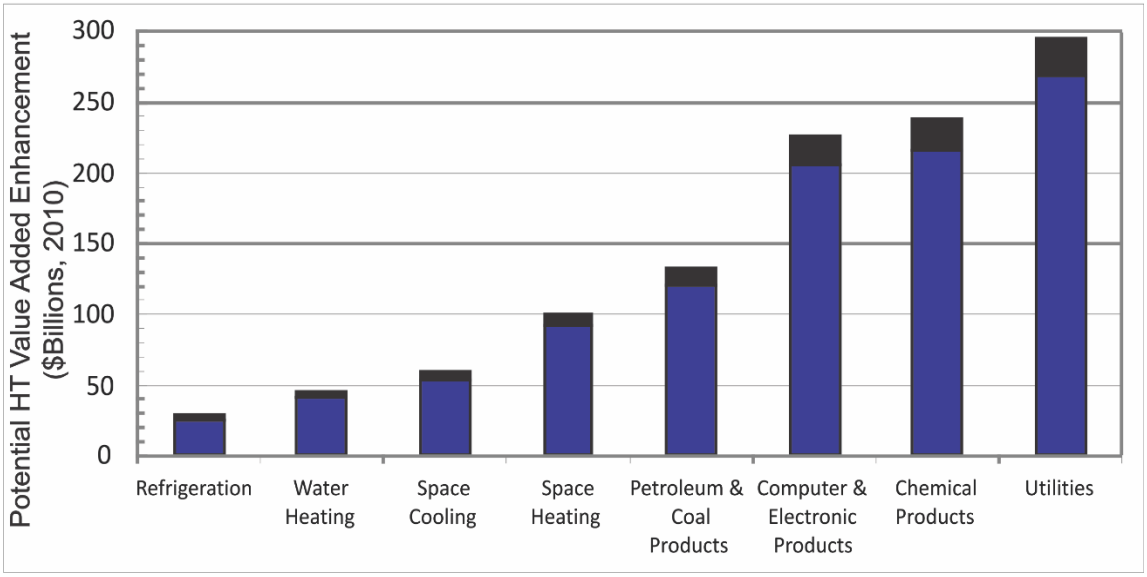

Figure 1.3 Revenue from heat transfer enhancement research [6]

Heat transfer enhancement is not a new concept. For decades active as well as passive techniques have been explored but with little significant insights due to limitations of experimentation, manufacturing, and numerical analysis. As far as 1980s, Kakac extensively investigated effective ways to improve flow of heat including correlations for different geometries [7]. Similarly, traditional techniques of enhancing the effectiveness of heat exchanger by adding fins have also been employed but with the precaution of justifying enhancement relative to added costs and weights. Problems like these changed the trend from manufacturing research to enhancement by use of HTF. Higher thermal conductivity, low density, and inertness of nanofluids have enable them to be used in applications ranging from computer chip cooling to power plants.

1.4 Nanofluids

Nanotechnology is one area that has enabled efficient heat transfer by the use of nano sized additives in fluids. These dilute suspensions called “nanofluids” were first investigated by Choi in 1995 [8]. Nanofluids are colloidal suspensions of these nanoparticles in a fluid. Nanoparticles increase thermal conductivity of nanofluid thus increasing convective heat transfer. Though nanofluids are being applied in other heat transfer mechanisms like mixed convection [9], natural convection [10], entropy generation minimization [11], boiling and condensation [12], there major application remains in pure convective heat transfer due to the ubiquitous nature of flows inside closed conduits (such as pipes, tubes, channels, nozzles, pumps, and tanks). There is a huge potential of heat transfer by nanofluids in solar energy as shown in Fig. 1.2. [13]

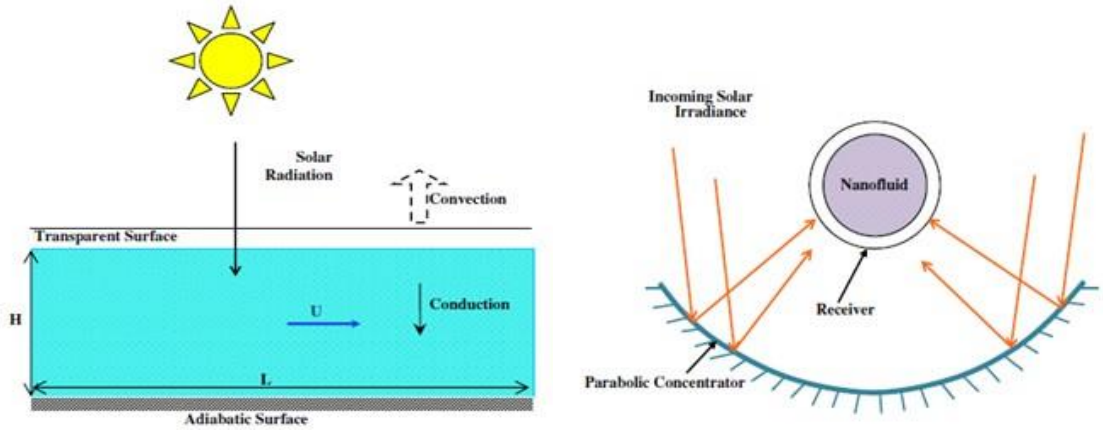

Figure 1.4 Direct absorption and parabolic trough solar collectors with nanofluid [13]

This research focuses on passive heat transfer enhancement using nanofluids to increase thermal conductivity and convective heat transfer. The hypothesis of critical heat flux (CHF) enhancement is based on the fact that at least some form of heat transfer characteristics are responsible and has something to do with nanoparticles. According to a study in 2008 in United States alone changing the heat transfer fluid from water to nanofluid can save 1 trillion BTUs per year of energy and usage of nanofluid in closed loop cooling cycles can save 10-30 trillion BTUs per year [14].

1.5 Working Principle

Due to the minute size of the particles, certain interesting phenomena are believed to present in nanofluids but are not found in conventional mixtures containing larger sized particles. These include thermal dispersion, intermolecular energy exchange, and liquid layering on the solid–liquid interface as well as phonon effects on the heat transport inside the particle itself. When using nanofluids HTC increases decreasing the surface area needed for heat transfer for the same temperature difference and more thermal energy is transferred as a result.

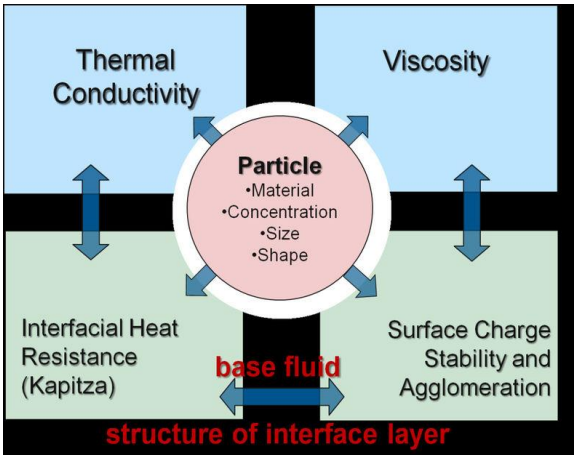

Figure 1.5 Effect of multiple parameters on working of heat transfer by nanofluids [15]

1.6 Motivation

Nanofluids were the preferred choice in conducting heat transfer analysis because of high thermal conductivity of particles. This fact is coupled with the ease of carrying accurate numerical analysis in a commercial CFD code which has dramatically reduced research time. With the discovery of nanofluids, heat transfer is dominated by in-situ control of fluid properties. Provided stable suspensions, they provide the following benefits.

- Applicability to different conditions by changing thermophysical properties like density, specific heat, thermal conductivity, and viscosity by changing concentration.
- Decreased clogging of closed systems (like pipes) as compared to previous generation of microfluidic thermal fluids and slurries.
    - Increased specific surface area enabling more thermal energy transfer between the

fluid and nanoparticles.

- Dependence on not only particle concentration but also size (increasing heat transfer with decrease in size). This was not possible in sediment fluids and microslurries.
- Maintenance of Newtonian behavior at low concentrations giving the advantage of a low increase in pressure drop due to increase in viscosity.

1.7 Research Questions

An accurate CFD analysis of heat transfer and particularly heat transfer enhancement with results that are in agreement with experimental analysis from literature, depends on the assumptions, conditions, and limitations imposed on the problem. The inherent nature of the problem has helped shaped many important questions regarding heat transfer enhancement using nanofluids in pipe flows. These are as follows.

- How to does nanofluid affect the entry length as heat transfer in this region is important for most applications?
- How nanofluids properties affect the average friction factor and heat transfer coefficient (HTC) in short pipes for the complete section of pipe?
- What CFD models are suitable to capture the flow and heat transfer physics of the forced convection problem out of the many models available to predict heat transfer?
- What empirical correlations account for the different thermophysical properties (particularly thermal conductivity) and how accurately?
- What barriers are there to design nanofluid based heat transfer in closed conduits and how could those challenged be addressed?

1.8 Goals and Objectives of Research

Major objectives of this research are as follows.

- Modeling and simulation of forced convective laminar and turbulent fluid flow and heat transfer in a heated pipe using single phase and multiphase models.
- Selection of design factors of concentration, diameter, flow rate, heat flux, inlet temperature, Re number, and type of nanofluid.
- Investigation of the effect of design factors on HTC, Nusselt (Nu) number, pressure drop (ΔP), flow and thermal boundary layers for different axial and radial locations.

- Application of constant property (thermophysical) nanofluid model with different correlations and comparison with the experimental and theoretical data available.

1.9 Methodology and Organization of Thesis

Following process was adopted for studying heat transfer enhancement in nanofluids.

- Chapter 1 Introduction
  Background, Nanofluids, Motivation, Research Questions, Working Principle, Research Goals, and Methodology
- Chapter 2 Literature Review
  Heat Transfer Enhancement, Nanofluids, Thermophysical Properties, Forced Convection, and CFD Numerical Modeling and Simulation
- Chapter 3 Methodology
  Single Phase Flow, Two Phase Flow, State Equations, Heat Transfer Equations, and Pre Analysis Correlations
- Chapter 4 Modeling and Simulation
  Preprocessing and Solving, Post Processing, Grid Independency, and Experimental and Theoretical Validation
- Chapter 5 Single Phase Heat Transfer
  Pressure, Temperature, and Velocity Distributions, and Effect of Different Parameters on Nanofluid Single Phase Heat Transfer
- Chapter 6 Two Phase Heat Transfer
  Pressure, Temperature, and Velocity Distributions, and Effect of Different Parameters on Nanofluid Two Phase Heat Transfer
- Chapter 7 Entropy Generation
  Fluid Flow, Heat Transfer, and Total Entropy Distribution, and Effect of Different Parameters on Total Entropy
- Chapter 8 Conclusions and Recommendations
- Chapter 9 Supercritical CO_2 for Concentrated Solar Energy (OSU)

References

[1] M. Shahbaz, “Electricity consumption, financial development and economic growth nexus: a revisit study of their causality in Pakistan,” Munich Personal RePEc Archive (MPRA), issue. 35588, 2011.

[2] S. E. Wasti et al., “Pakistan Economic Survey 2016-17,” Islamabad, 2017.

[3] K. Vignarooban et al., “Heat transfer fluids for concentrating solar power systems – A review,” Applied Energy, vol. 146, issue , pp. 383-396, 2015.

[4] H. E. Ahmed, H. A. Mohammed, and M. Z. Yusoff, “An overview on heat transfer augmentation using vortex generators and nanofluids: Approaches and applications,” Renew. Sustain. Energy Rev., vol. 16, no. 8, pp. 5951–5993, 2012.

[5] S. Noor, M. M. Ehsan, S. Salehin, and A. K. M. S. Islam, “Heat transfer and pumping power using nanofluid in a corrugated tube,” no. , pp. 1–4, 2014.

[6] R. A. Taylor et al., “Socioeconomic impacts of heat transfer research,” International Communications in Heat and Mass Transfer, vol. 39, issue 10, 1467-1473.

[7] R. L. Webb, Enhancement of single-phase heat transfer. In S. Kakac, R. K. Shah, and W. Aung, editors, *Handbook of Single-Phase Convective Heat Transfer*, chapter, 17. Wiley-Interscience, New-York, 1987.

[8] S. U. S. Choi and J. A. Eastman, "Enhancing thermal conductivity of fluids with nanoparticles," Proceedings of the 1995 ASME International Mechanical Engineering Congress and Exposition, ASME, San Francisco, CA, USA, vol. 231, pp. 99–105, 1995.

[9] N. Mittal, A. Satheesh, D. S. Kumar, “Numerical simulation of mixed-convection flow in a lid-driven porous cavity using different nanofluids,” Heat Transfer Asian Research, vol. 43, pp. 1–16, 2014.

[10] X. Meng and Y. Li, “Numerical study of natural convection in a horizontal cylinder filled with water-based alumina nanofluid,” Nanoscale Research Letters, 10: 142, pp. 2–11, 2015.

[11] P. K. Singh et al., “Entropy generation due to flow and heat transfer in nanofluids,” International Journal of Heat and Mass Transfer, vol. 53, issues 21–22, pp. 4757–4767, 2010.

[12] S. J. Kim, Subcooled boiling heat transfer and critical heat flux in water based

nanofluids at low pressure. PhD Thesis, Massachusetts: MIT, 2009.

[13] K. V. Wong et al., “Applications of nanofluids: current and future,” Advances in Mechanical Engineering, vol. 2, no. , pp. , 2010.

[14] V. Khullar et al., “Solar energy harvesting using nanofluids-based concentrating solar collector,” ASME. Journal of Nanotechnology in Engineering and Medicine, vol. 3, issue 3, pp. 031003-031003-9, 2013.

[15] E. V. Timofeeva et al., “Nanofluids for heat transfer: an engineering approach,” vol. 6, issue 1, pp. 182, 2011.

Chapter 2: Literature Review

2.1 Heat Transfer Enhancement

Theoretical studies formed the basis of additive-fluid mixture research dating as far as late 1800s when Maxwell proposed the first thermal conductivity correlation at low concentrations for millimeter or micrometer sized particles [1]. It was not until many years later that another model for thermal conductivity was developed by Bruggeman in 1935 [2]. The study gave insight into the interactions between random particles in binary homogenous mixtures containing spherical particles. As compared to Maxwell there was no restriction to the concentration of particles. Particle-liquid flow in pipes in turbulent regime was first practically studied after World War 2 in 1964 by Kofanov [3]. The result was a derivation of the following heat transfer correlation.

$$Nu_D = 0.026 Re_D^{0.8} Pr^{0.4} F_p \tag{2.1}$$

where F_p is a property group defined as

$$F_P = \left(\frac{x_v}{1-x_v}\right)^{0.15}\left(\frac{\rho}{\rho_p}\right)^{0.15}\left(\frac{c_p}{c_{p,p}}\right)^{0.15}\left(\frac{d_i}{d_p}\right)^{0.02} \tag{2.2}$$

This correlation was based on 18 data sets from five different authors. Particles were of chalk, coal, sand, aluminum, copper, graphite, and glass in base fluids of water and ethylene glycol (EG). It was found that the mixture density and viscosity depended on particle volume fraction but specific heat and thermal conductivity depended on mass fraction. Another study of convective forced laminar flow involving glass beads in oil revealed an enhancement of 40% [4]. At low concentrations and velocities, particles having low thermal conductivity caused fouling in pipes.

2.2 Nanofluids

With the advancement in nanotechnology, nanometer sized particles started being used in fluids. Heat transfer in nanofluids have been the subject of investigation since 1995 when Choi et al. [5] put forward the term during research at the Argonne National Labs, U.S.A. It was found that the Bruggeman correlation agrees better than Maxwell correlation at higher concentrations and also agreed well with the experimental data.

$$k_{eff}^2(-2) + k_{eff}\left(3\emptyset(k_p - k_{bf}) + 2k_{bf} - k_p\right) + k_{bf}k_p = 0 \tag{2.3}$$

Solving gives

$$k_{eff} = \frac{-\left(3\emptyset(k_p - k_{bf}) + 2k_{bf} - k_p\right) \pm \sqrt{\left(3\emptyset(k_p - k_{bf}) + 2k_{bf} - k_p\right)^2 + 8(k_{bf}k_p)}}{-4} \quad (2.4)$$

Eastman et al. [6] concluded that nanoparticles because of their minute size and density can remain stably suspended in solutions for weeks. Experiments for synthesis of nanofluids for different heat transfer analysis and applications indicated that stability of nanofluids depends on factors like diameter of nanoparticles, dispersant, magnetic stirring, pH, and/or ultrasonication, and most importantly method of preparation.

Stable and highly conductive nanofluids are produced by one-step and two-step production methods. Both approaches suffer from agglomeration of nanoparticles, which is a problem in technologies involving nanopowders. Synthesis and suspension of nearly non-agglomerated or monodispersed nanoparticles in liquids is the key to significant enhancement in thermal properties of nanofluids. All physical synthesis mechanisms have a critical length scale below which the physical properties of materials are changed. Thus, particles smaller than 100 nm exhibit properties different from conventional solids. Two-step method first makes nanoparticles by any of the processing techniques mentioned above and then disperses them in base fluids e.g. VEROS (vacuum evaporation onto a running oil substrate) [7-8]. The single-step method simultaneously makes and disperses nanoparticles directly into base fluids. In either case, a well-mixed and uniformly dispersed nanofluid is needed for successful production or reproduction of enhanced properties and interpretation of experimental data. Thus, thermophysical properties must be measured. It has been noted that making nanofluids containing oxide nanoparticles and nanotubes using two step method is easier than one step method [9].

2.3 Thermophysical Properties of Nanofluids

Several models have been proposed to describe the thermophysical behavior of these suspensions, but none has revealed to be rigorously reliable. This may be due to uncertainty in the experimental measurements or ineffective benchmarking, characterization, and standardization of the factors affecting thermophysical properties. Thus, physics governing the real behavior of nanofluids is far from being understood.

Three main categories of new models were proposed for enhanced thermal conductivity of nanofluids i.e. conduction, nanoscale convection, and near-field radiation.

- Figures 2.1 shows the first static model called the classical EMT or Maxwell model. This model predicts thermal conductivity of milli or micro sized particle mixtures but not nanofluids. Nonetheless it has been used for nanofluids by some researchers.
- The nano-convection model [10] divides conduction in nanofluids into four modes: (1) collision of base fluid molecules with each other, (2) thermal diffusion of nanoparticles in fluids, (3) collision of nanoparticles with each other, and (4) Brownian motion-induced nano-convection by the particles suspended in nanofluids.

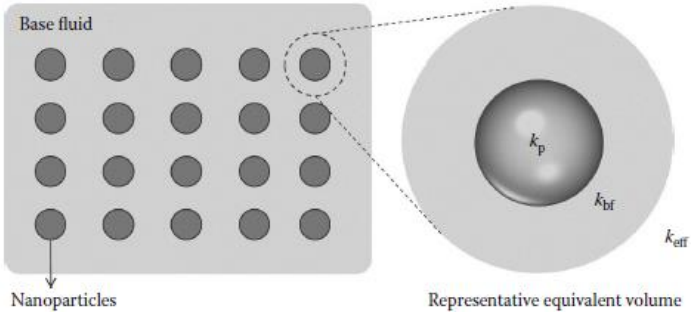

Figure 2.1 Classical EMT or Maxwell model for thermal conductivity [10]

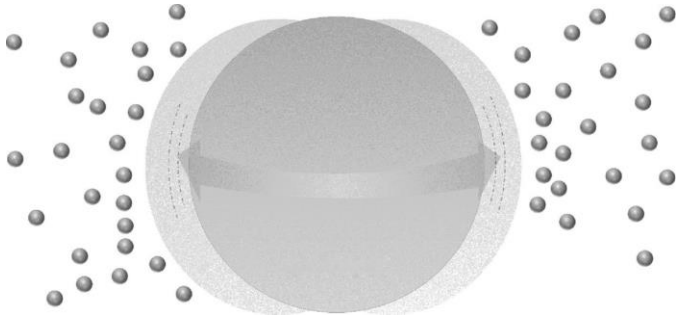

Figure 2.2 Brownian motion-induced nano-convection dynamic model [10]

2.4 Experimental Forced Convection in Nanofluids

Pak et al. in 1998 conducted an experimental forced convective analysis with constant wall heat flux in turbulent regime for Al_2O_3-water and TiO_2-water nanofluids. Both h and Nu number increased with concentration and Re number but at the same average velocity, h decreased by 12% as compared to base fluid. Moreover, the Dittus Boelter correlation

underpredicted the h and Nu number but matched for non-dimensionalized (with respect to Pr number) Nu number. A new correlation was given [11].

Copper-water nanofluids were investigated by Li et al. for laminar and turbulent flow. At same Re number, h increases by 60% for a maximum concentration of 2%. For turbulence, h increased dramatically with Re number, maximizing at 12000 at highest concentration of 2% and Re number of 20000. A new correlation was introduced [12].

An experimental closed loop setup was designed for forced convection of Cu-water nanofluids. Constant wall heat flux was applied in turbulent region. The results revealed that although heat transfer enhances with concentration and Re numbers, flow resistance increases with increase in viscosity. Though it is equal at same Re number, it increases slightly till 2% concentration implying use of conventional single phase correlation [13].

A work on entrance length convective heat transfer in laminar regime was carried out by Wen et al. Alumina-water nanofluids were employed in this study. The thermal developing length was found to be higher than the base fluid along with an increased heat transfer in the entrance length. Apart from thermal conductivity, particle migration was a factor taken into account in h enhancement [14].

Williams et al. evaluated an in-depth experiment studying the effect of design factors such as concentration, flow rate, heat flux, and inlet temperature on full developed turbulent convective heat transfer of Al_2O_3-water and ZrO_2-water nanofluids. Temperature dependent properties were used to calculate Nu number, Pr number, and Re number and as result no anomalous heat transfer was observed. The h increases for upto a concentration of 1.8% and then decreases till 3.6% with a maximum of 19.1 kW/m^2K at a concentration of 0.9%, flow rate of 0.0002283 m^3/s or 3.574 g/m, inlet temperature of 63.81°C, and power of 8.64 kW [15].

2.5 CFD Numerical Modeling and Simulation of Nanofluids

The advancement of computing performance coupled with customer friendly interfaces has enabled the resurgence of CFD after decades of dormancy. Although present from 1960s, CFD was limited to applications of aerospace, automotive, and power generation. Now it has spread to almost all areas and prevalent in industry. In fact, over the last two decades many problems of fluid flow and heat transfer have been solved.

CFD not only reduces development time but also costs. No doubt there is a certain amount of time (such as around 50% in making domain and grid) as well as investment involved in the form of hardware, licenses, and personnel. CFD more than makes up these costs by removing the high fixed cost and variable costs of an experimental facility as its very convenient to test a large number of data points and configurations.

The start of 21st century marked the generation of numerical research in nanofluids. In 2004 Maiga et al. investigated Al_2O_3-water and Al_2O_3-EG laminar and convective heat transfer in a circular tube with uniform heat flux. Heat transfer was found to increase for increased concentration but at a compromise of detrimental effect of wall shear. Furthermore, Al_2O_3-water had less enhancement than Al_2O_3-EG nanofluid [16–17].

Labonte et al. took into account temperature dependent thermophysical properties of Al_2O_3-water nanofluids in a circular pipe with constant wall heat flux. Interestingly lower values for h were obtained for constant properties model and a higher wall shear stress as compared to temperature dependent properties. A maximum h enhancement of 40% was obtained for a modest concentration of 4% [18].

Apart from Brownian diffusion and forces and sedimentation, the dispersion (thermal) model has been shown to be the reason for heat transfer enhancement in nanofluids. Chaotic motion of particles (hydrodynamic dispersion) and thermal dispersion increases energy exchange rate and normalize temperature gradients. S. Z. Heris et al. applied factors such as dispersed thermal conductivity (k_d) in axial and radial direction in form of thermal diffusivity in energy equation terms to account for dispersion in numerical

analysis of circular laminar pipe with constant wall temperature [19]. The k_d depended on average axial velocity, concentration and diameter of particle, and nanofluid properties. Following papers reporting heat transfer characteristics of nanofluids in conduits are summarized in the form of Table 2.1 below.

Table 2.1 Key findings from modeling and simulation researches

References	Nanofluid	Model	Conclusions/Findings
A. Aghaei et al. [20]	Al_2O_3-water	Two phase	Nu_{ave} increases till ϕ=1% at constant Re and Nu_{ave} increases 700% at constant ϕ for Re=10000-100000
A. M. Khdher et al. [21]	Al_2O_3-water, and Al_2O_3-ethylene glycol (EG) and water mixture	Single phase	h_{ave}: 12.5% at ϕ=4% and Re = 30000
A. T. Utomo et al. [22]	Al_2O_3-water and TiO_2-water		h_{ave}: 1.5% at ϕ=9%, constant Q and h_{ave}: 5% at constant Re
E. E. Bajestan et al. [23]	Al_2O_3-water	Single phase	h_z:87.5% at ϕ=6% and Re = 832.8 and Q = $6.308x10^{-5}$ m^3/s at entrance region
E. E. Bajestan et al. [24]	Al_2O_3-water, and Al_2O_3-EG and water mixture, CuO- water and CuO-EG and water mixture, carbon nanotube (CNT)-water and CNT- EG and water mixture	Single phase	h_z:26.92% at ϕ=6% and Re = 1460 (Al_2O_3-water) h_z:15.38% at ϕ=6% and Re = 1460 (Al_2O_3-EG and water mixture) h_z:38.46% at ϕ=0.0384% and Re = 1460 (CNT- water) h_z: 7.69% at ϕ=6% and Re = 1460 (TNT-water) at entrance region
G. Sekrani and S. Poncet [25]	Al_2O_3-water and Cu-water	Single phase and two phase	h_z: 74% at ϕ=1.6% Re = 1600
J. Labonte et al. [18]	Al_2O_3-water	Single phase	h: 40% at ϕ=4%
S. E. B. Maiga et al. [16]	Al_2O_3-water and Al_2O_3-EG	Single phase	h: 40% at ϕ=4%
S. E. B. Maiga et al. [17]	Al_2O_3-water and Al_2O_3-EG mixture	Single phase	h_{ave}: 205% at ϕ=10% and Re=1000 (Al_2O_3-water)

Summary

The use of nanofluids as HTF for thermal energy applications is promising. Heat transfer enhancement using nanofluids can decrease costs, decrease energy and water usage, and increase efficiency of process in a symbiotic way. The most prominent mechanism to do that has shown to be thermal conductivity enhancement. Different empirical and theoretical models have been developed to better understand the behavior of nanofluids under different conditions. The mode of heat transfer has been the dominant factor in determining the nature of these correlations and models. The investigation of both experimentation and modeling has been geared towards quantifying effective thermophysical properties such as density, specific heat, thermal conductivity and viscosity.

An overview of the evolution, characterization, experimentation, modeling and simulation, and convective forced heat transfer of nanofluids has been done keeping in view an eye on the shortcomings in current research. Numerical methods and simulation using tools such as CFD reveal important information on heat transfer characteristics. No general consensus has yet been made on the preferred modeling scheme for nanofluid forced convection problems. Generally speaking, two-phase models seem to give better results in certain cases, but in other situations, they were found to differ considerably from available experimental data. Other studies confirmed that the simplest approach based on the single-phase assumption can lead to satisfactory results, provided adequate nanofluid properties are specified.

A justification is therefore necessary for assumptions and correlations used in convective forced heat transfer by nanofluids.

References

[1] J. C. Maxwell, A Treatise on Electricity and Magnetism, Clarendon Press, Oxford, 1873.

[2] D. A. G. Bruggeman, “Calculation of various physical constants of heterogeneous substances. I. dielectric constants and conductivities of the mixed body of isotropic substances,” Annals of Physics, vol. 416, issue 7, pp. 636–679, 1935.

[3] V. I. Kofanov, “Heat transfer and hydraulic resistance in flowing liquid suspensions in piping,” Int. Chem. Eng., 4(3), pp. 426–430, 1964.

[4] R. W. Watkins et al., “Entrance region heat transfer in flowing suspensions,” International Journal of Heat and Mass Transfer, vol. 19, issue 6, pp. 693–695, 1976.

[5] S. U. S. Choi and J. A. Eastman, "Enhancing thermal conductivity of fluids with nanoparticles," Proceedings of the 1995 ASME International Mechanical Engineering Congress and Exposition, ASME, San Francisco, CA, USA, vol. 231, pp. 99–105, 1995.

[6] J. A. Eastman et al., “Enhanced thermal conductivity through the development of nanofluids,” Nanophase Composite Matter, II, pp. 3–11.

[7] S. Yatsuya et al., “Magnetic properties of extremely fine particles of iron pepared by vacuum evaporation on running oil substrate,” Japanese Journal of Applied Physics, 17, pp. 355–359, 1978.

[8] S. Yatsuya et al., “Ultraafine particles produced by vacuum evaporation onto a running oil substrate (VEROS) and the modified method,” Journal of Crystal Growth, 70, pp. 533–535, 1984.

[9] W. Yu et al., “Review and comparison of nanofluid thermal conductivity and heat transfer enhancements,” Heat Transfer Engineering, 29, pp. 432–460, 2008.

[10] V. Bianco et al., Mechanisms and models of thermal conductivity in nanofluids, in: S-H Lee and S. P. Jang (Eds.), Heat transfer enhancement with nanofluids, CRC Press Taylor and Francis Group, Florida, pp. 73–102, 2015.

[11] B. C. Pak and Y. I. Cho, "Hydrodynamic and heat transfer study of dispersed fluids with submicron metallic oxide particles," Experimental Heat Transfer, vol. 11, issue 2, pp. 151–170, 1998.

[12] Q. Li and X. Yimin, “Convective heat transfer and flow characteristics of Cu-water nanofluid,” Science in China Series E: Technolgical Science, vol. 45, issue 4, pp. 408–416, 2002.

[13] Y. Xuan and Q. Li, “Investigation on convective heat transfer and flow features of nanofluids,” Journal of Heat Transfer, vol. 125, issue 1, pp. 151–155, 2003.

[14] D. Wen and Y. Ding, “Experimental investigation into convective heat transfer of nanofluids at the entrance region under laminar flow conditions,” International Journal of Heat and Mass Transfer, vol. 47, issue 24, pp. 5181–5188, 2004.

[15] W. Williams et al., “Experimental investigation of turbulent convective heat transfer and pressure loss of alumina/water and zirconia/water nanoparticle colloids (nanofluids) in horizontal tubes,” Journal of Heat Transfer, vol. 130, issue 4, 042412, 2008.

[16] S. E. B. Maiga et al., “Heat transfer behaviours of nanofluids in a uniformly heated tube,” Superlattices and Microstructures no. vol. 35, issues 3–6, pp. 543–557, 2004.

[17] S. E. B. Maiga et al., “Heat transfer enhancement by using nanofluids in forced convection flows,” vol. 26, issue 4, pp. 530–546, 2005.

[18] J. Labonte et al., “Heat transfer enhancement in laminar flow using Al_2O_3-water nanofluid considering temperature-dependent properties,” International Conference on Heat Transfer, Thermal Engineering and Environment pp. 331–336, 2006.

[19] S. Z. Heris et al., “Numerical investigation of nanofluid laminar convective heat transfer through a circular tube,” Numerical Heat Transfer, Part A: Applications, vol. 52, issue 11, pp.1043–1058, 2007.

[20] A. Aghaei at al., “Numerical investigation of turbulent forced-convective heat transfer of Al_2O_3-water nanofluid with variable properties in tube,” Ain Shams Engineering Journal, vol. 6, issue 2, pp. 577–585, 2015.

[21] A. M. Khdher et al., “Experimental and numerical investigation of heat transfer augmentation using Al_2O_3-Ethylene Glycol/Water nanofluids under turbulent flows in a tube,” The National Conference for Postgraduate Research, 2016.

[22] A. T. Utomo et al., “Experimental and theoretical studies of thermal conductivity, viscosity and heat transfer coefficient of titania and alumina nanofluids,”

International Journal of Heat and Mass Transfer, vol. 55, issue 25–26, pp. 7772–7781, 2012.

[23] E. E. Bajestan et al., “Flow and heat transfer of nanofluids with temperature dependent properties,” ASME 2010 8th Int. Conf. Nanochannels, Microchannels, Minichannels Collocated with 3rd Jt. US-European Fluids Eng. Summer Meet. ICNMM2010, no. August, 2010.

[24] E. E Bajestan et al., “Numerical investigation of effective parameters in convective heat transfer of nanofluids flowing under a laminar flow regime,” International Journal of Heat and Mass Transfer, vol. 54, issue 19–20, pp. 4376–4388, 2011.

[25] G. Sekrani and S. Poncet, “Further investigation on laminar forced convection of nanofluid flows in a uniformly heated pipe using direct numerical simulations,” Applied Science, vol. 6, issue 11, p. 332, 2016.

Chapter 3: Methodology

The numerical method used to solve the nanofluid heat transfer research problem is CFD. The technique is based on finite volume method (FVM) that is used to solve a matrix of conservative form of governing equations that may be in differential or integral form. CFD is applied to approximate physics of a practical problem of heat transfer, fluid flow and related phenomenon like chemical reactions, phase change etc.

A set of conservative partial differential equations (PDEs) is converted to a system of algebraic equations (a combination of linear and non-linear terms) at discrete points that are solved by a computer. For fluid flow the Newtonian form of conservation equations i.e. the Navier Stokes equations and for heat transfer the energy equation are solved iteratively. Fluid flow is conserved as conservation is built into the FVM procedure.

The laminar flow is a viscous flow in which shear stresses are only due to molecular interaction or transport (diffusion). This is manifested as Newton's law of viscosity or shear stress law defined as

$$\tau_{yx} = \mu \frac{\partial u}{\partial y} \tag{3.5}$$

This behavior is called Newtonian and is approximated by single component nanofluid. Incompressible steady 3D flow is assumed to simplify the dynamics of the flow. Furthermore, no body forces like buoyancy, gravity or electromagnetism or other forces like pressure, viscosity, or rotation are taken into account. The governing equations are composed of the fundamental continuity or mass equation, momentum equation(s) (Navier Stokes equation(s)), and energy equation.

3.1 Single Phase Flow

Single phase flows are flows that assume negligible motion slip between the dispersed and continuous phase and thermal equilibrium conditions prevail between the two components with effective thermophysical properties as a function of the properties of components and their respective concentrations.

3.1.1 Continuity Equation

The equation is defined as [1]:

$$\frac{\partial \rho}{\partial t} + \nabla . \rho \boldsymbol{u} = 0 \tag{3.6}$$

where ρ=density,

$\nabla = \frac{\partial}{\partial x} + \frac{\partial}{\partial y} + \frac{\partial}{\partial z}$ is the divergence,

and $\mathbf{u} = u\hat{\imath} + v\hat{\jmath} + w\hat{k}$ is the velocity vector. The first term is the rate of change of density and second term is convective term for the net mass flow rate out of element. For incompressible flows, the equation reduces to

$$\nabla . \boldsymbol{u} = 0 \tag{3.3}$$

3.1.2 Momentum Equation

Conservation of momentum principles were used to derived the equation defined as [1]:

$$\rho \frac{Du_i}{Dt} = -\gamma \nabla h - \nabla P + \nabla . \tau_{ji} + F_i \tag{3.4}$$

where $\frac{D}{Dt} = \frac{\partial u_i}{\partial t} + \nabla . u_i u_j$ is the material derivative,

γ= ρg is the specific weight,

h is the distance opposite to the direction of body force (e.g. weight),

P is the static pressure,

$\tau_{ji} = \left[\mu\left(\frac{\partial u_j}{\partial x_i} + \frac{\partial u_i}{\partial x_j}\right)\delta_{ji}\right] - \frac{2}{3}\mu \frac{\partial u_m}{\partial x_m}\delta_{ji}$ is the stress tensor,

δ_{ji}=1 if j=i and δ_{ji}=0 if j≠i and is the Kronecker delta. It is a second order tensor, and

F_i is the body forces

3.1.3 Energy Equation

The equation is defined as [1]:

$$\frac{\partial(\rho h_{tot})}{\partial t} - \frac{\partial P}{\partial t} + \nabla . (\rho \boldsymbol{u} h_{tot}) = \nabla . (k \nabla T) + \nabla . (\boldsymbol{u} . \tau) + \boldsymbol{u} . \boldsymbol{S}_M + \boldsymbol{S}_E \tag{3.5}$$

where $h_{tot} = h + \frac{1}{2}\boldsymbol{u}^2$ is the total enthalpy,

h=h(p,T) is the static enthalpy,

k is the thermal conductivity,

∇.(k∇T) is the conduction heat transfer,

$\nabla.(\mathbf{u}.\tau)$=viscous work-internal heating by viscous stresses and negligible for the study

$\mathbf{u}.\mathbf{S}_M$ is the external momentum sources work, and

S_E is volumetric heat source (optional)

3.2 Two Phase Flow

Particulate or two phase flows are flows that compose of a disperse/particle phase and base/carrier/continuous phase. Density of disperse phase is usually different from carrier phase. If the concentration of dispersed particles is small then only the carrier phase influences dynamics of dispersed phase and is called one-way coupling. If concentration is appreciable there is a mutual influence of both phases and is called two-way coupling.

In the present study Eulerian-Eulerian/static frame of reference model is used. Furthermore, the model is homogeneous without the use of a free surface model. In Eulerian-Eulerian model, base fluid is continuous and dispersed phase is solid and treated as a continuum thus they are distinct but influencing fluids with continuum equations solved. The equations for this model are defined below.

3.2.1 Base Fluid Continuity Equation

$$\frac{\partial \rho}{\partial t} + \nabla.\rho\boldsymbol{u} = 0 \tag{3.6}$$

3.2.2 Nanoparticle Conservation of Volume Equation

$$\frac{\partial \rho}{\partial t} U.\nabla\phi = \nabla.(D_B \nabla\phi + D_T \frac{\nabla T}{T}) \tag{3.7}$$

where $D_B=\frac{k_b T}{3\pi\mu d_p}$ is the Brownian diffusion coefficient,

$D_T=(\frac{\mu}{\rho})(0.26\frac{k_f T}{2k_f+k_p})\phi$

3.2.3 Momentum Equation

$$U.\nabla U = \frac{-1}{\rho_{nf}}\nabla P - \frac{\mu_{nf}}{\rho_{nf}}\nabla.(\nabla U + (\nabla U)^T + g \tag{3.8}$$

where T is the transpose

3.2.4 Energy Equation

$$U.\nabla T = \nabla\left(\alpha_{nf}\nabla T\right) + \frac{\rho_p \rho_p}{c_{nf} c_{nf}}\left(D_B \nabla\phi.\nabla T + D_T \frac{\nabla T.\nabla T}{T}\right) \tag{3.9}$$

3.3 State Equations

The equations of state along with the transport equations form the governing equations. This is required for the development of a closed system. Thermophysical properties are defined of density, specific heat, and enthalpy are defined as a function of state variables pressure and temperature. The default generalized form of these equations in ANSYS is defined as [2]

$$\rho = \rho(P, T) \tag{3.10}$$

$$c_p = c_p(P, T) \tag{3.11}$$

$$dh = c_p dT + \frac{\partial h}{\partial P}|_T dP \tag{3.12}$$

where $c_p = \frac{\partial h}{\partial t}|_P$ is the specific heat,

$\frac{\partial h}{\partial P}|_T dP = v - T\frac{\partial v}{\partial T}|_P$, and

$v = \frac{1}{\rho}$ is the specific volume

Thermodynamically consistent defined expressions i.e. exact differentials mathematical properties are satisfied i.e. defined as [2]

$$\frac{\partial c_P}{\partial P} = \frac{\partial}{\partial T}\left(v - T\frac{\partial v}{\partial T}|_P\right) \tag{3.13}$$

3.2.1 Incompressible Equation of State

The incompressible equation of state is defined as

$$\rho = \rho_{user\ specific} \tag{3.14}$$

$$c_p = c_p(T) \tag{3.15}$$

$$dh = c_p dT + \frac{dP}{\rho} \tag{3.16}$$

3.4 Heat Transfer Equations

A special form of energy equation called the thermal energy equation is used as it is suitable for laminar low speed flows and stable as compared to total energy equation that is more appropriate for estimating high speed flows, large variation density, or specific heat flows (that uses a CEL expression, RGP table, or Redlich Kwong equation of state) or acoustic analysis (e.g. of speed of sound).

3.4.1 Thermal Energy Equation

Thermal energy equation comes by considering mechanical energy K and is defined as

$$\frac{\partial(\rho h)}{\partial t} + \frac{\partial P}{\partial t} + \nabla.(\rho \boldsymbol{u}\mathrm{h}) = \nabla.(\mathrm{k}\nabla\mathrm{T}) + \boldsymbol{u}.\nabla\mathrm{P} + \tau{:}\nabla\boldsymbol{u} + \boldsymbol{S}_E \tag{3.17}$$

where $\tau{:}\nabla\mathbf{u}$ is the viscous dissipation or internal heating and is negligible and positive

Assuming $h = e + \frac{P}{\rho} \sim e$ and neglecting -P∇.$\mathbf{u}$ gives the following form that was used.

$$\frac{\partial(\rho h)}{\partial t} + \nabla.(\rho \boldsymbol{u}\mathrm{h}) = \nabla.(\mathrm{k}\nabla\mathrm{T}) + \tau{:}\nabla\boldsymbol{u} + \boldsymbol{S}_E \tag{3.18}$$

3.4.2 Conjugate Heat Transfer Energy Equation

Solving for heat transfer in solid domains involve conduction, solid motion, and volumetric heat sources (done by applying a subdomain for the solid portion and applying a source term (linear source coefficient or value) to the subdomain). It doesn't involve flow. The same energy equation is used but with a little modification. This enables the use of conservative or hybrid variable values at a solid-fluid interface.

The conjugate heat transfer energy equation is defined as

$$\frac{\partial(\rho h)}{\partial t} + \nabla.(\rho \boldsymbol{u}_s\mathrm{h}) = \nabla.(\mathrm{k}\nabla\mathrm{T}) + \boldsymbol{S}_E \tag{3.19}$$

where $\mathbf{u}_s$=optional solid velocity-term that accounts for solid motion with respect to reference frame and the rest of the terms are the same as in the previous equation.

3.5 Pre Analysis Correlations

The hydrodynamic entrance length is defined as [4]

$$L_e = 0.05ReD \tag{3.20}$$

The pressure drop is defined as [4]

$$\Delta P = \frac{C_f \rho V^2 z}{2D} \tag{3.21}$$

where $C_f = \frac{\tau_w}{0.5\rho V^2} = \frac{0.05VD^2}{\alpha} = \frac{16}{Re}$ is the normalized wall shear or skin friction coefficient-

a factor to check associated with entrance length,

τ_w is the wall shear equal to $\mu \frac{\partial w}{\partial y}|_w$,

w is the axial centerline velocity,

V is the average freestream velocity, and

D is the diameter of pipe.

Entrance heat transfer is sensitive to Prandtl (Pr) number defined as [4]

$$Pr = \frac{\nu}{\alpha} = \frac{c_p \mu}{k} \tag{3.22}$$

where ν is the momentum diffusivity (kinematic viscosity or viscous diffusion rate),

α is the thermal diffusivity (thermal diffusion rate).

The Re number is defined as [4]

$$Re = \frac{\rho VD}{\mu} \tag{3.23}$$

The thermal entrance length is defined as [4]

$$L_t = 0.05DRePr = \frac{0.05VD^2}{\alpha} \tag{3.24}$$

In the fully developed region w will approach twice that of the average velocity according to the analytical solution of parabolic velocity profile [].

$$\frac{w}{V} = 2(1 - (\frac{y}{Y})^2) \tag{3.25}$$

The Nu number is defined as []

$$Nu = \frac{hD}{k} \tag{3.26}$$

where $h = \frac{q}{T_w - Average\ Bulk\ Mean\ Temperature}$ is the heat transfer coefficient.

For fully thermally developed flow Nu=4.364.

Summary

In this chapter the main governing equations of fluid flow and heat transfer are presented. Moreover, the numerical methodology along with their main equations, adopted in modeling nanofluids are also discussed briefly.

References

[1] H. K. Versteeg, W. Malalasekera, “An introduction to computational fluid dynamics: the finite volume method,” John Wiley and Sons Inc., New York, 1995.

[2] ANSYS® ANSYS CFX, Release 15.0, Help System, ANSYS Documentation CFX Theory Guide, ANSYS, Inc.

[3] Z. Haddad et al., “A review on natural convective heat transfer of nanofluids,” Renewable and Sustainable Energy Reviews, vol. 16, issue 7, pp. 5363–78, 2012.

[4] M. Massoud, Engineering Thermofluids Thermodynamics, Fluid Mechanics, and Heat Transfer, first edition, Springer, Berlin Heidelberg New York, 2005.

Chapter 4: Modeling and Simulation

CFD is a numerical method to model and simulate an engineering problem. It consists of preprocessing (i.e. geometry creation, grid generation, boundary and domain conditions assignment) and solving, and post-processing. Grid independency (grid refinement) is carried out along with experimental and theoretical validation. Following approach was adopted for the analysis of convective heat transfer by nanofluids in closed conduits.

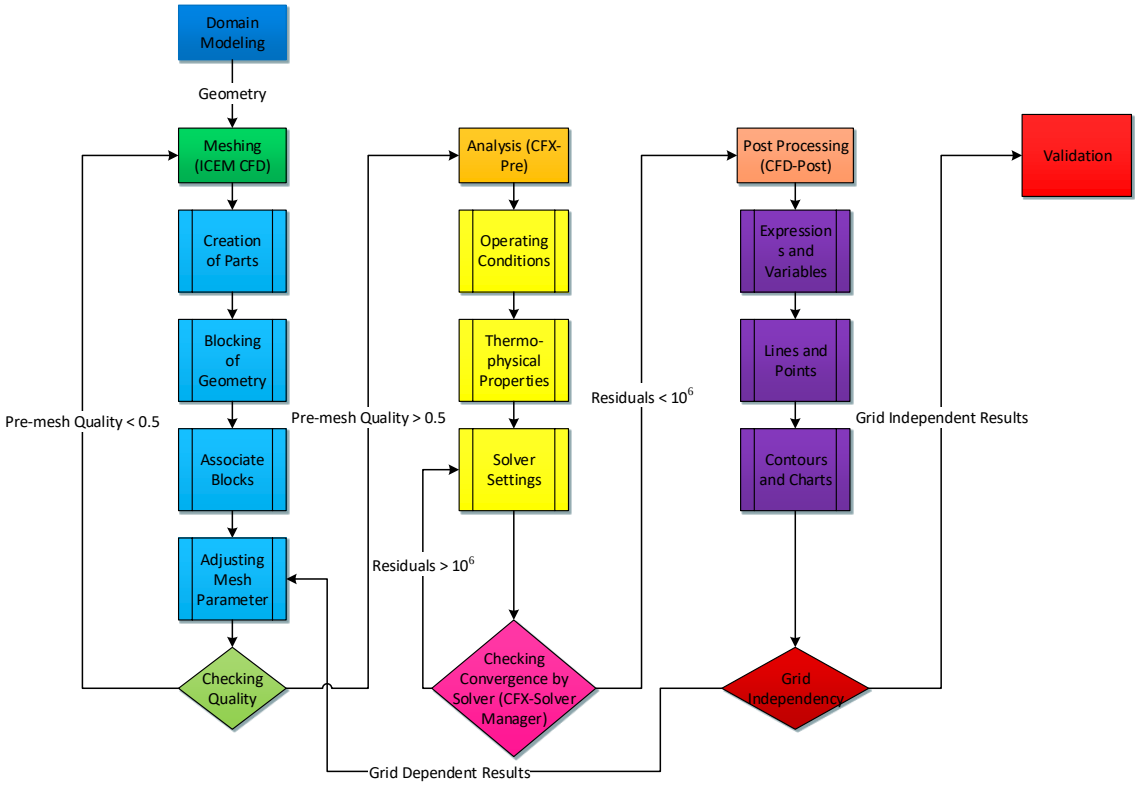

Figure 4.1 Modeling and simulation approach

4.1 Preprocessing and Solving (CFX-Pre)

Code used in simulating the model is ANSYS 16 with following steps for preprocessing.

4.1.1 Geometry and Grid Creation

Computational domain is a geometry developed in DesignModeler, a sub-component of ANSYS. The domain is a key input for the mathematical model (governing equations plus boundary conditions) to be solved over it. Grid creation is carried by discretizing domain

in small cells or elements in ICEM CFD, another sub-component of ANSYS and doesn't affect the mathematical model but only affects the numerical method.

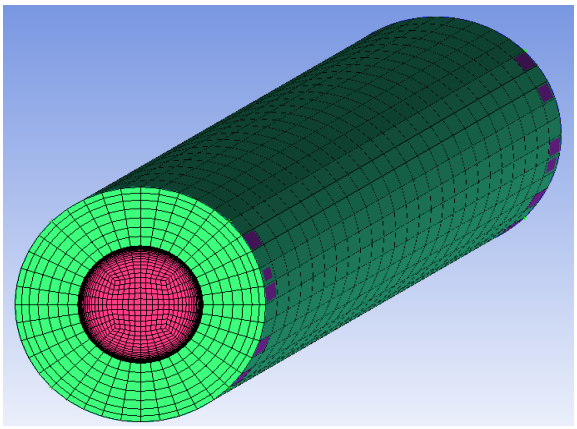

Figure 4.2 Double O-grid in ICEM CFD

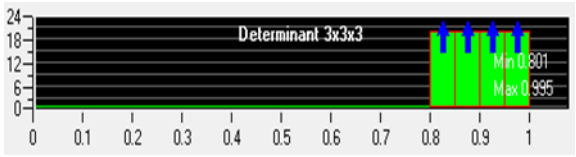

Figure 4.3 Quality metrics

4.1.2 Boundary Conditions and Domain Assignment (Model Setup)

Boundary conditions, fluid properties, and governing equations are assigned in CFX-Pre. The analysis type is steady state, domain is nanofluid, and the physical model is laminar model. Full second order discretization scheme has been employed to minimize discretization errors and ensure accuracy. Treatment of nanofluid as a single phase or multiphase determines what type of heat transfer correlations can be formed and used.

4.1.2.1 Density and Specific Heat

Density and specific heat capacity were calculated as mass averaged quantities and a function of properties of nanoparticle and base fluid. Expressions using Pak and Cho developed density and specific heat models [2] were inserted in nanofluid material.

$$\rho_{nf} = (1 - \emptyset)\rho_f + \emptyset\rho_p \tag{4.1}$$

$$(\rho c_p)_{nf} = (1 - \emptyset)(\rho c_p)_f + \emptyset(\rho c_p)_s \tag{4.2}$$

4.1.2.2 Thermal Conductivity

Classical effective medium theory (EMT) was used to define thermal conductivity below to model static effect. It is static because particles are fully dispersed in base fluid and hence a static mechanism [3].

$$(k_{eff})_{nf} = k_f\left(\frac{k_p + 2k_f + 2\emptyset(k_p - k_f)}{k_p + 2k_f - \emptyset(k_p - k_f)}\right) \tag{4.3}$$

4.1.2.3 Viscosity

Classical mixture theory based static theoretical viscosity models were employed [4-5].

$$\mu_{eff} = \mu_f \frac{1}{(1-\emptyset)^{2.5}} \tag{4.4}$$

Table 4.1 Thermophysical properties of base fluid and nanoparticles

Material	**Density (kg/m^3)**	**Specific Heat (J/kgK)**	**Thermal Conductivity (W/mK)**	**Viscosity (kg/ms or Pas)**
Water	997	4181.7	0.6069	8.899×10^{-4}
Alumina	3950	718	35.4	-
Cupric Oxide	6315	460	20	-

Following conditions shown in Table 4.2 were applied to the boundaries of the problem.

Table 4.2 Boundary conditions

Region or Zone	**Boundary Type**	**Value**
Inlet	Velocity	Variable
Outlet	Pressure Outlet	0 Pa
Wall	Heat Flux No Slip	10000 Wm^{-2}

4.1.3 Numerical Method of Solving

For resolving the advection terms, a "high resolution" advection scheme is employed together with a convergence control of 1000 iterations to ensure that the solution is sufficiently converged and minimize the linearization errors. Timescale control is chosen

to be “physical timescale” as the internal laminar pipe flow is an advection dominated flow requiring relaxation of non-linearities and a value of 2 s is chosen to get a steady state solution. Solver output gives a maximum Re number in laminar regime validating the model as shown in Fig. 4.4. All residuals converge to a value below 10^{-6}. The residual (aggregate imbalance) should be less than specified tolerance and defined as [6].

$$R = \frac{\Sigma|R_i|}{Scaling\ Factor} \tag{4.5}$$

In order to set guess values at all cell centers, the domain is globally initialized with the gauge pressure equal to 0 and velocity equal to the average inlet velocity. This is checked by displaying cell center values at longitudinal traverse contour of the complete pipe. The nodal values go from a value of the inlet velocity to a value of 0 near the pipe wall, also placing a check on the boundary condition. The effect of boundary conditions on cell center values is checked by first running one iteration and checking the contour again. The value at the wall decrease with respect to inlet velocity that shows the effect of the wall boundary condition. The mass imbalances in solver output are scaled by a factor of 10^6 as compared with the contours and agree.

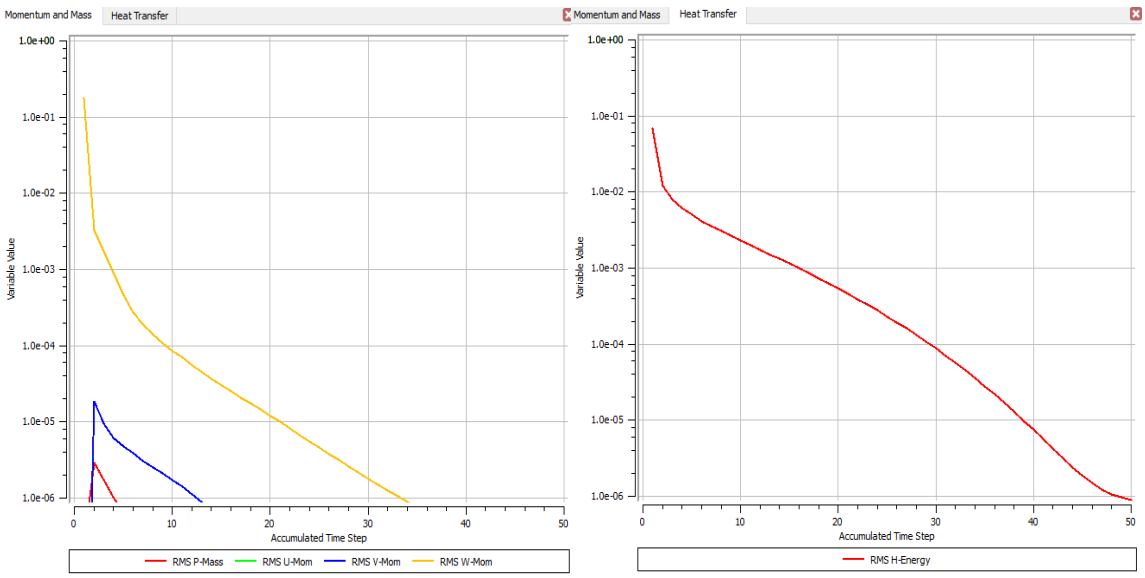

Figure 4.4 Convergence history of mass, momentum, and energy equations parameters

4.1.4 Assumptions and Simplifications

There are no buoyancy effects, domain motion, thermal dispersion effects or mesh

deformation in fluid domain modeling. Heat transfer and turbulence models of thermal energy and laminar are selected in fluid domain physical models. Scalable wall functions are used as the boundary layer. Non sphericity of particles is not taken into account. Only sphere particles are considered.

4.2 Post Processing

After convergence of solution parameters, the last stage in CFD analysis is processing of results in the form of displayed charts, contours, streamlines, and vector plots. In ANSYS this task is dedicated to CFD-Post. Expressions made in CFX-Pre are automatically imported into CFD-Post when it is opened. Other expressions were created using functions and variables existing in the ANSYS database.

4.2.1 Expressions

The following expressions were created in CFD-Post.

- Average HTC 1= areaAve(Wall Heat Transfer Coefficient)@Wall
- Average HTC 2=areaAve(WHTC 2)@Wall
- WHTC 2= (Wall Heat Flux)/(Tw 2-Tm2 or Tmx)
- Tw 2=(Wall Heat Flux/Wall Heat Transfer Coefficient)+Wall Adjacent Temperature
- Tm2 or Tmx=(Inlet Velocity [K])+((Wall Heat Flux [W/m^2]*3.142*D [m]*Z)/(Density*3.142*(D [m])^2*Inlet Velocity [m/s]*Specific Heat Capacity at Constant Pressure))
- Average Nu 1= (Average HTC 1*D[m])/keff
- Average Nu 2= (Average HTC 2*D[m])/Thermal Conductivity
- Eta=((massFlow()@Inlet*cpnf*(massFlowAve(T)@Outlet-massFlowAve(T)@Inlet))/(Input Energy))*100
- IE=areaInt(Wall Heat Flux)@Wall
- Nu 1=(Wall Heat Transfer Coefficient*D [m])/Thermal Conductivity
- Nu 2= (Wall Heat Flux*D [m])/(Thermal Conductivity*(Tw 2-Tm2 or Tmx))
- SFC=Wall Shear/(0.5*Density*(Inlet Velocity [m/s])^2)
- (Wall Shear/Density)^0.5

- (Density*Y*Friction Velocity)/Dynamic Viscosity

4.2.2 Variables

These expressions were then used to create the following variables which were then used in plotting contours, graphs, and reports.

- Average Bulk Temperature=Tm2 or Tmx
- Friction Velocity=Utau
- Nu Number 1=Nu 1
- Nu Number 2=Nu 2
- Skin Friction Coefficient=SFC
- Wall Heat Transfer Coefficient 2=WHTC 2
- Wall Temperature 2=Tw 2
- Y Plus=Yplus

4.2.3 Lines, Polylines, and Points

Different user locations were created to assist in extracting parameters of interest at different areas of domains. These included the following.

- Centerline-to calculate pressure, temperature and velocity at the center of conduit
- Central YZ plane
- Polyline made by intersection of a central YZ plane and pipe wall-to calculate heat flux, HTC, Nu number, Fanning friction factor or skin friction coefficient, temperature and yplus

4.2.4 Contours

Contours were then created using in built variables and user defined variables at six points along the length of the pipe (inlet or 0 m, 0.25 m, 0.5 m, 0.75 m, and outlet or 1 m) at cross sections and one in longitudinal direction along YZ plane.

- Pressure Contours
- Temperature Contours
- Velocity Contours

4.2.5 Charts

Apart from contours CFD post processor has the capability to display main results in the form of charts.

4.3 Grid Independency

In order to remove dependency of results on the grid, a refinement was carried out to accurately account for effects of boundary layer and near wall gradients. As a consequence, the following grid independency was applied at a Re number of 500 with Nu number, maximum temperature, and maximum velocity as the comparison criteria.

Table 4.3 Grid independency

Grid elements	Nusselt number	Maximum temperature (°C)	Maximum velocity (m/s)
13500	4.471	104.3	0.0448
72800	4.523	103.5	0.0447
448800	4.532	103.3	0.0447
3070400	4.436	103.3	0.0447

An extensive mesh refinement was applied to decrease discretization error and improve accuracy. A grid of 72800 elements was chosen with 19, 20, and 50 elements in the radial, azimuthal (tangential) and axial directions. Further mesh improvement did not further resolve physics features and a stable maximum temperature of 103.5°C, Nu number of 4.523, and velocity of 0.0447 m/s was reached at the outlet at a Re number of 500.

4.4 Experimental and Theoretical Validation

Mostly h_{avg} is associated with an average bulk mean temperature but defined in ANSYS as

$$h_{avg} = \frac{q}{T_w - Adjacent\ Wall\ Temperature} \tag{4.6}$$

Adjacent Wall Temperature was defined by setting expert parameter “tbulk for htc”. This sets a locally defined bulk temperature for calculation. The h_{avg} can also be defined as

$$h_{avg} = \frac{1}{L}\int_0^L h(z)dz \tag{4.7}$$

There is excellent agreement of Nu number with empirical correlation of Shah and London [7] shown in Fig. 4.5. The correlation was chosen because of its application in constant wall heat flux laminar forced convection in relatively big diameter (~1-20 mm) pipes.

$$Nu = 3.302(x_*)^{-\frac{1}{3}} - 1 \text{ if } x_* \leq 0.00005 \tag{4.8}$$

$$Nu = 1.302(x_*)^{-\frac{1}{3}} - 0.5 \text{ if } 0.00005 < x* < 0.0015 \tag{4.9}$$

$$Nu = 4.264 + 8.68(10^3 x_*)^{-0.506} e^{-41x_*} \text{ if } x* > 0.001 \tag{4.10}$$

Averaging over pipe length, correlation for average Nu number for entrance region is

$$Nu_{average} = 1.953 * (L_*)^{-\frac{1}{3}} \text{ if } L_* \leq 0.03 \tag{4.11}$$

$$Nu_{average} = 4.364 + 0.0722 * (L_*)^{-1} \text{ if } L_* > 0.03 \tag{4.12}$$

where $L_* = \frac{L}{DRePr}$

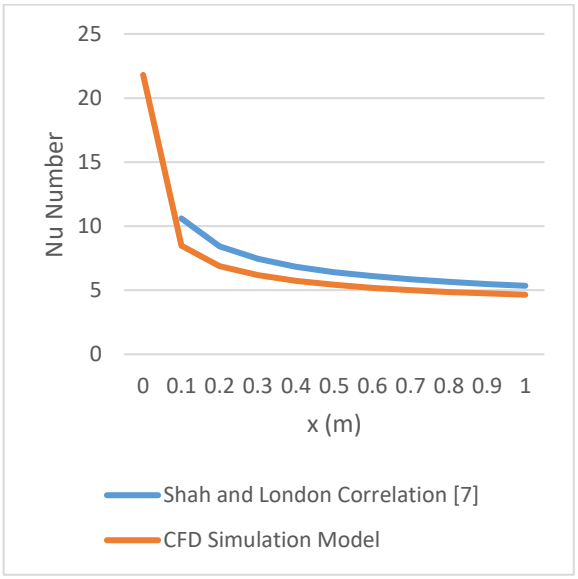

Figure 4.5 CFD model and correlation comparison of Nu number at Re number 500

Summary

Modeling and simulation approach of heat transfer in nanofluids has been presented in this chapter. This chapter covers the complete method to accurately and reliably design and solve a CFD thermal energy analysis for convective laminar steady state heat transfer in closed conduits. Each and every step of the process step is fully described followed by detail explanation.

References

[1] H. K. Versteeg, W. Malalasekera, “An introduction to computational fluid dynamics: the finite volume method,” John Wiley.

[2] B. C. Pak and Y. I. Cho, “Hydrodynamic and heat transfer study of dispersed fluids with submicron metallic oxide particles,” Experimental Heat Transfer, vol. 11, issue 2, pp. 151–170, 1998.

[3] J. C. Maxwell, A Treatise on Electricity and Magnetism, Clarendon Press, Oxford, 1873.

[4] A. Einstein, “A determination of molecular dimensions,” Annals of Physics, vol. 324, issue 2, pp. 289-306, 1906.

[5] H. C. Brinkman, "The viscosity of concentrated suspensions and solutions," Journal of Chemistry Physics, vol. 20, pp. 571-581, 1952.

[6] ANSYS® ANSYS CFX, Release 15.0, Help System, ANSYS Documentation CFX Reference Guide, ANSYS, Inc.

[7] R. K. Shah and A. L. London, “Laminar flow forced convection in ducts,” Advances in Heat Transfer, Academic Press, New York, 1978.

Chapter 5: Single Phase Heat Transfer

The results of CFD numerical analysis are described in detail. These were benchmarked against the geometry of Kim et al. [1]. It was selected as the base case because it had in common the same geometry and dimensions thus, providing an accurate and reliable basis of comparison. The published results of that experimental apparatus were used to validate the modeling and simulation results. Once it was determined that the model is robust, the effect of different characteristic factors of concentration, diameter of nanoparticle, inlet temperature and Re number on thermal efficiency and heat transfer performance (i.e. on characteristics of h and Nu number) was examined in detail. In the following chapters the effect of these on heat transfer as well as fluid flow from a second law of thermodynamics is scrutinized to analyze entropy generation and possible minimization.

5.1 Base Fluid

Base fluid chosen for this study is water. The reason for selecting this particular liquid lies in the many unique properties that favor nanoparticles suspensions. from both an experimental and simulation point of view. These include abundance in nature, medium density, good working temperature for single phase analysis (boiling point of 100°C), high specific heat, and well established correlations that can be extended to nanofluids.

5.1.1 Velocity and Pressure Distribution

Results were validated by comparing them with theoretical calculations and axial centerline velocity increases along the length of the pipe becoming twice that of the average free stream inlet velocity i.e. 0.0446 m/s in fully developed region. The profile consequently becomes parabolic as the boundary layer subtly develops along the wall slows down the fluid there due to viscous effects and pushes the fluid towards the center. Pressure linearly decreases along the length of the pipe to 0 Pa confirming our check on the outlet boundary condition as the pressure difference forces the fluid along the length of the pipe.

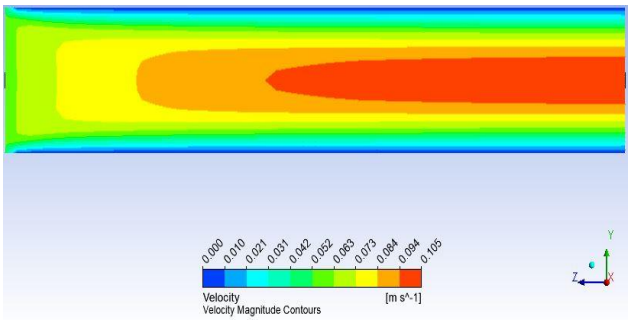

Figure 5.1 Velocity distribution along pipe at an average Re number of 1200

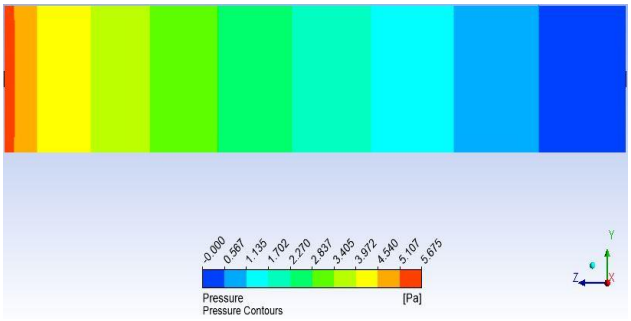

Figure 5.2 Pressure distribution along pipe at an average Re number of 1200

5.1.2 Temperature Distribution

The temperature varies along the radial direction in a way that maximum temperature occurs along the wall due to impingement of heat flux. The thermal boundary layer is subtler as compared to velocity due to the nature of terms in the energy equation of governing equations. Maximum heat transfer takes place at the end of the pipe where a maximum wall temperature of 77.8°C occurs at the wall.

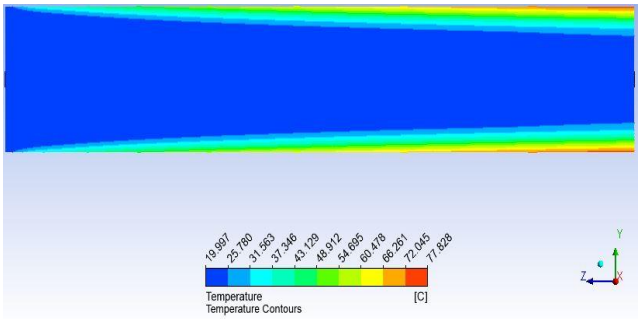

Figure 5.3 Temperature distribution along pipe at an average Re number of 1200

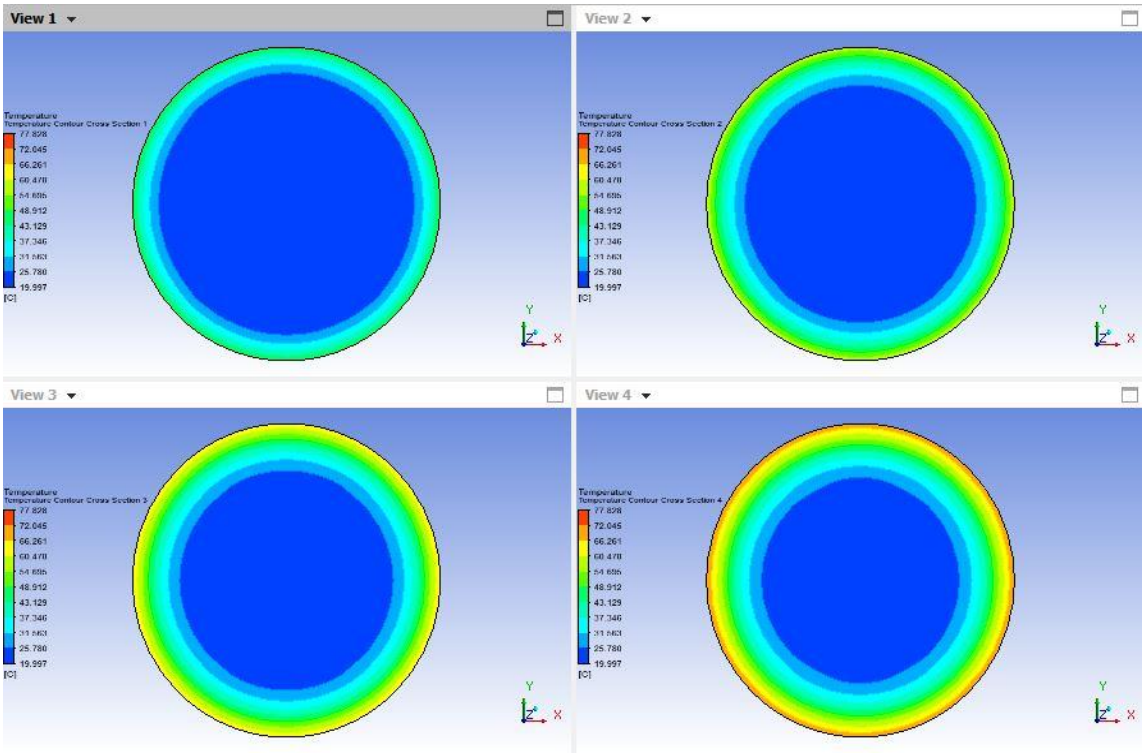

Figure 5.4 Cross section temperatures at an average Re number of 1200 at distances of 0.2 m (top left), 0.4 m (top right), 0.6 m (bottom left), and 0.8 m (bottom right) from inlet

5.2 Nanofluid

5.2.1 Velocity and Pressure Distribution

As the fluid enters the pipe the boundary layer in entrance region pushes fluid towards central position increasing its velocity and consequently try to develop a uniform velocity at the center as a result of conservation of flow and mass. The velocity is marginally decreased due to presence of nanoparticles as density and viscosity is increased by a very small amount. Velocity and pressure distribution of CuO-water nanofluid is similar to that of Al_2O_3-water nanofluid. Higher density of CuO hinders development of velocity boundary layers thus a lower centerline velocity of 0.097 m/s is achieved at the outlet. This decrease is minor as compared to other nanofluid but may be significant at higher concentration and Re number. Parabolic velocity profile along with centerline velocity of Al_2O_3-water and CuO-water nanofluids is shown in Fig. 5.5.

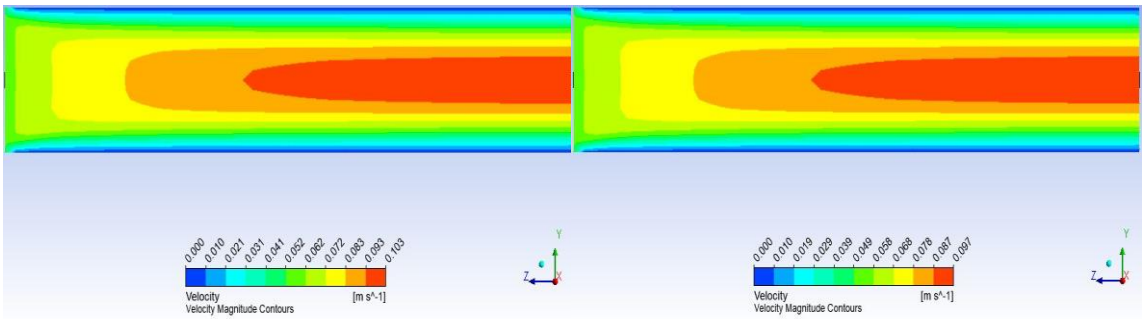

Figure 5.5 Velocity distribution of Al_2O_3-water nanofluid (left) and CuO-water nanofluid (right) along length of the pipe at an average concentration of 3% and an average Re number of 1200

Unlike sharp velocity gradients at the wall the pressure remains almost constant throughout different sections of the pipe respectively. Despite this characteristic the pressure of a nanofluid is distinct as compared to base fluid in Fig. 5.2 and the pressure is 6.132% higher at the inlet. Moreover, throughout a cross section the pressure remains constant as well along a certain length of the pipe which increases with distance along the pipe. For CuO, pressure difference is relatively higher because of direct influence of concentration and density. It is clear at the inlet where pressure of Al_2O_3-water nanofluid is 6.526% higher than CuO-water nanofluid. Viscosity of nanofluids cause a change in pressure drop of nanofluids but as its correlation used is not temperature dependent there is not much of a difference between the two nanofluids at same inlet temperature and Re number. Pressure map of Al_2O_3-water and CuO-water nanofluids is shown in Fig. 5.6.

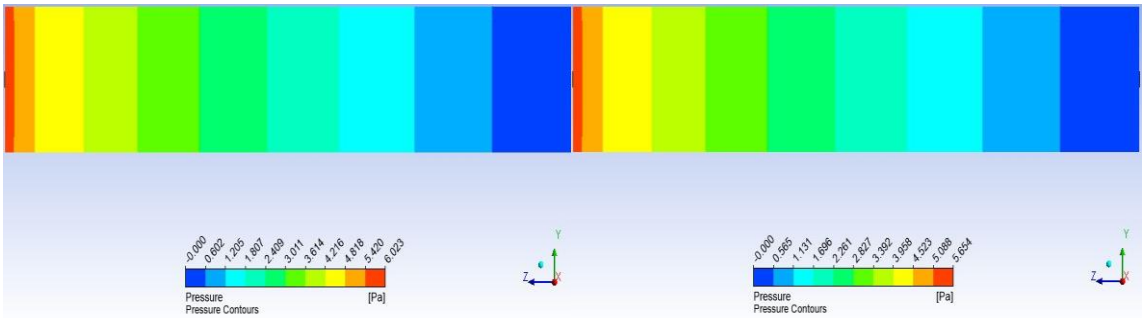

Figure 5.6 Pressure distribution of Al_2O_3-wawater nanofluid (top) and CuO-water (bottom) long length of the pipe at an average concentration of 3% and an average Re number of 1200

5.2.2 Temperature Distribution

With the introduction of nanofluid in base fluid the Nu number decreases in the laminar flow regime. Nu number approaches 4.364 as the grid is refined at the end of the pipe validating hand calculations. The wall temperature decreases when the fluid is changed from base fluid to nanofluid as shown in Fig. 5.7. A consequence of the combination of constant wall heat flux boundary condition and higher thermal conductivity of nanoparticle, it leads in CuO-water nanofluid a continuous increase in bulk wall temperature along the length of the pipe once again confirming the combined entrance transitional length of the problem. For any cross section, the nanofluid temperature increases from center to the wall. Highest temperature increases along the axial length unlike the velocity profile that fully develops approximately at the mid of the pipe.

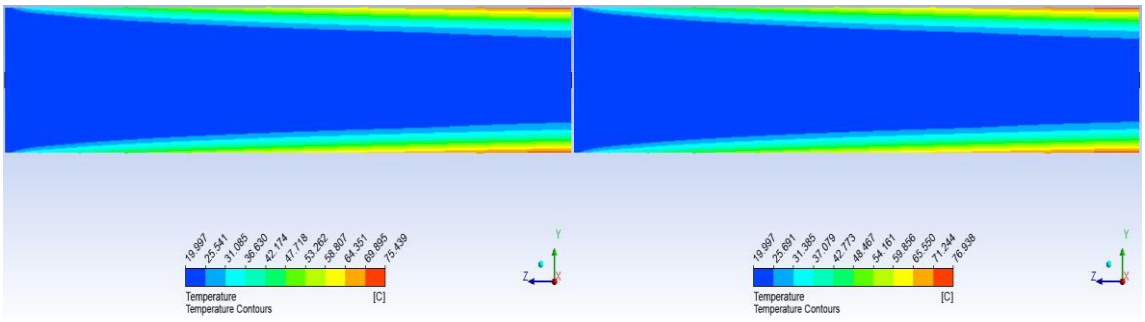

Figure 5.7 Temperature distribution of Al_2O_3-water nanofluid (left) and CuO-water nanofluid (right) along length of pipe at an average concentration of 3% and an average Re number of 1200

As the velocities have been kept the same for both the base fluid and nanofluid there is a slight increase of around 2.5°C. Increasing the concentration to 3% the boundary layer development is more pronounced as more fluid volume is heated leading to lower wall temperature as more heat has been transferred leading to a higher h value. It is also the reason why most heat transfer occurs early near inlet and evident in a comparison of Fig. 5.3 and Fig. 5.8 (bottom right).

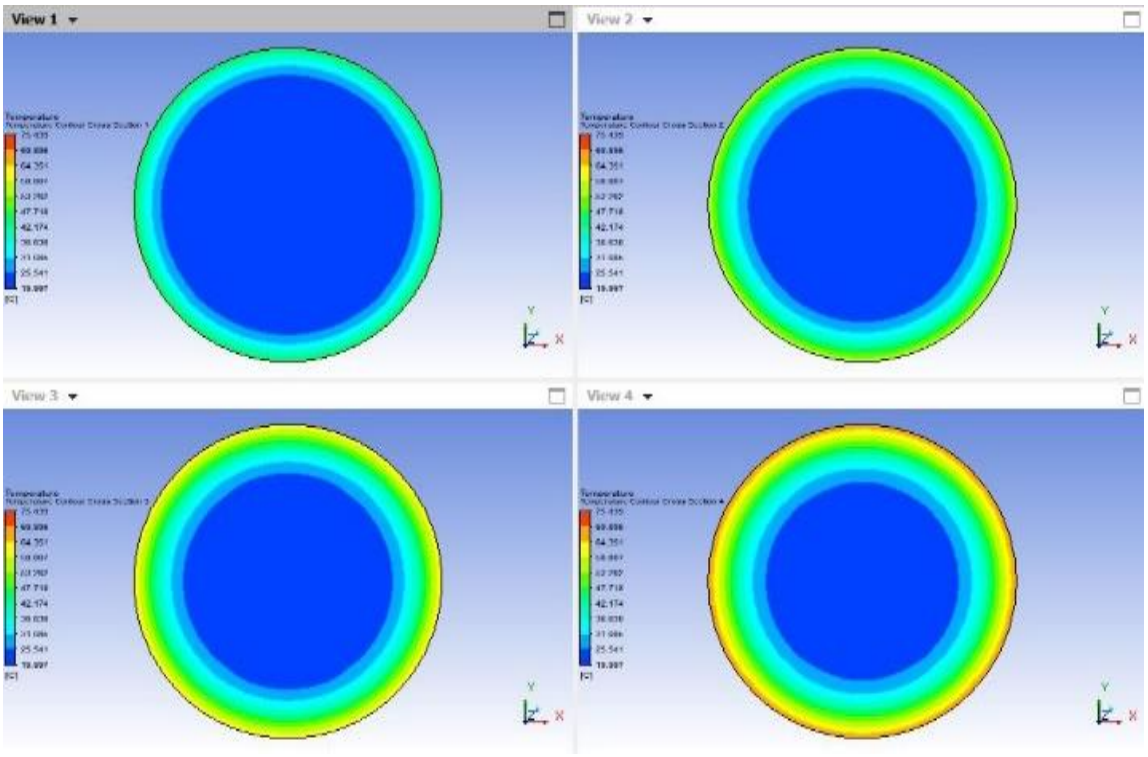

Figure 5.8 Cross section temperatures of Al_2O_3-water nanofluid at an average concentration of 3% and an average Re number of 1200 at distances of 0.2 m (top left), 0.4 m (top right), 0.6 m (bottom left), and 0.8 m (bottom right) from inlet

5.2.3 Effect of Axial Length

Performance factor evaluated is local HTC and defined when defining Nu number. Increasing axial length causes h to continuously decrease for constant properties model because most heat is convectively transferred in entrance area. Along the length of the pipe HTC remains almost equal for the two nanofluids as shown in Fig. 5.10 because HTC is dependent only on local wall temperature and local bulk temperature. As wall temperature increases so does bulk temperature but wall temperature increases sharply than bulk temperature at entrance and HTC consequently decreases. Beyond the entrance region it remains constant along the length of pipe. For CuO-water nanofluid despite having lower thermal conductivity and higher density, HTC doesn't change much. CuO-water nanofluid has lower heat transfer due to disturbance of thermal boundary layers.

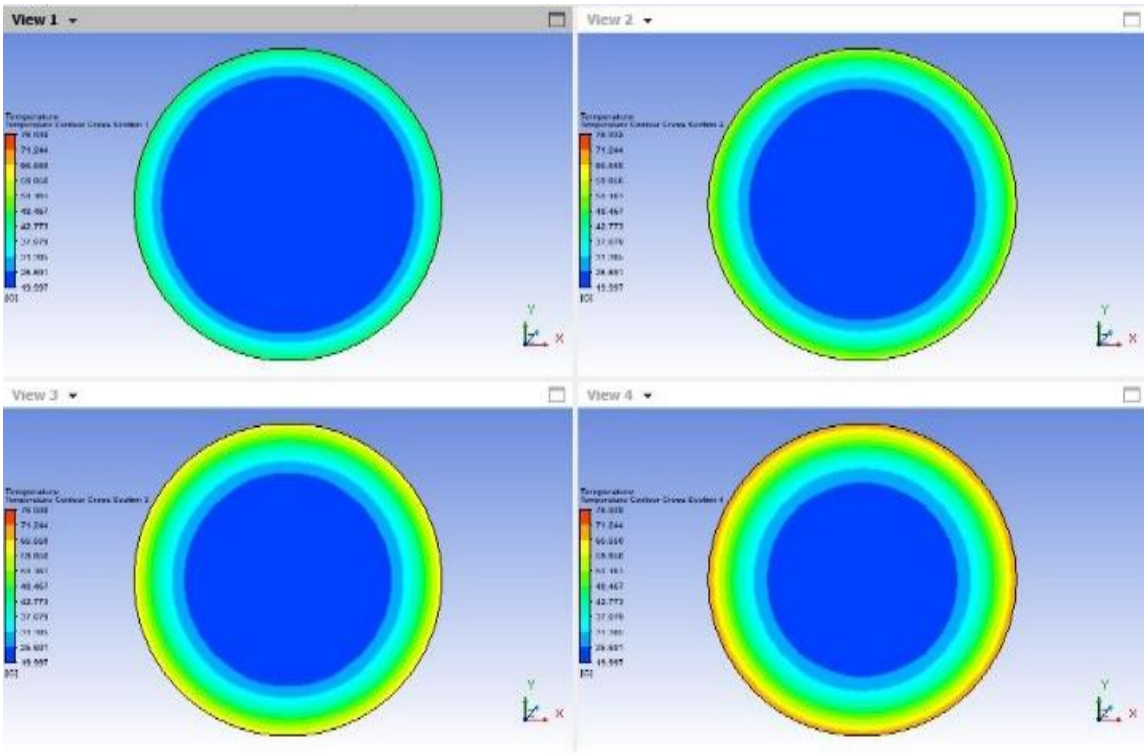

Figure 5.9 Cross section temperatures of CuO-water nanofluid at an average concentration of 3% and an average Re number of 1200 at distances of 0.2 m (top left), 0.4 m (top right), 0.6 m (bottom left), and 0.8 m (bottom right) from inlet

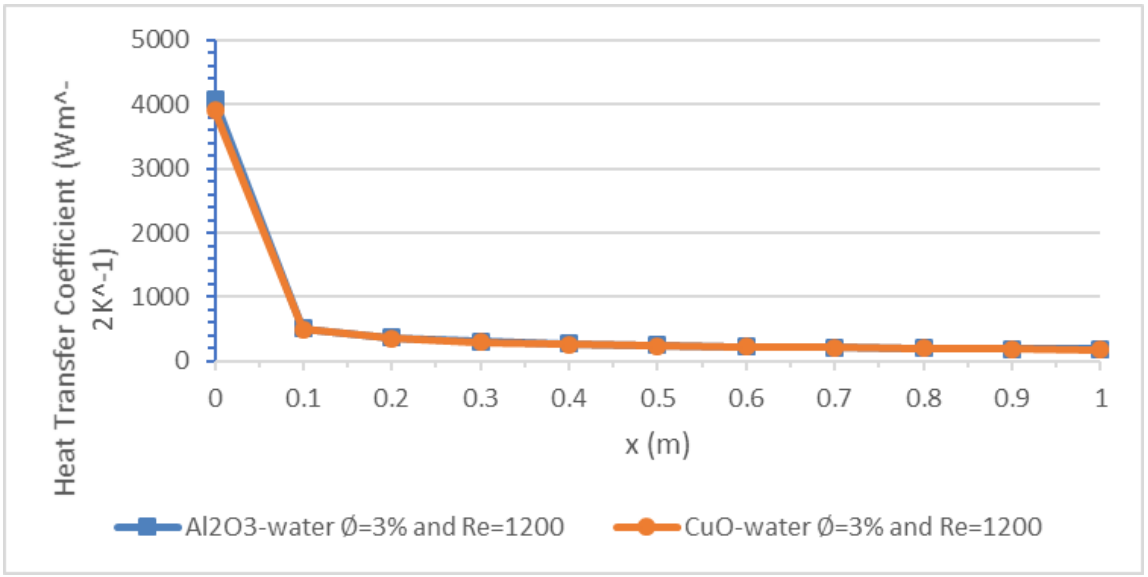

Figure 5.10 Equal axial length comparison of nanofluids

5.2.4 Effect of Concentration

At the same concentration Al_2O_3-water nanofluid exhibits a higher value of h_{avg} than CuO-water nanofluid. At concentration of 1% or 0.01, h_{avg} enhancement of Al_2O_3-water nanofluid is 1.354% whereas theoretical enhancement is 1.644% (Shah averaged correlation) compared to base fluid. This difference increases explicitly for higher values of concentration with values of 2.257% and 4.613% at a concentration of 5%. Again, higher thermal conductivity of Al_2O_3 is attributed for considerably high values. Similarly, for CuO-water nanofluid it is 0.3511% whereas theoretical enhancement is 0.8406% and increases with concentration with values of 2.257% and 4.613% at a concentration of 5%. Concentration marks largest difference between the values as it directly affects the fluid as shown in Fig. 5.11.

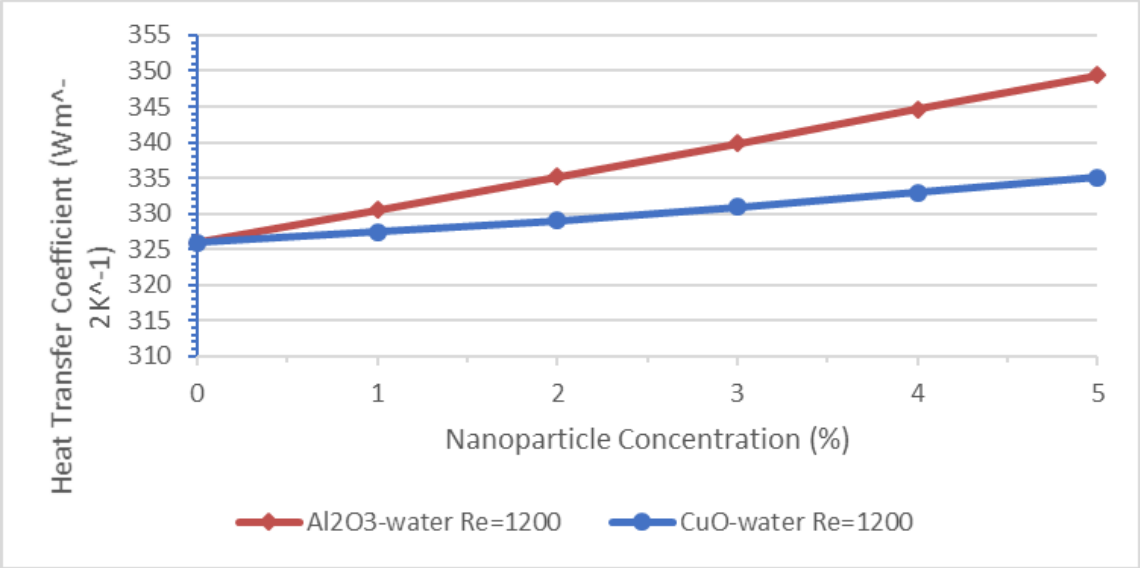

Figure 5.11 Equal concentration comparison of nanofluids

5.2.5 Effect of Diameter

Changing the diameter of nanoparticle inversely influences h i.e. increasing diameter decreases h. This may be due to effects such as Brownian motion, nanolayer thickness, and dispersion. Correlation of Khanafer and Vafai [2] was used.

$$(k_{eff})_{nf} = (1 + 1.0112\emptyset + 2.4375\emptyset\left(\frac{47}{d}\right) - 0.0248(\frac{k_p}{0.613}))k_f \quad (5.1)$$

For same size of nanoparticles, CuO-water nanofluids has a distinctively less impact on

h_{avg} as compared to Al_2O_3-water nanofluids even though it has a lower thermal conductivity which should give a relatively high value of h_{avg} as increase in d outweighs impact of lower thermal conductivity. Nanolayer for lower thermal conductivity may influence effect of diameter with a h_{avg} decrease of 8.076% for d value from 20 to 100 nm. A comparison reveals effect of diameter in Fig. 5.12. Increasing size decreases nanofluid temperature which is more in case of CuO-water nanofluid. This decrease is due to high density and lower thermal conductivity of CuO that decreases heat transfer. Interesting to note is that both nanofluids have exactly same trend and consequently same difference with Al_2O_3-water nanofluids having 1.724% higher values.

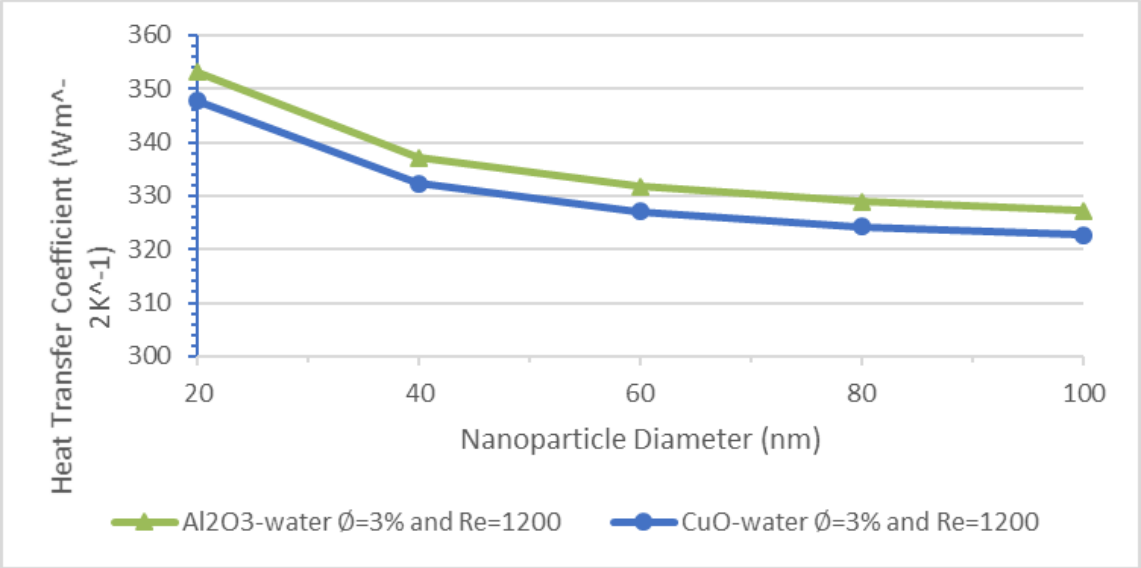

Figure 5.12 Equal diameter comparison of nanofluids

5.2.6 Effect of Inlet Temperature

Amount of heat transferred from the wall to the bulk of wall boundary condition being constant, increasing inlet temperature decreases h as differential between wall and bulk temperature increases. This effect is enhanced for nanofluids as outlet wall temperature decreases with concentration. A low-medium optimum temperature would be required to get a higher of h. Trend can be seen in Fig. 5.13.

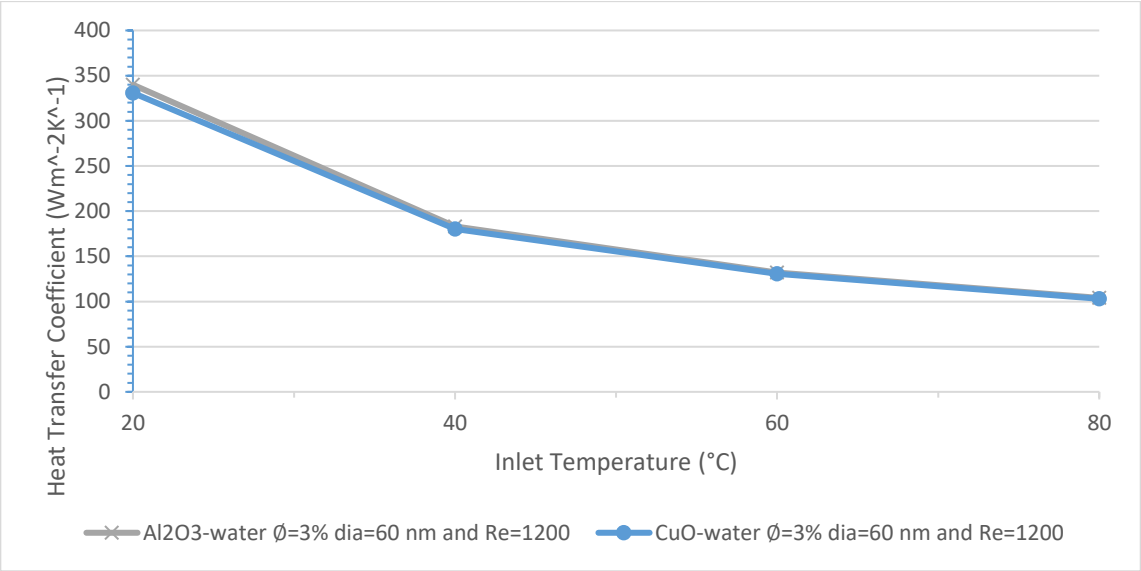

Figure 5.13 Equal inlet temperature comparison of nanofluids

5.2.7 Effect of Re Number

In reality, Re number of a fluid changes with time along pipe. Increasing Re number increases heat transfer from wall to the bulk of the nanofluid with higher Re number having a higher h and is a manifestation of an increase in velocity and possible increase of wall temperatures. At same Re numbers, same velocities are chosen to get different enhancements ratios for the two fluids. As seen in Fig. 5.14 Al_2O_3-water nanofluid gives a higher heat transfer enhancement than CuO-water. This is because of much higher thermal conductivity and lower specific heat capacity as compared to CuO-water nanofluid. Increasing Re number increases the turbulence effects in the fluid enabling better mixing of the nanoparticles with the base fluid. Re number has the highest effect on efficiency and performance of circular pipe in transferring heat to nanofluids. In fact, inclusion of d under predicts h_{avg} at the same inlet temperature. The effect of Re number for CuO-water nanofluids is increased as the highest temperature achieved is around 76.94°C as compared to 75.44°C for Al_2O_3-water. Higher wall temperatures occur due to lower thermal conductivity and cause h_{avg} to be less than Al_2O_3-water nanofluid.

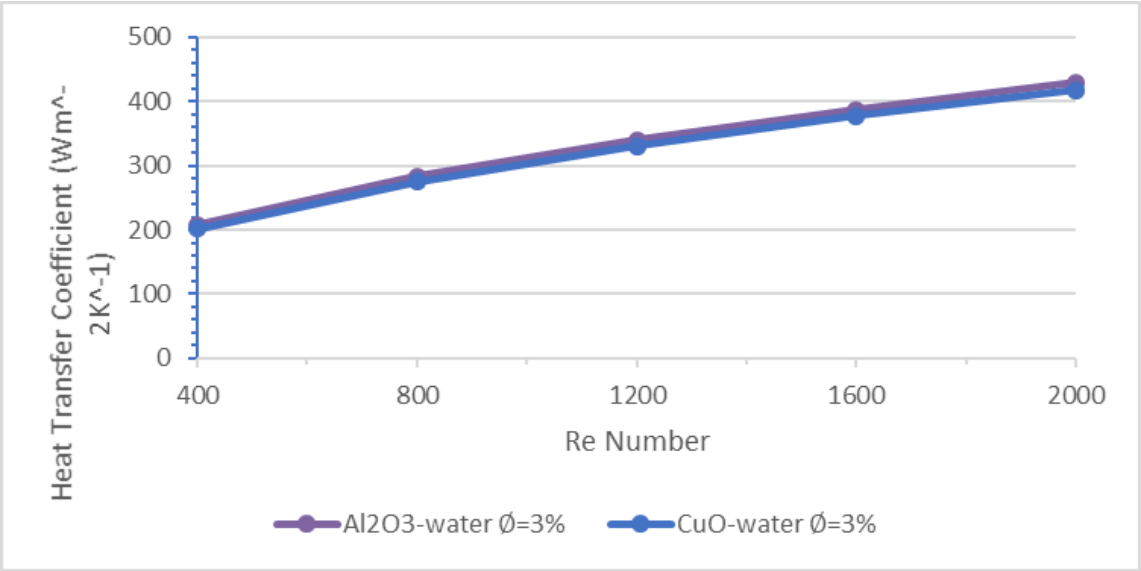

Figure 5.14 Equal Re number comparison of nanofluids

Summary

A CFD modeling and simulation analysis of single phase heat transfer of nanofluids has been presented in this chapter. Base fluid water has been selected because of its advantageous and unique properties. The correlations used for approximating thermophysical properties of nanofluids had been discussed and explained in the previous chapter. Full description and behavior of base fluid and nanofluid heat transfer and fluid flow field in the form of pressure, velocity, and temperature distribution has been provided. The insights reveal that density and viscosity have a slight effect on pressure and velocity fields at low concentrations and Re number whereas thermal conductivity effects thermal boundary layer in temperature maps. To highlight the importance of this phenomenon both longitudinal and cross sectional maps are given.

The second half of the chapter deals with the effects of characteristic factors of axial length, concentration of particle, diameter of particle, inlet temperature, and Re number on heat transfer by investigating the behavior of HTC. The HTC increases with increase in concentration and Re number and decreases with axial length, diameter and inlet temperature. Thermal conductivity increase has been identified as the responsible mechanism for increasing heat transfer and is also the strongest factor among all. Increase

in velocity and HTC is determined to be the reason for increased HTC with increase in Re number. Local HTC decreases along direction of pipe as wall temperature increases sharply than bulk fluid temperature. Diameter and inlet temperature have an inverse relationship with heat transfer due to irreversibility discussed in Chapter 7.

References

[1] D. Kim et al., “Convective heat transfer characteristics of nanofluids under laminar and turbulent flow conditions,” Current Applied Physics, vol. 9, issue 2, pp. 119–123, 2009.

[2] K. Khanafer and K. Vafai, “A critical synthesis of thermophysical characteristics of nanofluids,” International Journal of Heat and Mass Transfer, vol. 54, issues 19-20, pp. 4410–4448, 2011.

Chapter 6: Two Phase Heat Transfer

The accuracy of the assumption of treating nanofluid as a homogeneous fluid can be determined by estimating amount of difference in temperature and velocity between the phases and the concentration distribution. The multiphase model that gives best and more uniform distribution of concentration for a large range of concentrations and types of particles determines whether there is a negligible amount of slip and the suitability of homogeneous model. This is a consequence of the interphase transfer rate being very large. As concentration of particles is small only the carrier phase influences the dynamics of dispersed phase in one-way coupling. Here too, the effect of different characteristic factors on fluid flow and heat transfer performance (i.e. on characteristics of h and Nu number) has been examined in detail.

6.1 Eulerian Eulerian Two Phase Model

6.1.1 Velocity and Pressure Distribution

The velocity profiles remain the same as the dilute concentration of nanoparticles does not control the flow field of the base fluid. Axial velocity at the tube center increases while velocity gradient at the wall decreases with increasing axial position until x=0.5 m where flow is almost fully developed. There is no slip between fluid and particle phases and velocities are almost equal. Velocity of nanofluid is shown in Fig. 6.1.

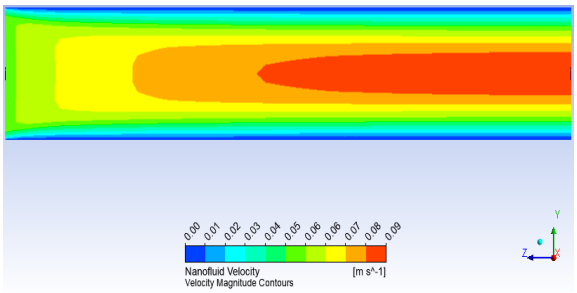

Figure 6.1 Velocity distribution of two phase nanofluid along length of the pipe at an average concentration of 3% and an average Re number of 1200

Interestingly, the pressure drop is not the same in two phase flow as in single phase flow. In fact, it is the complete opposite. There is a pressure drop of 1.339% compared to base

fluid at the inlet. Unlike sharp velocity gradients at wall, pressure remains almost constant in different sections of pipe and along a certain length of pipe which increases with distance along pipe. Pressure map of two phase nanofluid is shown in Fig. 6.2.

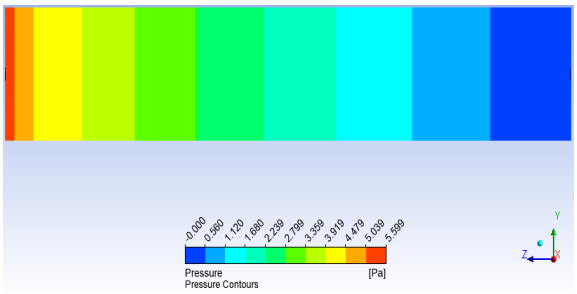

Figure 6.2 Pressure distribution of two phase nanofluid along length of the pipe at an average concentration of 3% and an average Re number of 1200

6.1.2 Temperature Distribution

For the two phase model, the nanofluid exhibits a much smaller average bulk temperature. At 0.2 m the bulk temperature increases by 16°C from 20°C at the center of pipe to 36°C at the wall. This temperature increases along the length and at 0.8 m the temperature increases by 30°C from 20.19°C to 49.21°C. The temperatures further increase along the length of pipe. Introduction of a separate phase for particles stabilize the mixture more uniformly. Increasing concentration to 3%, enhances boundary layer development as more fluid volume is heated leading to lower wall temperature and higher h value. Temperature maps of two phase nanofluids are shown in figures below.

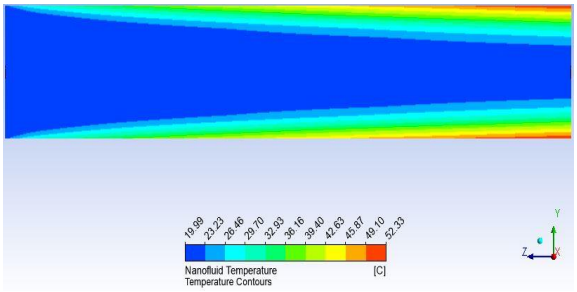

Figure 6.3 Temperature distribution of two phase nanofluid along length of pipe at an average concentration of 3% and an average Re number of 1200

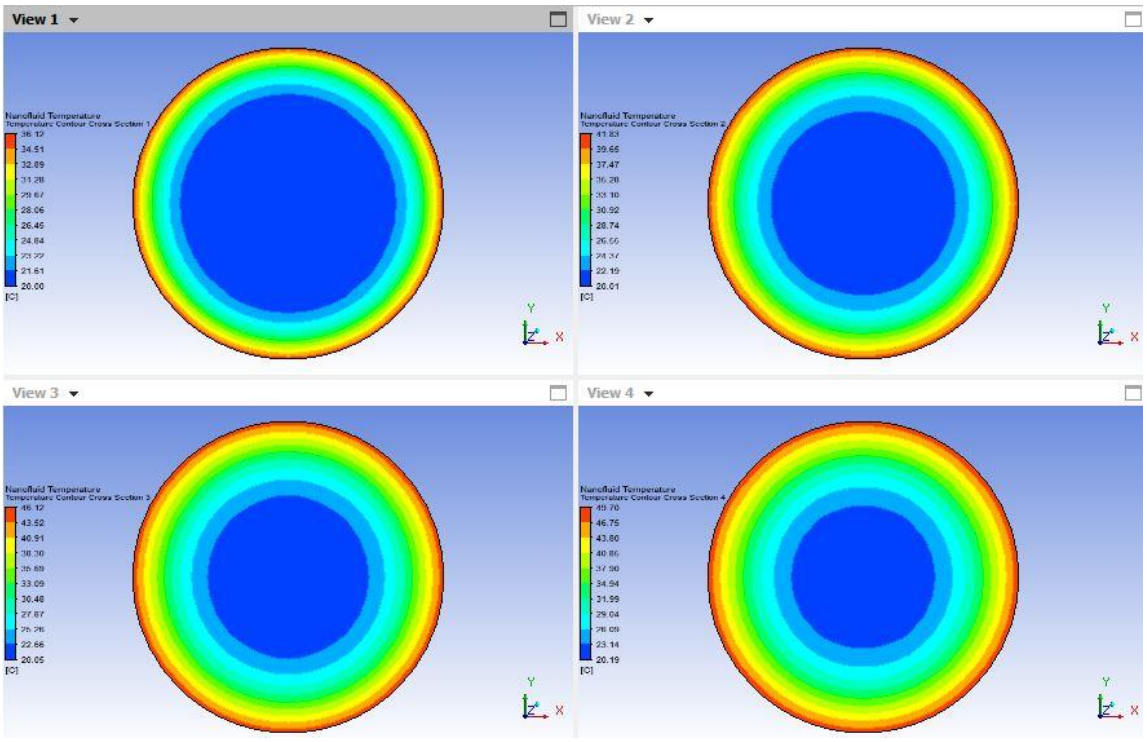

Figure 6.4 Temperature of two phase nanofluid at average concentration of 3% and Re number of 1200 at 0.2 m, 0.4 m, 0.6 m, and 0.8 m (clockwise from top left) from inlet

6.1.3 Effect of Axial Length

For two phase flow, heat transfer enhancements are more noticeable in the thermally developing region. Local HTC enhancement ratio (h_{eff}/h_{bf}) increases rapidly along the length of pipe and becomes constant after passing the entrance region. A maximum enhancement of almost 70% was observed. A part of it may be due to anomalous heat transfer and a better estimate of comparison might be at the same Pe number. But despite that fact, it is more than twice that of single phase fluid. An interesting trend occurs i.e. the local h_{eff}/h_{bf} decreases after crossing more than half the length of pipe. This is due to little pockets of particles aggregation that increases the temperature of fluid as compared to the wall causing local h to decrease. But this decrease is insignificant. The effect of axial length on local h_{eff}/h_{bf} is shown in Fig. 6.5.

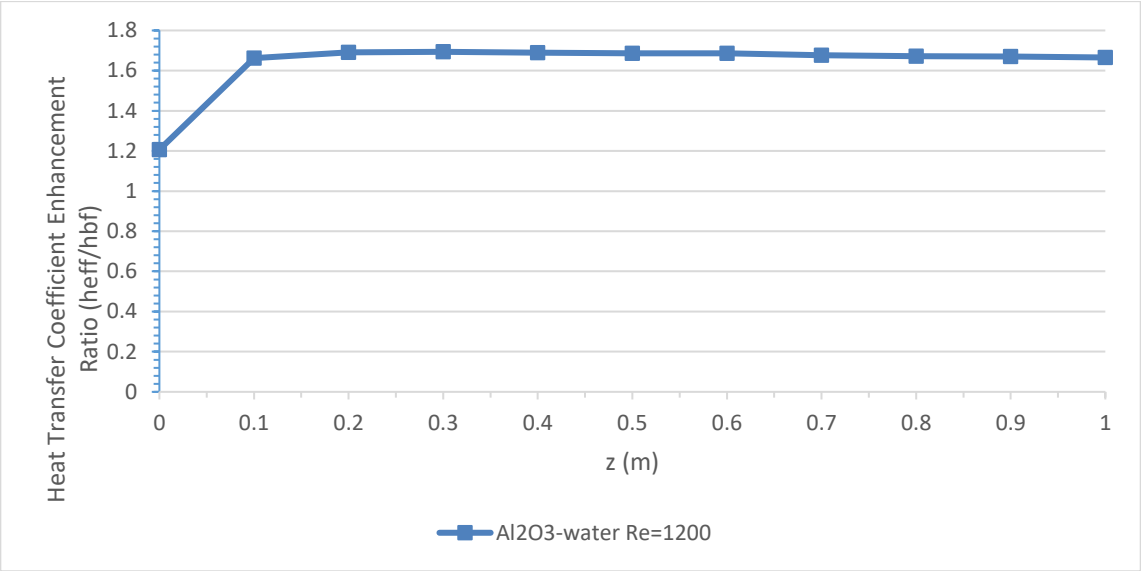

Figure 6.5 Axial variation of HTC enhancement ratio of nanofluid

6.1.4 Effect of Concentration

Nanofluid with small nanoparticles aggregates or concentration has higher ability for heat transfer. The effect of enhancement by smaller nanoparticle aggregates is more obvious at lower Reynolds number. At concentration of 1% or 0.01, h_{avg} enhancement of Al_2O_3-water nanofluid is 27.92% compared to base fluid. This difference increases explicitly for higher values of concentration with values of 70.48% at a concentration of 3%. Anomalous heat transfer is caused by relatively low concentration near wall as it creates there a comparatively low viscosity field generating high velocity and sharp temperature gradient. The linear portion is attributed to thermal conductivity linearly increases with concentration in static model of Maxwell. The trend is not perfectly linear and h_{avg} increases sharply at lower concentrations. The effect is shown in Fig. 6.6.

6.1.5 Effect of Inlet Temperature

As temperature distribution is not close to fully developed for high temperatures than for lower temperatures as compared to velocity profile along with the fact that amount of heat transferred from the wall to the bulk of fluid is constant, increasing inlet temperature decreases h as differential between wall and bulk temperature increases. Multiphase nature promotes mixing that sharply decreases HTC as shown in Fig. 6.7.

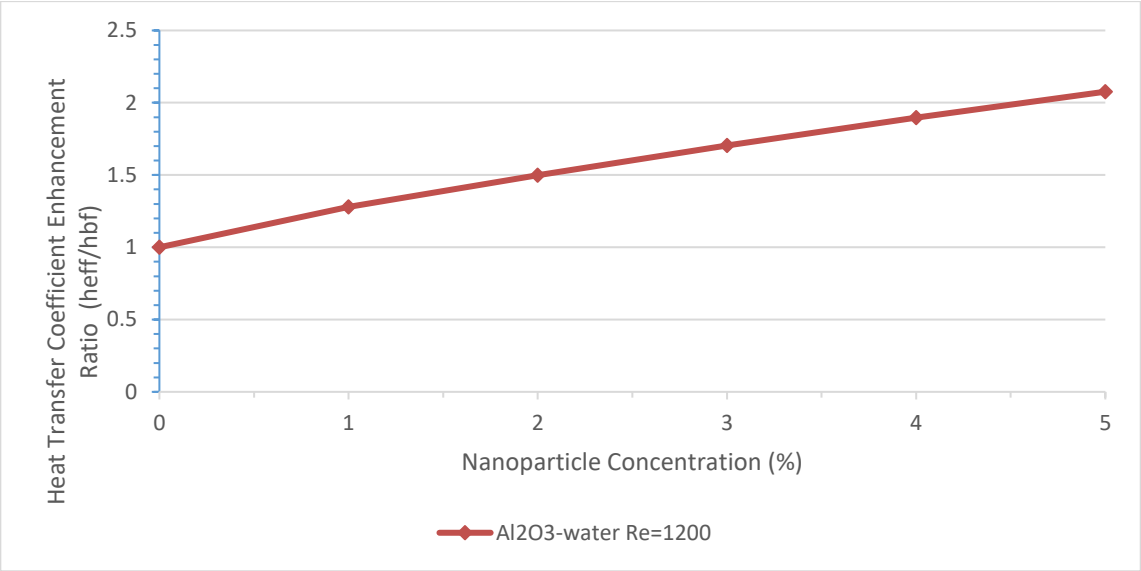

Figure 6.6 Effect of concentration on HTC ratio of nanofluid

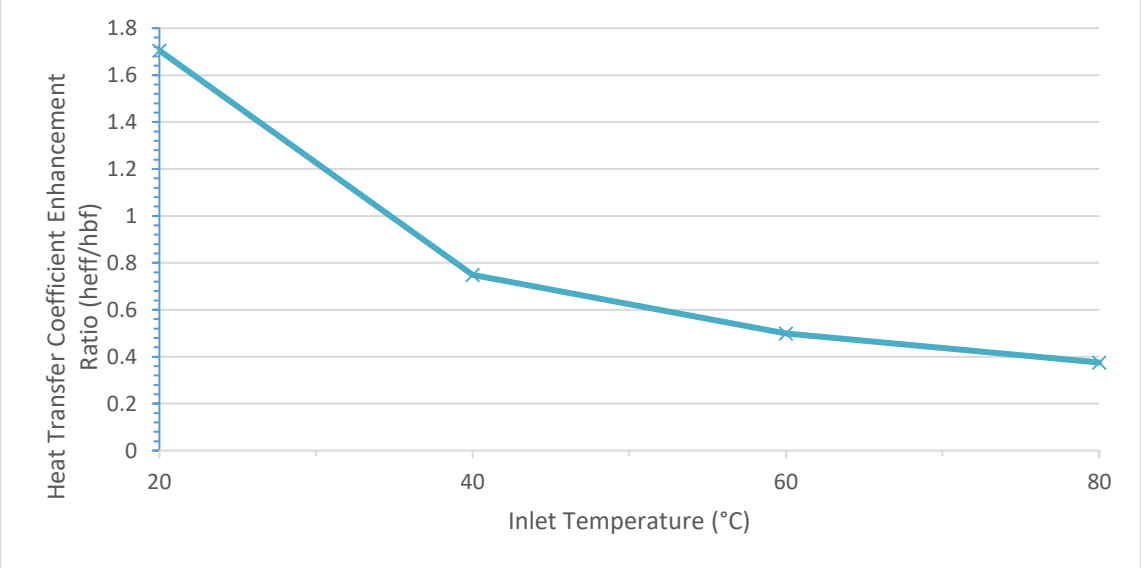

Figure 6.7 Effect of inlet temperature on HTC ratio of nanofluid

6.1.6 Effect of Re Number

The differences between predictions by the single-phase and two-phase models decrease as the Reynolds number increases but they remain significant in the case of temperature profiles. In multiphase flow, changing Re numbers by the same amount increases the wall temperature much more quickly than in single phase nanofluid. This cause sharp variations in temperature gradients and increase HTC tremendously [1]. At same Re

numbers, same velocities are chosen to get different enhancements ratios for the two fluids. Increasing Re number increases the turbulence effects in the fluid enabling better mixing of the nanoparticles with the base fluid. Re number has the highest effect on efficiency and performance of circular pipe in transferring heat to nanofluids. The effect of Re number on two phase nanofluid HTC is shown in Fig. 6.8.

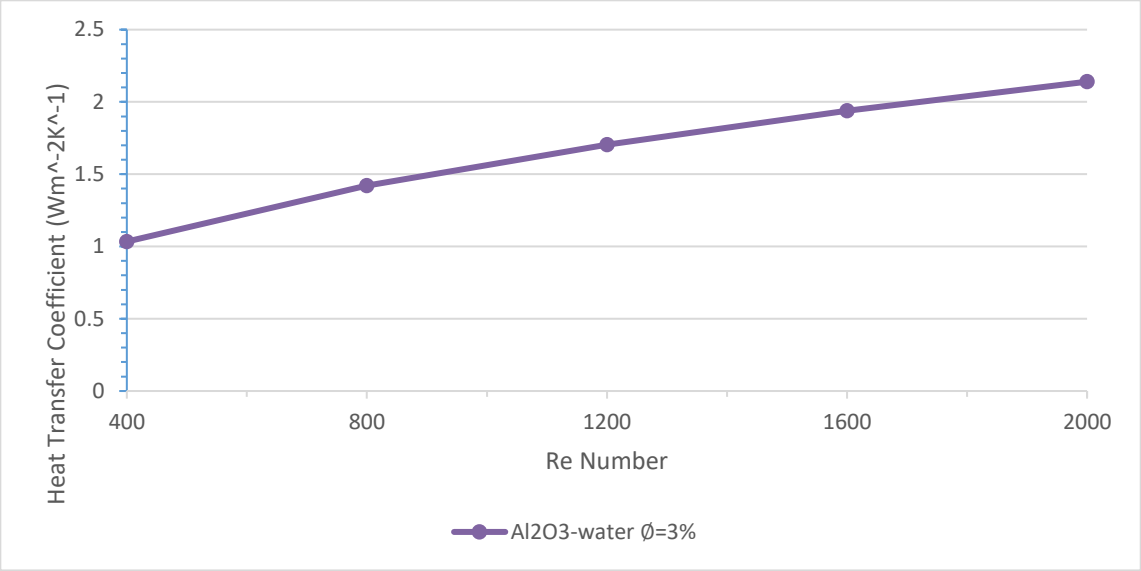

Figure 6.8 Effect of Re number on HTC ratio of nanofluid

Summary

The predictions of nanofluids by Eulerian Eulerian two phase fluid flow and heat transfer model were presented the same. The model overestimate convective HTC for equal range of axial length, concentration, inlet temperature, and Re number compared to the empirical correlations and experimental data than the single-phase model. Hydrodynamic field is almost same but thermal field is very different.

References

[1] S. Tahir and M. Mital, Numerical investigation of laminar nanofluid developing flow and heat transfer in a circular channel, vol. 39, issue , pp. 8–14, 2012.

Chapter 7: Entropy Generation

This research focuses on minimization of generated entropy in metal oxide Al_2O_3-water nanofluid due to the fact of getting higher heat transfer in the entrance region of conduits may come at the cost of increased viscous dissipation. The objective of this work is to understand the effect of axial length, concentration of particle (1-5%), diameter of particle (20-100 nm), inlet temperature (20-80 °C), and Re number (400-2000) on characteristic parameters of pressure drop and entropy generation in a pipe of length 1 m and diameter 20 mm. A constant wall heat flux boundary condition, laminar flow regime, single phase modeling, and steady state analysis is employed. The results presented are based on average values of inlet temperature of 60°C, nanoparticle concentration of 3%, diameter of 60 nm, and Re number of 1200 respectively.

7.1 Entropy Distribution

For circular convective flow pipe of constant wall heat flux, total entropy generation rate per unit length is defined as [1]

$$\dot{S}'_{gen=}(\dot{S}'_{gen})_{heat\ transfer} + (\dot{S}'_{gen})_{fluid\ flow} \tag{7.1}$$

where $(\dot{S}'_{gen})_{heat\ transfer} = \frac{q\pi D^2}{kT_{ave}^2 Nu(Re,Pr)}$ is the entropy generation due to heat transfer,

$(\dot{S}'_{gen})_{heat\ transfer} = \frac{32\dot{m}^3 f(Re)}{\pi^2\rho^2 T_{ave} D^5}$ is the entropy generation due to fluid flow,

$\dot{m} = \rho AV$ is the mass flow rate, and

$A = \pi R^2$ is the cross sectional area of pipe.

The pressure drop is defined as [2]

$$\Delta P = \frac{f\rho V^2 z}{2D} \tag{7.2}$$

The above approach requires use of correlations h and/or Nu number and pumping power and/f as momentum and energy equations are not solved and deals with total entropy generation rather than local entropy production. If the Darcy friction factor is desired to be used in place of Fanning friction factor, the 32 in second term is replaced by 8 but the final form for developed flow turns out to be the same. Average values of shear, temperature, and velocity were used.

In the second approach, total entropy generation per unit volume is calculated by calculation of momentum and energy equations and using the heat and flow field gradients.

$$\dot{S}'''_{gen=}(\dot{S}'''_{gen})_{heat\ transfer} + (\dot{S}'''_{gen})_{fluid\ flow} \tag{7.3}$$

where $(\dot{S}'''_{gen})_{heat\ transfer} = \frac{k}{T_{ave}^2}((\frac{\partial T_{ave}}{\partial x})^2 + (\frac{\partial T_{ave}}{\partial y})^2 + (\frac{\partial T_{ave}}{\partial z})^2)$ is the entropy generation due to heat transfer,

$$(\dot{S}'''_{gen})_{fluid\ flow} = \frac{\mu}{T_{ave}}(2\left(\left(\frac{\partial u}{\partial x}\right)^2 + \left(\frac{\partial v}{\partial y}\right)^2 + \left(\frac{\partial w}{\partial z}\right)^2\right) + \left(\frac{\partial u}{\partial y} + \frac{\partial v}{\partial x}\right)^2 + \left(\frac{\partial u}{\partial z} + \frac{\partial w}{\partial x}\right)^2 + \left(\frac{\partial v}{\partial z} + \frac{\partial w}{\partial y}\right)^2)$$ is the entropy generation due to fluid flow.

The Bejan number is defined as [1]

$$Be = \frac{(\dot{S}'''_{gen})_{heat\ transfer}}{\dot{S}'''_{gen}} \tag{7.4}$$

For Be number greater than 0.5, the heat transfer irreversibility dominates, for Be number less than 0.5 the fluid flow irreversibility dominates. For Be equal to 0.5, the effect of heat transfer on entropy is equal to the effect of fluid flow on entropy. It can be seen in Fig. 7.1 that near the walls, where greater velocity gradients exist, the friction entropy generation is maximum and it decreases to zero by approaching to the centerline because of the zero gradient boundary condition of velocity on the axis of the pipe. Moreover, it can be seen that there is some friction entropy generation due to inlet effects near the inlet region.

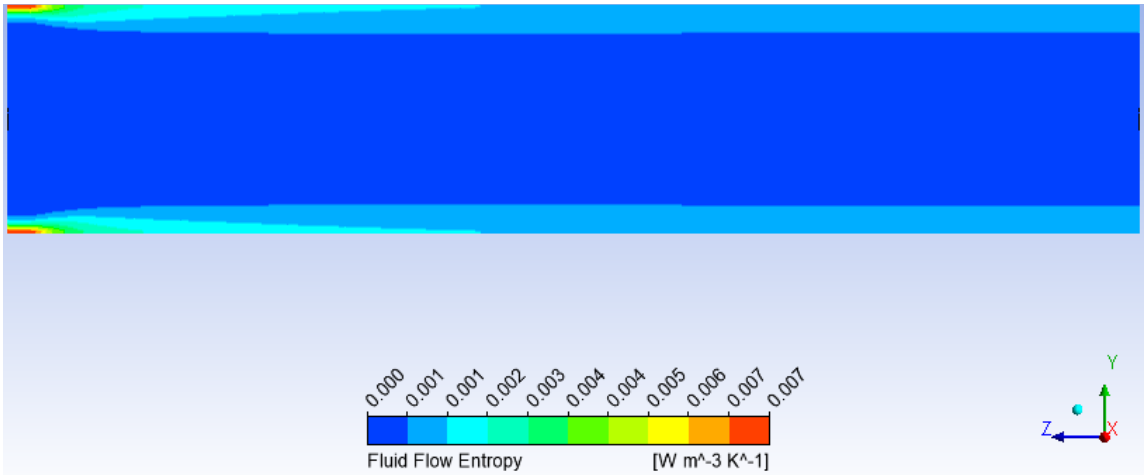

Figure 7.1 Fluid flow entropy distribution of Al_2O_3-water nanofluid along pipe at an average concentration of 3%, diameter of 20 nm, inlet temperature of 60°C, and Re number of 1200

The heat transfer entropy generation (as depicted in Fig. 7.2) is maximum near the constant heat flux walls where greater temperature gradients persist. Since the Pr number is greater than unity for water, the thermal boundary layer does not grow as fast as the hydrodynamic boundary layer. So, the zero thermal entropy generation region near the axis is larger than the zero friction (fluid flow) entropy generation region.

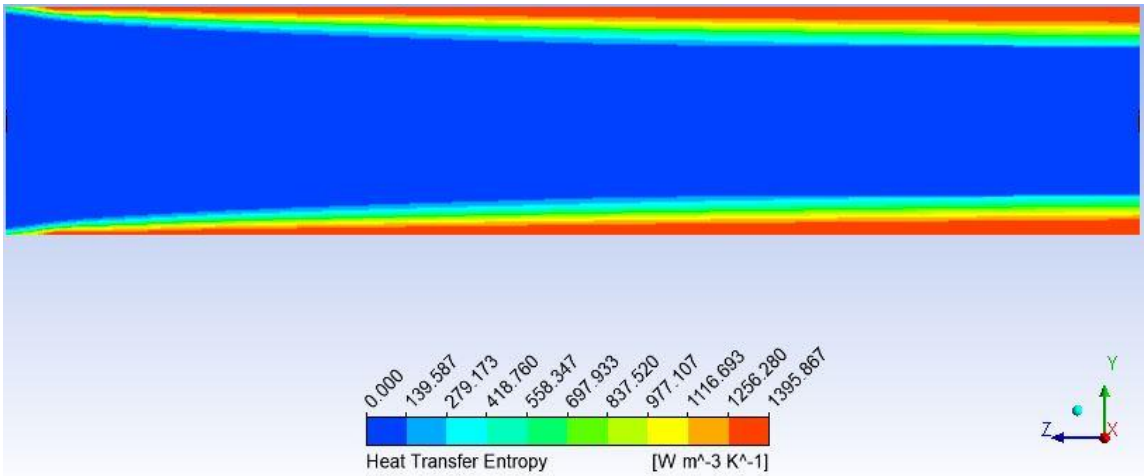

Figure 7.2 Heat transfer entropy distribution of Al_2O_3-water nanofluid along pipe at an average concentration of 3%, diameter of 20 nm, inlet temperature of 60°C, and Re number of 1200

Heat transfer entropy dominates entropy generation as velocity gradients are relatively small in the laminar regime. Near the wall, where heat transfer entropy is six orders of magnitude greater than fluid flow entropy, total entropy is affected mostly by the former. On the other hand, near centerline, total entropy is affected by fluid flow entropy because the thermal boundary layer is smaller than hydrodynamic boundary layer.

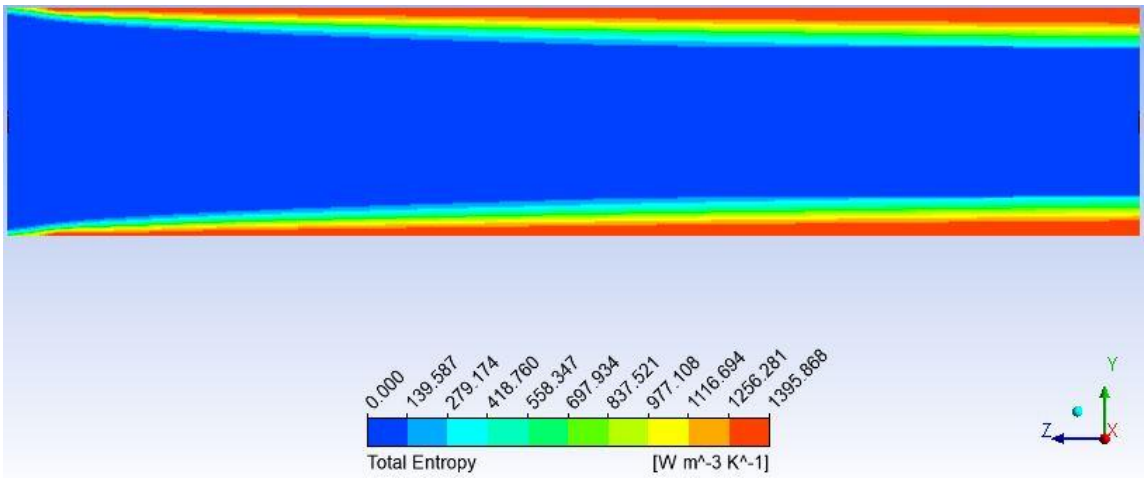

Figure 7.3 Total entropy distribution of Al_2O_3-water nanofluid along pipe at an average concentration of 3%, diameter of 20 nm, inlet temperature of 60°C, and Re number of 1200

7.2 Effect of Concentration

Adding nanoparticles to base fluid increases thermal conductivity of nanofluid. For constant wall heat flux boundary condition the temperature field experience a decrease in gradients. This causes the heat transfer entropy to decrease. As seen in Fig. 7.4, increasing the concentration by a maximum of 5% decreases the entropy generated by about 6.657% at a diameter of 20 nm and Re number of 1200.

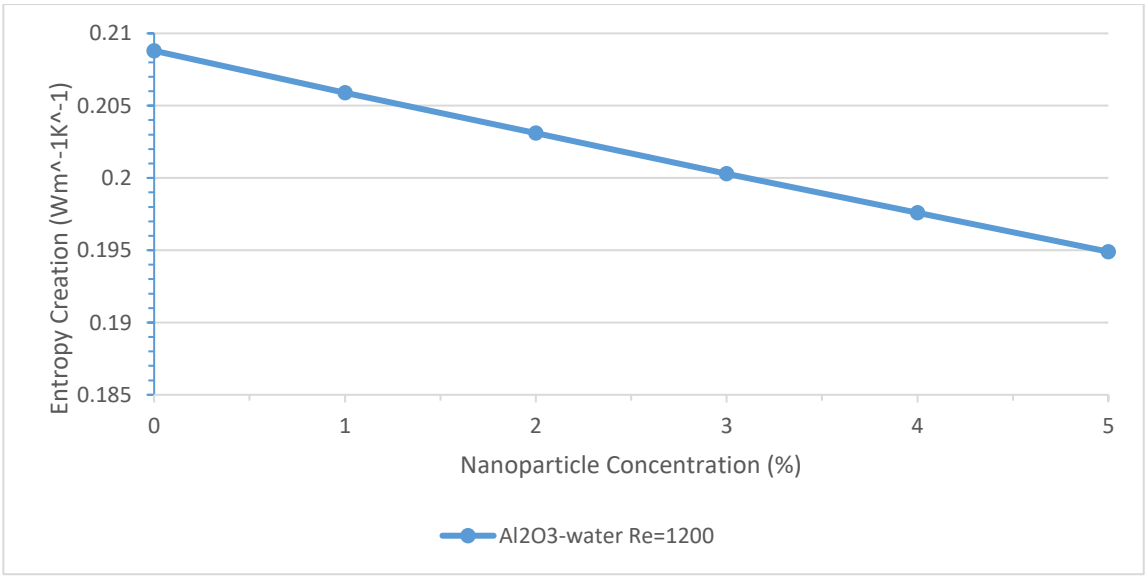

Figure 7.4 Effect of concentration on total entropy generation in Al_2O_3-water nanofluid

7.3 Effect of Diameter

Changing the diameter of nanoparticle inversely influences entropy. Khanafer and Vafai [3] correlation was used.

$$(k_{eff})_{nf} = (1 + 1.0112\emptyset + 2.4375\emptyset\left(\frac{47}{d}\right) - 0.0248(\frac{k_p}{0.613}))k_f \quad (7.5)$$

Insignificant effect of frictional entropy generation on total entropy generation is observed for different nanoparticles size diameter. Total entropy generation increases as the diameter decrease. This happens due to the significant increase of heat transfer rate as well as the increase of thermal conductivity of nanofluids too. Effect of diameter is shown in Fig. 7.5.

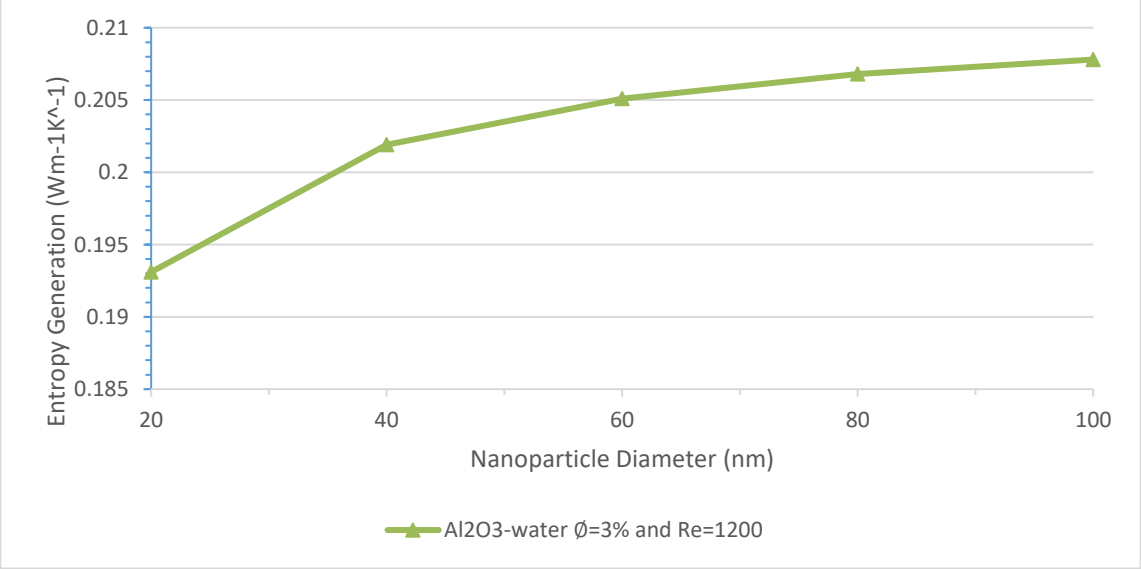

Figure 7.5 Effect of diameter on total entropy generation in Al_2O_3-water nanofluid

7.4 Effect of Inlet Temperature

The amount of heat transferred from the wall to the bulk of wall boundary condition being constant, increasing inlet temperature increases entropy as differential between wall and bulk temperature increases. This effect is enhanced for nanofluids as outlet wall temperature decreases with concentration. A minimum optimum temperature would be required to minimize entropy. Trend can be seen in Fig. 7.6.

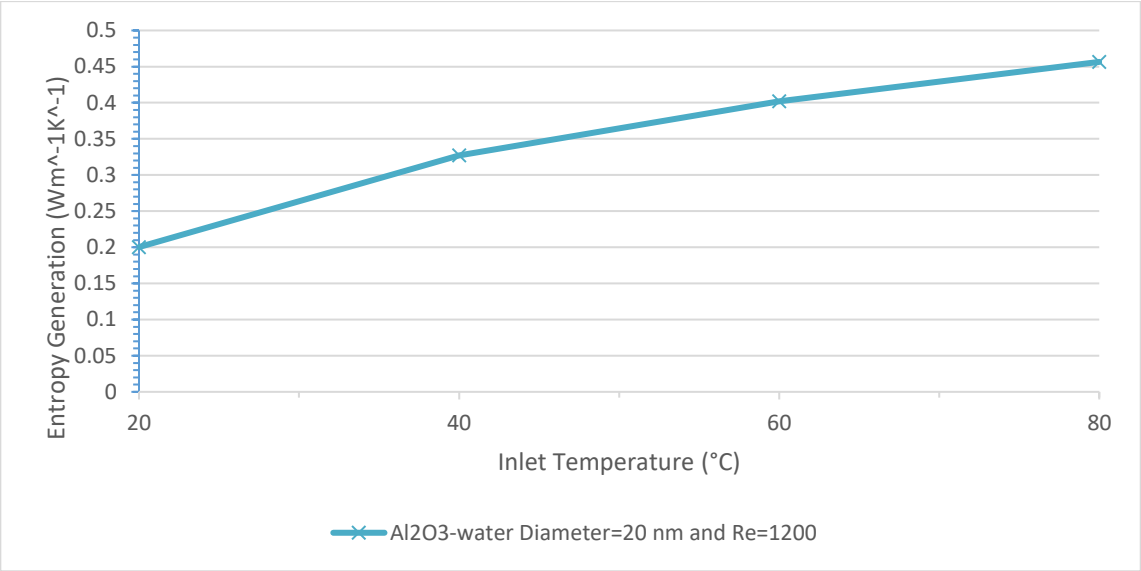

Figure 7.6 Effect of temperature on total entropy generation in Al_2O_3-water nanofluid

7.5 Effect of Re Number

Total entropy generation decreases as the Re number increases and rapidly for small values of diameter due to enhancement of thermal conductivity and h_{ave} due to smaller field temperature gradients. Also, rapid reduction of total entropy means that effect of friction entropy is negligible and effect of thermal entropy becomes more significant. Thus, an optimal Re number exists where entropy is minimum.

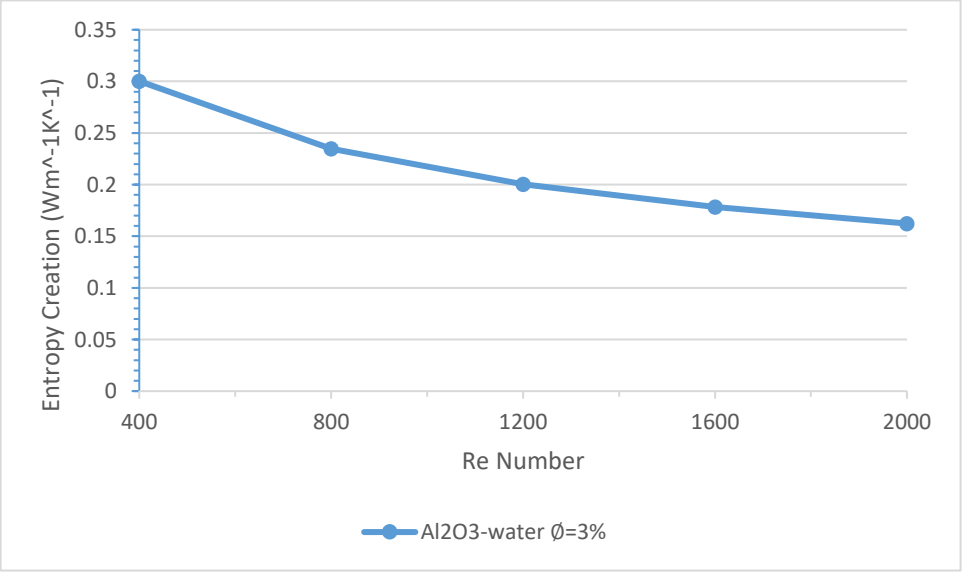

Figure 7.7 Effect of Re number on total entropy generation in Al_2O_3-water nanofluid

Summary

Heat transfer analysis of nanofluids in circular pipes is done from a second law of thermodynamics perspective. The role of heat transfer and fluid flow or frictional dissipation irreversibilities on entropy generation is studied. Two approaches have been taken for determining the losses associated with this phenomenon. In the first, the standard Bejan correlation is used to calculate entropy generated per unit length of pipe using available correlations for friction factors and pumping power and HTC and Nu numbers. The second approach involved using gradients of heat transfer and fluid flow to calculate local entropy generation per unit volume and then average to get the total.

References

[1] A. Bejan, Entropy Generation through Heat and Fluid Flow, Wiley, New York, 1982.

[2] M. Massoud, Engineering Thermofluids Thermodynamics, Fluid Mechanics, and Heat Transfer, first edition, Springer, Berlin Heidelberg New York, 2005.

[3] K. Khanafer and K. Vafai, "A critical synthesis of thermophysical characteristics of nanofluids," International Journal of Heat and Mass Transfer, vol. 54, issues 19-20, pp. 4410–4448, 2011.

Chapter 8: Conclusions and Recommendations

The following conclusions were drawn on the basis of these research simulations.

- The difference in h enhancement between the simulation and theoretical results is most probably due to non-inclusion of viscosity Batchelor model of nanofluid which directly affects the pressure drop for forced convection in pipes.
- Heat transfer coefficient of nanofluid decreases along the axial length of the pipe. The trend is almost the same for both nanofluids. Highest heat transfer occurs at the entrance of the tube due to largest difference between bulk temperature and wall temperature.
- Increasing concentration increases average HTC by 4.296% and 1.534% for Al_2O_3-water and CuO-water nanofluids at an average concentration of 3% and Re number of 1200 respectively. Increase for Al_2O_3-water is more than CuO-water.
- Diameter has an inverse effect on average HTC. For lower sizes h is higher due to higher mobility of nanoparticles within base fluid. This enhance heat transfer between partlces and the fluid layers around it which then convect the heat throughout the fluid.
- For CuO-water nanofluid the pressure is a little higher at the beginning due to high density of CuO as compared to Al_2O_3.
- Heat transfer is more for Al_2O_3-water nanofluid compared to CuO. This is due to the lower thermal conductivity and higher density of CuO.

Improvements in convective forced heat transfer by nanofluids can certainly be made and the following future work is advocated to advance using nanofluids in energy applications.

- The complicated phenomenon of agglomeration and maybe sedimentation in nanofluids flow should be clustering in future simulations.
- For practical applications like pipe heat exchanger it is observed that a lower value of ϕ and inlet temperature and higher Re may optimize system.
- This can counter the adverse affects of higher pressure drops at higher concentrations.
- Experimental studies are advised to determine the exact concentration distribution during convective heat transfer.

Chapter 9: Supercritical CO_2 for Concentrated Solar Thermal Energy

9.1 Introduction

Solar thermal energy systems form an important part of solar energy for the future. Economic and design constraints demand large scale expansion of solar thermal energy and in this area there is a reinvigoration in the interest of concentrated or high temperature solar thermal energy around the world. The current global installed operating capacity at the end of 2015 was 4.8 GW. Out of this about 90% is owned by Spain and USA [1]. Despite innovations in design, manufacturing, and integration of these systems in global energy grid there is still a tremendous potential to be exploited. Component design of collector optical system (field layout or heliostat), heat transfer fluid, power block system, thermal energy storage, tracking as well as cycle analysis continue to take on a more aggressive approach.

In particular design and modeling engineering is enabling new technologies to surface in collector design, tracking, and use of alternative clean fuels. Storage continues to be an issue but materials such as latent heat storage and nanofluids promise to emerge as the next generation of storage mediums. Latent heat storage can tackle the problem of intermittency of the high temperatures achieved in the receiver and other components as well as decreases costs by reducing the size storage of the concentrated solar thermal energy system [2]. The dream of making concentrated solar power (CSP) a reality can be accomplished by increasing competitiveness, developing analysis and insight into optimization, and short to long term goal evolution. Short term gas fired backup is commonly considered included to smooth out transients.

Within the domain of CSPs process intensification is playing an important role in the development of alternative cycles and heat transfer fluids. Superheated and supercritical regimes can provide a lot of energy. In particular, this research addresses carbon dioxide (CO_2) direct Brayton cycle at or near supercritical point. The reason to operate the fluid

at this temperature is primarily to increase density (compared to water) and increase specific heat capacity, attributes which are very desirable in increasing equivalent or higher efficiencies without holding higher temperatures in receiver. The design also becomes modular as less piping is required decreasing costs. Also unlike water or steam Rankine cycles, supercritical CO_2 (s-CO_2) undergo no phase change and is compatible and matched to current molten salt technology. There is a possibility of imminent integration in the upcoming years with molten salt storage that can remove short term transients and provide stable power generation during the night.

9.2 Literature Review

Models for direct as well as indirect cycle CO_2 at or near supercritical pressures and temperatures have been investigated to date [3-4]. Further static or steady state and dynamic models further delineate the behavior and performance of such a system. A direct, dynamic model studying the effects of solar flux on mass flow rates, net power, pressures, and temperatures has been investigated by considering the effects of density, and thus mass and volume changes throughout the year. Consequently, control strategies have been suggested [5]. Innovation in the architectural design of power cycle has also sprung an interest in this field. This has led to modular tower concepts using the same direct, regenerative or recuperative cycle with the goal of decreasing land usage, maintenance costs, thermal mass, volume, and weight of the turbomachinery (increasing reliability), increasing cycle efficiency [6], and providing electricity for remote areas (which can also be scaled for large scale power generation). The charging and discharging mechanisms when thermal storage is also simple when modular blocks are used but with the disadvantage of high storage costs for two tank storage molten salt storage and ability to bridge only short term transients such as drifting clouds [7].

In high temperature solar thermal combined with the fickle nature of CO_2 at or near supercritical point, even small changes in design variables can have a huge impact on cost and reliability of power plant [8]. This is especially important for indirect cycle using CO_2 as the HTF in the receiver block is different from the working fluid in the power block. The sensitive effect of mass flow rates, heat exchanger effectiveness, and important

temperatures on cycle efficiencies has consistently required the optimization of heat exchanger for effective heat transfer which forms the basis of clean and sustainable energy [9]. The effect of source temperature (turbine inlet temperature), compressor inlet pressure (low side pressure), and expansion pressure ratio (turbine pressure ratio) on cycle efficiency, mass flow rate, irreversibility (gas cooler, specific, and total), and net work output has also been researched [10]. Efficiency, work output, and irreversibility seem to prop as the dominant performance indicators with mass flow rate being used both as a cause and effect [5-6]. The goal has been to increase cycle efficiency within supercritical region and achieve low sensitivity to source temperatures. Tradeoffs are almost always involved usually with parameters such as flow rate, source pressures, and temperatures.

9.3 Analysis and Discussion

9.3.1 Thermodynamic Cycle

The basic Brayton solar thermal cycle consists of a compressor, collector (concentrator/heliostat and receiver) and turbine in a closed cycle. Closing the same cycle with a low pressure or power turbine can increase the cycle efficiency. Furthermore, high pressure (HP) turbine is used to drive the compressor. Turbines can also be connected in parallel using two receivers to decouple the HP turbine from low pressure (LP) turbine and control the power from the second receiver.

9.3.2 Modifications to the Basic Cycle

The basic cycle is modified by introducing components that can increase the efficiency. The following cycle in Fig. 9.1 was modeled and simulated in TRNSYS. TRNSYS is a software that models and simulates transient systems. It was initially built to simulate solar energy systems but with time expanded to other engineering domains. The basic function is to optimize the system by evaluating its performance with changing design parameters. Typical meteorological year (TMY) data for Multan available in TRNSYS library is used simulate weather conditions. Creating a TRNSYS simulation consists of identifying components that accurately model physical process unit, connecting those components appropriately and input of parameters to mimic operating conditions of each unit in the

real system. The following components were used in the simulation of the plant over the course of a day in winter as the worst-case scenario.

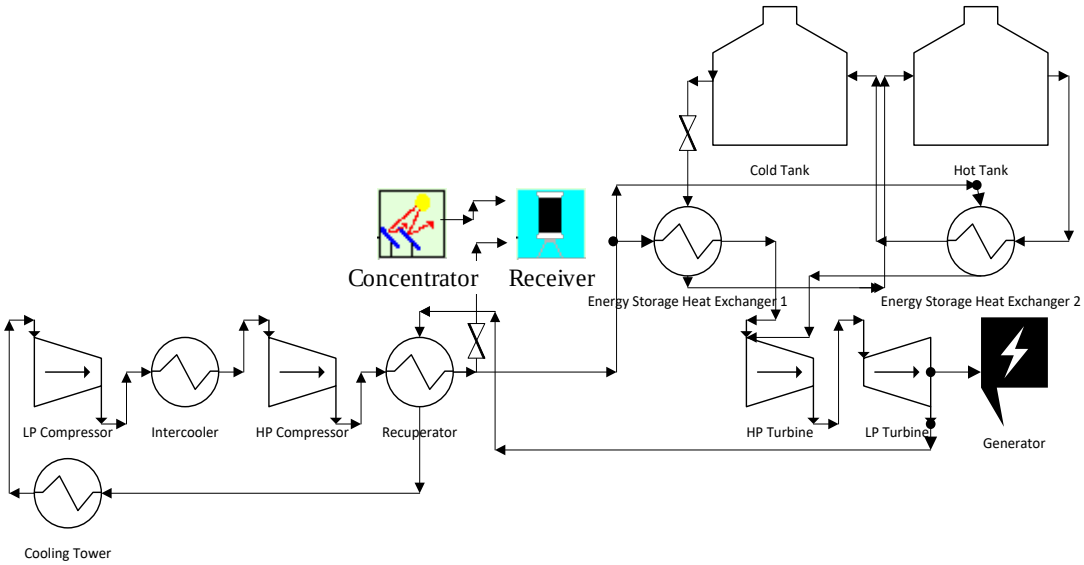

Figure 9.1 Central receiver plant using s-CO_2 in TRNSYS

Weather Data Processor (Type16g): The component reads data at regular time intervals from a data file and make it available to other components as time varying forcing functions. It gives solar azimuth and solar zenith at different locations and time of year. This output is used to interpolate the heliostat field efficiency matrix provided by user.
Heliostat Field (Type194): It tells the area of field, efficiency matrix of field, net electric output, heliostats number, start-up and tracking among other outputs.

Receiver Tower (Type195): The component has output of demand flowrate required to get the desired outlet s-CO_2 pressure and temperature.

Power Cycle: It contains the models used in conventional power plant, like the compressor stages, compressor controller, generator, pumps, turbine stages, turbine controller, etc. Due to the CSP power plant simulation based research focus is on efficiency performance, the above components in power cycle are not defined here.

The recuperator or regenerator is used to extract the exhaust CO_2 energy leaving he HP turbine. When a heat exchanger is used, less energy is required in the receiver assuming that the source temperature doesn't change. The net work output doesn't change ensuring the increase in cycle efficiency.

The cooling tower cools the gases down to a pressure and temperature required for LP compressor again increasing the efficiency. However, low rejection temperature requires heat rejection to environment that may have a higher ambient temperature, making heat rejection difficult. By operation in supercritical regime the same thermal efficiency increase be generated by decreasing maximum cycle temperature, decreasing costs or increasing performance.

Intercooler is used to decrease work input of compressors and thus, increase the net work output and consequently the work ratio. But cycle efficiency is also decreased which is why the recuperator is used to offset. The availability and cost of cooling water supply is met by identifying the ideal location for wet cooling. Critical temperature and classification as a dry or wet fluid is important in determining a fluid stability for an application. For example, dry fluid is not suitable for use at supercritical conditions for turbine inlet as they increase need of additional heating components. Moreover, different regimes of criticality also have different thermal conversion efficiencies, cycle efficiencies, heliostat size, temperature range and storage size.

9.3.3 Assumptions

- Pressure ratios of all turbo-machinery is the same.
- Inlet temperatures of both compressors are the same. Both assumptions ensure work input is minimum.
- There are no losses in recuperator no matter what outlet temperatures are used.
- Maximum cycle temperature does not change to ensure heat supplied in the receiver is reduced.
- Pressure losses are neglected in all components.

9.3.4 Thermodynamic Equations

A compression isentropic process (reversible adiabatic) relates state variables as follows

$$\frac{T_{2s}}{T_1} = \left(\frac{p_2}{p_1}\right)^{\frac{\gamma-1}{\gamma}} \tag{9.1}$$

Compression efficiency is defined as

$$\eta_c = \frac{T_{2s} - T_1}{T_2 - T_1} \tag{9.2}$$

$$Work\ input\ of\ compressor = c_{p1}(T_2 - T_1) \tag{9.3}$$

Work output of HP turbine is defined as

$$\dot{W}_{HPt} = \frac{2\dot{W}_c}{\eta} = c_{p10}(T_{10} - T_{11}) \tag{9.4}$$

Turbine efficiency is defined as

$$\eta_{HPt} = \frac{T_{10} - T_{11}}{T_{10} - T_{11s}} \tag{9.5}$$

$$\frac{p_{10}}{p_{11}} = \left(\frac{T_{10}}{T_{11s}}\right)^{\frac{\gamma}{\gamma-1}} \tag{9.6}$$

$$\frac{p_{11}}{p_{12}} = \frac{\frac{p_4}{p_1}}{\frac{p_{10}}{p_{11}}} \tag{9.7}$$

Similarly, for expansion isentropic process at LP turbine

$$\frac{T_{11}}{T_{12s}} = \left(\frac{p_{11}}{p_{12}}\right)^{\frac{\gamma-1}{\gamma}} \tag{9.8}$$

$$\eta_{LPt} = \frac{T_{11} - T_{12}}{T_{11} - T_{12s}} \tag{9.9}$$

Net work output is cumulative work of both compressors and turbines and is defined as

$$\dot{W} = c_{p11}(T_{11} - T_{12})\eta \tag{9.10}$$

Thermal ratio of heat exchanger is defined as

$$TR = \frac{T_6 - T_4}{T_{12} - T_4} \tag{9.11}$$

Net heat is only input by the receiver

$$\dot{Q} = c_{p6}(T_7 - T_6) \tag{9.12}$$

The cycle efficiency, gross work output, and cycle efficiency are then calculated

$$\eta_{cycle} = \frac{\dot{W}}{\dot{Q}} \tag{9.13}$$

$$\dot{W_g} = \dot{W_{HPt}} + \frac{\dot{W}}{\eta} \tag{9.14}$$

$$Work\ ratio = WR = \frac{\dot{W}}{\dot{W_g}} \tag{9.15}$$

$$\dot{m} = \frac{P_{elec}}{\dot{W}} \tag{9.16}$$

9.4 Methodology

9.4.1 Main Components of Solar Power Plant

9.4.1.1 Heliostat Field

Flux density must be focused/increased at a surface. Large number of tracking mirrors used for focusing the light on a focal point to get the maximum radiation on a certain point for achieving high temperature are called heliostats. They consist of a flat or curving mirror, frame body, steel support and tracking mechanism. No of these mirrors in a field depends upon the power output of the system. Being large in number, shadowing effect of one heliostat on other minimize the reflectivity, so distance between mirrors is kept large to block shadowing effect and hence land area for installation the plant increases. Mirrors should have good optical properties for high reflectivity. Heliostats optical efficiency depends upon atmospheric attenuation, blocking effect, cosine effect, mirror reflectivity, and receiver spillage.

9.4.1.2 Solar Collector

In power tower technology reflected sun rays from the mirrors are received on a central point which acts both as a receiver and a heat exchanger. In fact, small circular pipes welded to each other form a circular shape at a specific height from the earth supported by the steel structure. Heat is taken by HTF flowing inside the receiver tubes. On the basis of HTF and receiver geometry, receivers can be classified into different types.

9.4.1.3 Heat Transfer Fluid

Heat transfer fluids act as the transporter by receiving heat energy and deliver it to the steam generation unit. Desired characteristics of a HTF include

Table 9.1 Factors affecting HTF performance

Number	**Characteristic**	**Desired**
1	Corrosion with metallic alloy	Low
2	Heat capacity	High
3	Thermal stability	High
4	Thermal conductivity	High
5	Vapor pressure	Low
6	Viscosity	Low

In Brayton cycle, gas turbines with air or other gases at high pressure rotate shaft of turbine and generator's rotor at fixed rpm by striking them. At supercritical conditions cycle efficiency can be increased for intermediate pressures and temperatures by increasing source temperatures. Depending on the power required, the design parameter span a range of values as indicated by the experimental or simulation research for that s-CO_2 plant.

9.5 Designing of Model

Receiver size depends upon the desired output temperature of receiver. Receiver temperature rises because of the radiation fall on it. Designing a 1 MW system requires that the input should be greater than 1 MW due to losses occurs within the Brayton cycle. Considering those losses 3.75 MW input power would need to run a 1 MW plant as shown below.

$$Output\ power\ need = 1\ MW$$

$$Efficieny\ of\ turbogenerator = 40\%$$

$$Piping\ network\ efficieny = 99\%$$

$$Thermal\ storage\ efficieny = 99\%$$

$$Plant\ wide\ availability = 95\%$$

$$Total\ thermal\ to\ electric\ conversion = 40 * 99 * 99 * 95 = 37.34\%$$

$$Input\ power\ needed = \frac{1}{37.34\%} = 2.67 \cong 2.70\ MW$$

Considering optical losses

$$Receiver\ efficiency = 90\%$$

$$Heliostats\ efficieny = 95\%$$

$$Total\ input\ power\ required = \frac{2.70}{0.9 * 0.95} = 3.15\ MW$$

$$Available\ flux\ limit = 630\ {}^{W}/_{m^2}$$

$$Area\ required\ for\ heliostats = \frac{3.15}{630} = 5000\ m^2$$

$$Area\ of\ a\ single\ heliostats = 64\ m^2$$

$$Total\ heliostats\ required = \frac{5000}{64} = 78$$

Available limiting maximum solar flux value is defined as

$$0.35 - 0.5\ \frac{MW}{m^2}$$

$$Area\ required\ for\ receiver = \frac{3.15}{0.35} = 9\ m^2$$

Dimensions of a single circular tube and total number of tubes are defined as

$$Length\ of\ a\ single\ tube = 1\ m$$

$$Diameter\ of\ single\ tube = 1\ cm$$

$$Area\ of\ single\ tube = 2\pi rh = 0.0314\ \text{m}$$

$$Total\ tubes\ required = \frac{9}{0.0314} = 287$$

9.6 Model Without Storage

The following model was developed.

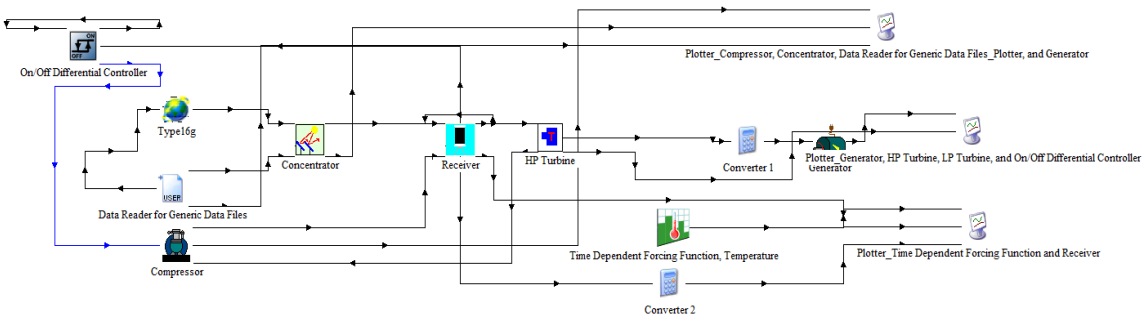

Figure 9.2 Brayton cycle model without storage

Points 1, 2, and 3 correspond to compressor inlet, receiver inlet, and turbine inlet

At

$$\dot{m} = 19.6\ kg/s, p_1 = 8\ MPa, \frac{p_2}{p_1} = 3\ and\ T_3 = 850°C$$

Table 9.2 Effect of mass flow rate on cycle pressures and temperatures without storage

Points	1	2	3
Mass flow rate m (kg/s)	19.6	19.6	19.6
Pressure (MPa)	8 (initial) then 13.64	24	24
Temperature T (°C)	690.6 (day) - 483.4 (night)	847 (day) - 611 (night)	850 (day) - 611 (night)

Receiver

For a 24-hour cycle, during the day the receiver flow rate demand increases due availability of solar radiation and becomes 0 at night. The outlet temperature is stable during the day at a value of 850°C but decreases during the night to 611°C due to non-availability of radiation. Both the flow rate and temperature vary in order to keep the pressure at a fixed value of 240 bar.

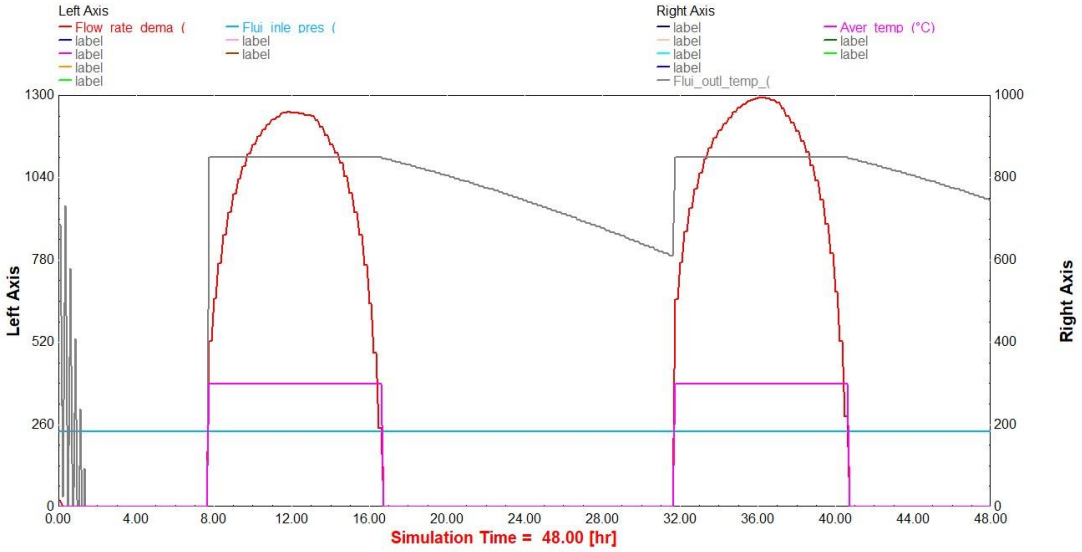

Figure 9.3 Receiver output

Turbine

The turbine flow rate is very high and stable as high speed is required to expand the fluid and convert enthalpy into work. It remains stable as the pressure of the receiver is stable. Similarly, the output pressure is stable at a value of 136.4 bar. Both of these trends are shown in Figures 9.4 and 9.5. Moreover, the temperature follows the same trend as the outlet temperature of receiver as its directly connected to it.

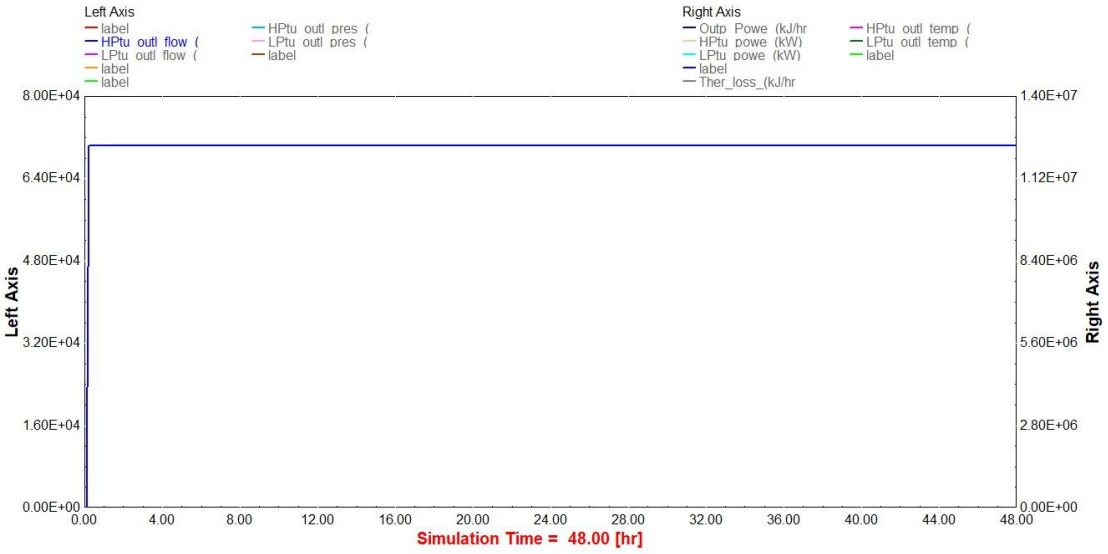

Figure 9.4 Turbine flow rate

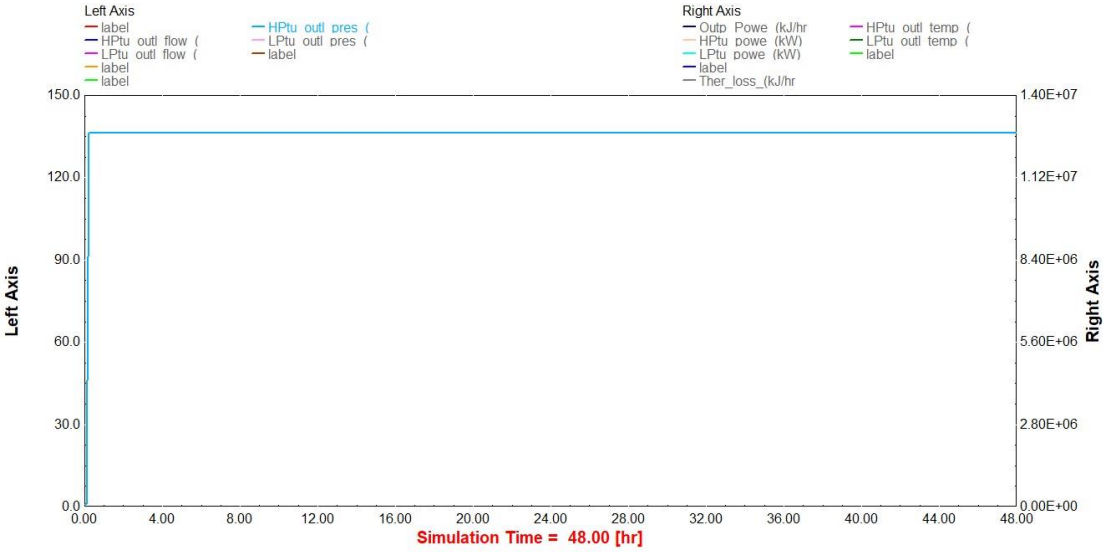

Figure 9.5 Turbine pressure

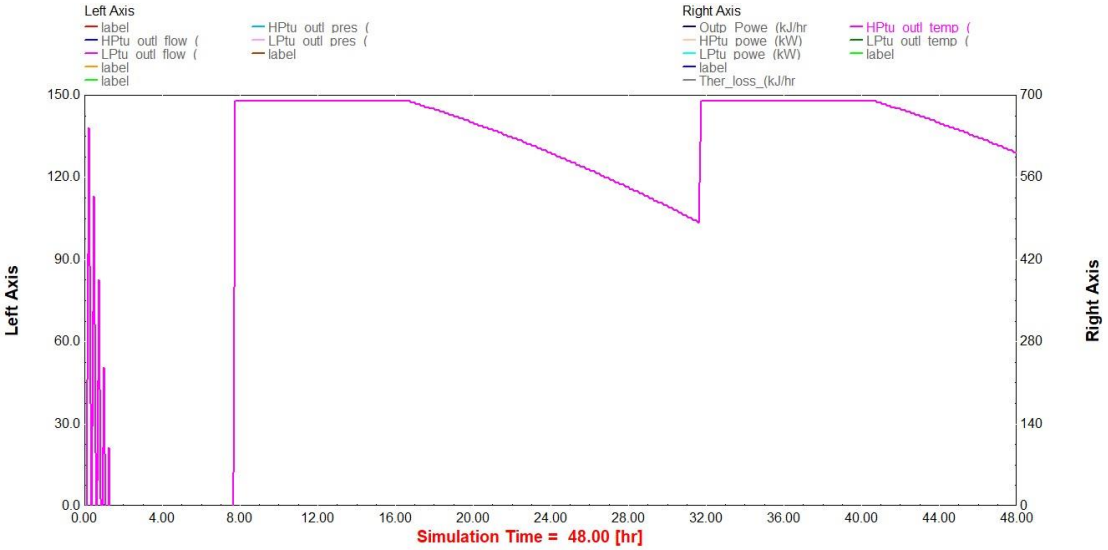

Figure 9.6 Turbine temperature

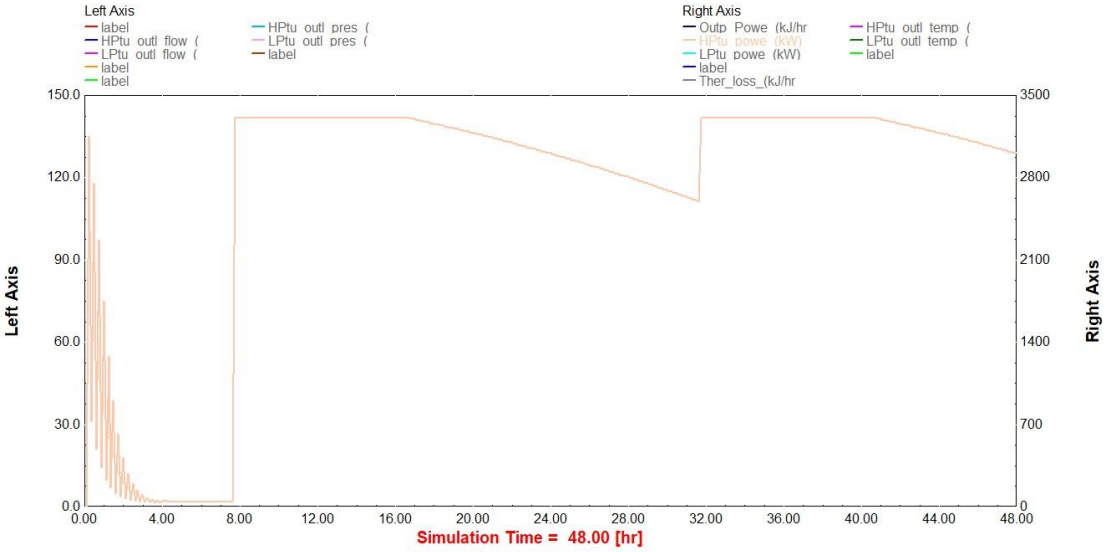

Figure 9.7 Turbine power

Generator

The generator power is around 2.78 MW without considering losses after which it becomes 1 MW.

9.7 Model With Storage

The following model was developed.

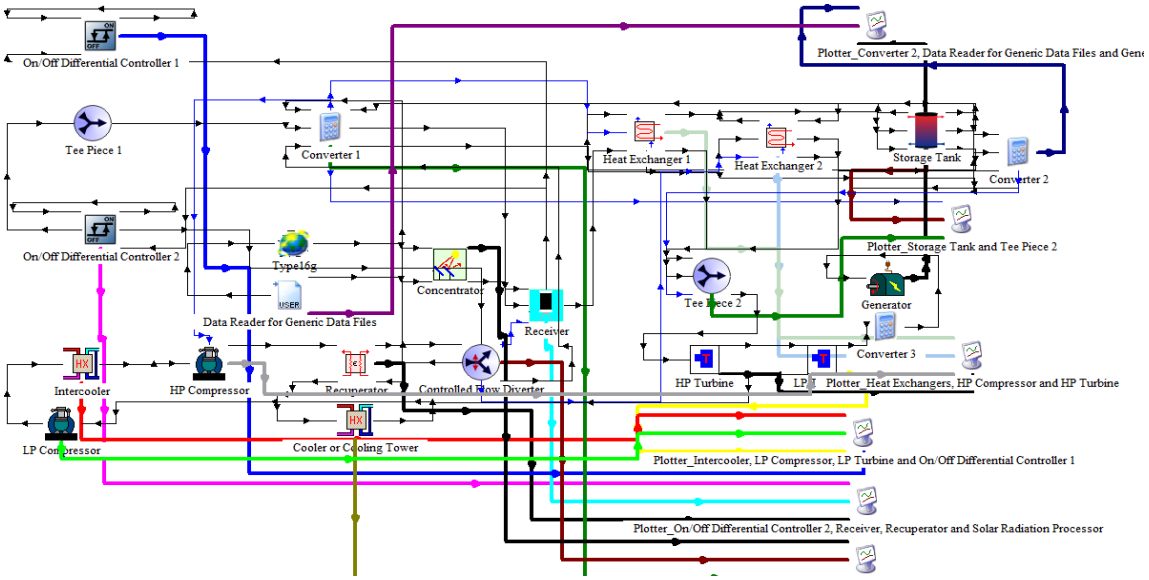

Figure 9.8 Brayton cycle model with storage and associated units

Effect of Compressor Ratio

Increasing the compressor pressure ratio increases the work output and is more for turbine as compared to compressor as shown below. It is lower for higher inlet pressures.

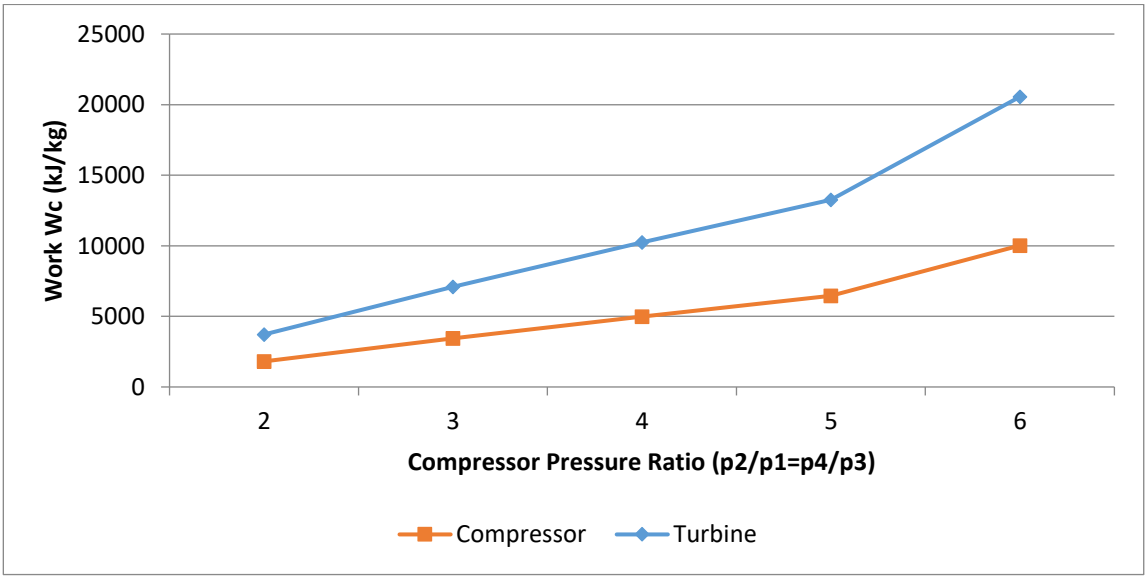

Figure 9.9 Effect of compressor pressure ratio on work output at p1 of 7.8 MPa

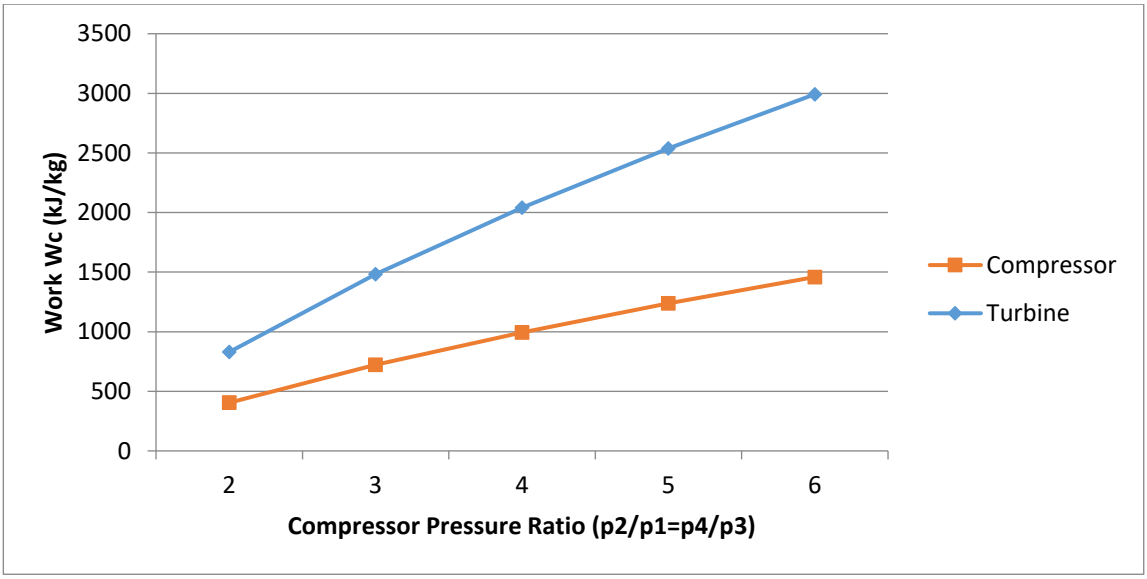

Figure 9.10 Effect of compressor pressure ratio on work output at p1 of 25 MPa

The work output considerably reduces for a single compressor and turbine model at subcritical or normal conditions.

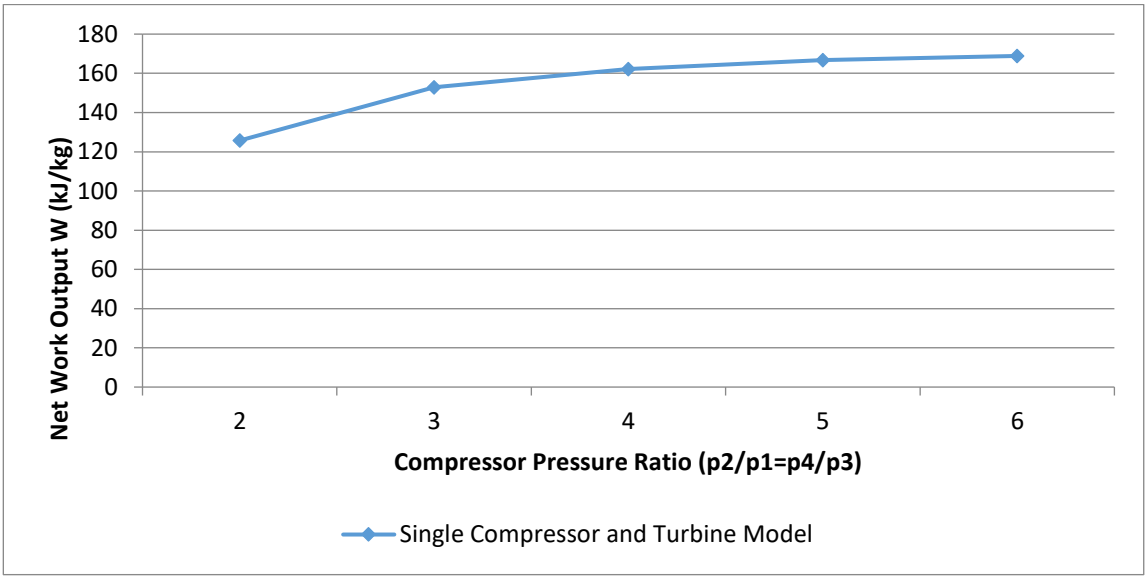

Figure 9.11 Effect of compressor pressure ratio on work output at p1 of 0.2 MPa

Table 9.3 Effect of mass flow rate on cycle pressures and temperatures with storage

Points	1	2	3
Mass flow rate m (kg/s)	19.6	19.6	19.6
Pressure (MPa)	8 (initial) then 13.64	24	24
Temperature T (°C)	690.6 (day) - 483.4 (night)	847 (day) - 611 (night)	850 (day) - 611 (night)

Effect of Collector Area on Solar Fraction

Area of heliostat is maximized to get supercritical pressures as shown in Fig. 9.12.

Figure 9.12 Effect of area of collectors or number of heliostats on solar fraction

9.8 Conclusions

Following insights were gained by doing this research.

- Net output power of 1 MW is stable during the day with storage.
- Also, even though generator power doesn't go to zero but decreases.
- The dynamic modeling of a s-CO_2 depends on several factors like mass flow rate, pressure, and, temperature.
- Area, flow, pressures, and temperatures have been varied.
- Receiver outlet/turbine inlet temperature is dominant factor.

9.9 Recommendations

Following the recommendations below can aid in the development of efficient and optimized Brayton s-CO_2 cycle for CSP applications.

- Storage cycle can be improved by using PID controller to control mass lumping based transients and optimizing the storage tanks as heat exchanger optimization is not enough.
- Generated power could be made stable

References

[1] J. L. Sawin et al., Renewables 2016. Global Status Report. 2016.

[2] B. Xu et al., "Application of phase change materials for thermal energy storage in concentrated solar thermal power plants: A review to recent developments," Applied Energy, vol. 160, issue , pp. 286–307, 2015.

[3] D. Milani et al., "A comparative study of solar heliostat assisted supercritical CO2 recompression Brayton cycles: Dynamic modelling and control strategies," The Journal of Supercritical Fluids, vol. 120, part 1, pp. 113–124, 2017.

[4] M. Atif and F. A. Al-Sulaiman, "Energy and exergy analyses of solar tower power plant driven supercritical carbon dioxide recompression cycles for six different locations," Renewable and Sustainable Energy Reviews, vol. 68, part 1, pp. 153–167, 2017.

[5] R. Singh et al., "Dynamic characteristics of a direct-heated supercritical carbon-dioxide Brayton cycle in a solar thermal power plant," Energy, vol. 50, issue 1, pp. 194–204, 2013.

[6] M. Valdés et al., "Thermal efficiency of direct, inverse and sCO_2 gas turbine cycles intended for small power plants," Energy, vol. 100, issue 1, pp. 66–72, 2016.

[7] Z. Ma and C. Turchi, "Advanced supercritical carbon dioxide power cycle configurations for use in concentrating solar power systems," Supercritical CO_2 Power Cycle Symposium, no. March, pp. 4–7, 2011.

[8] M. Persichilli et al., "Supercritical CO_2 power cycle developments and commercialization: Why sCO2 can displace steam," Power-Gen India Cent. Asia 2012, pp. 19–21, 2012.

[9] M. A. R. Belmonte et al., "Optimization of a recompression supercritical carbon dioxide cycle for an innovative central receiver solar power plant," vol. 112, issue 1, pp. 17–27, 2016.

[10] P. Garg et al., "Supercritical carbon dioxide Brayton cycle for concentrated solar power," Journal of Supercritical Fluids, vol. 76, pp. 54–60, 2013.

Acknowledgments

I am thankful to Almighty Allah who is creator of the universe and everything and the most gracious and the most merciful. Without Your guidance, this research and nothing in fact nothing in my life would have been possible. It was Your continuous opportunity and support towards me that made me stand where I am. Every event directly or indirectly was steered by Your sheer will and You are the only One who shall prevail.

My deepest respects go towards my late father who developed a sense security for me during my childhood and encouraged me to fulfill his dream of becoming a successful engineer. Although, he is no longer with me, his spirit remains in my heart and is one of the major driving force for what I have achieved in life. I am forever indebted to his memory along with the continuous sacrifice and support of my mother and siblings.

Mere words cannot describe the guidance, motivation, patience, and support of my supervisor Dr. Majid Ali in the tenure of this study. His priceless knowledge and experience of CFD has helped me overcome obstacles in a field that was new to me. In fact, he was the one that encouraged me to pursue this work and take an additional optional course on CFD during summer apart from Nuclear Energy Engineering in my coursework.

An important role was played by Dr. Brian Fronk in successful completion of my investigation at OSU. My sincerest regard goes to him.

I express thanks to guidance and examination committee (GEC) members Dr. Muhammad Zubair, and Dr. Emad Ud Din for their guidance and support during this research which was supported by Thermal Energy laboratory, USPCAS-E, NUST, Islamabad, Pakistan. Especial appreciation goes to my research fellows Hamza Ahmad Raza, Ibadullah Safdar, Sara Sultan, and Sufyan Naeem for their valuable cooperation and insights.

Finally, I would like to express my gratitude to all the individuals who took a considerable amount of their precious time in making this investigation a reality.

Annex I

Journal Article: "Effect of characteristic parameters on nanofluid thermal energy performance"

Under Review in: International Journal of Sustainable Energy

Abstract

Heat transfer forms the basis of conversion of one form of energy to another. Increasing heat transfer area by using conventional methods of geometry design can increase the output temperature but this leads to a bulky and costly thermal system. Passive techniques can decrease the cost. The research presented revolves around enhancment of heat transfer using nanofluids. Nanofluids are colloidal suspensions of nanoparticles in a base fluid (thermal fluids) such as water with excellent thermal characteristics. They enhance heat transfer by increasing the convective heat transfer and thermal conductivity of nanofluid as compared to base fluid by increasing heat transfer area. An analysis of hydrodynamically and thermally developing laminar forced convection of nanofluids in circular pipes subjected to a constant wall heat flux boundary condition has been perfomed by numerical method. The numerical analyis was conducted using parametric three dimensional (3D) computatational fluid dynamics (CFD) simulation code ANSYS CFX. Alumina (Al_2O_3) and copper oxide (CuO) nanoparticles were employed in water as base fluid in a liquid single phase constant thermophysical properties model. The effect of design factors of concentration, diameter, heat flux, Reynold (Re) number, and type of nanofluid on heat transfer coefficient (h), Nusselt (Nu) number, and pressure drop (ΔP) is investigated for different axial locations. Results reveal that increasing particle concentration from 1% to 5% increases the HTC for Al_2O_3-water by more than 5% similar to that by Re number. CuO shows little heat transfer enhancement due to high density and low thermal conductivity. Velocity increases along the length of the pipe. Moreover, the results were validated with empirical and theoretical correlations and agreed with an error less than 5%.

Keywords: Convective heat transfer, nanofluid, nanoparticle, boundary condition, thermophysical, friction factor, heat transfer coefficient, Nusselt number, pressure drop, Reynold number, concentration, single phase

1. Introduction

The rapid growth in global economy, lifestyle, and population has put tremendous strains on the energy sector. Big power plants continue to dominate the world energy mix. A crucial quantitative measure of an energy system is heat transfer. The mode of heat transfer can be enhanced by changing flow geometry, boundary conditions, or fluid thermophysical properties [1-2]. Modeling and simulation of heat transfer is important to optimize the model. The issue of insufficient thermal conductivity of conventional fluids is crucial to the successful operation of thermal energy systems. It is directly related to the efficieny of a process or system. Consequently, the HTC depends on the dimensions of device, fluid, geometry, temperature difference, and time. The fluid is the most important parameter and should be chosen for high thermal conductivity, that gives easy availability, high boiling point, high HTC, and nontoxic behavior. If boiling is to be added in design latent heat of vaporization becomes an important parameter to obtain a high heat transfer

coefficient. The problem can be addressed using several different methods that can increase heat transfer. The successful implementation depends on the consideration of several different design and modeling parameters. The best method for passive heat transfer is using nanofluids. Nanofluids are dilute mixtures of sub micron (nanometer (nm)) sized particles in a base fluid. Choi developed the first nanofluid in 1995 [3]. Different theories have been proposed to explain the behavior of heat transfer by nanofluids. Heat transfer of nanofluids include brownian motion of nanoparticles, liquid layering of base fluid surrounding nanoparticles, and nanoparticle aggregation [1]. Higher concentration has shown increase in heat transfer [2]. Most investigation has showed that nanofluid have a very strong temperature dependent thermal conductivity at low concentrations believed to be one of the most important factor in increasing heat transfer [4]. Applications include cooling in electronics, engine, machining, and transformer oil, diesel generator, heat exchangers, nuclear energy, and solar thermal [5]. Previously investigations have been carried out by researchers on both the experimentation and modeling and simulation of nanofluids for the past two decades. Problems arise during practical application of nanofluids like agglomeration, cost, increased pressure drop, pumping power, and unstability and reactivity among others [6]. Despite these challenges there is a very strong potential in nanofluids and there is a consistent rise in the research being carries out in this field [7].

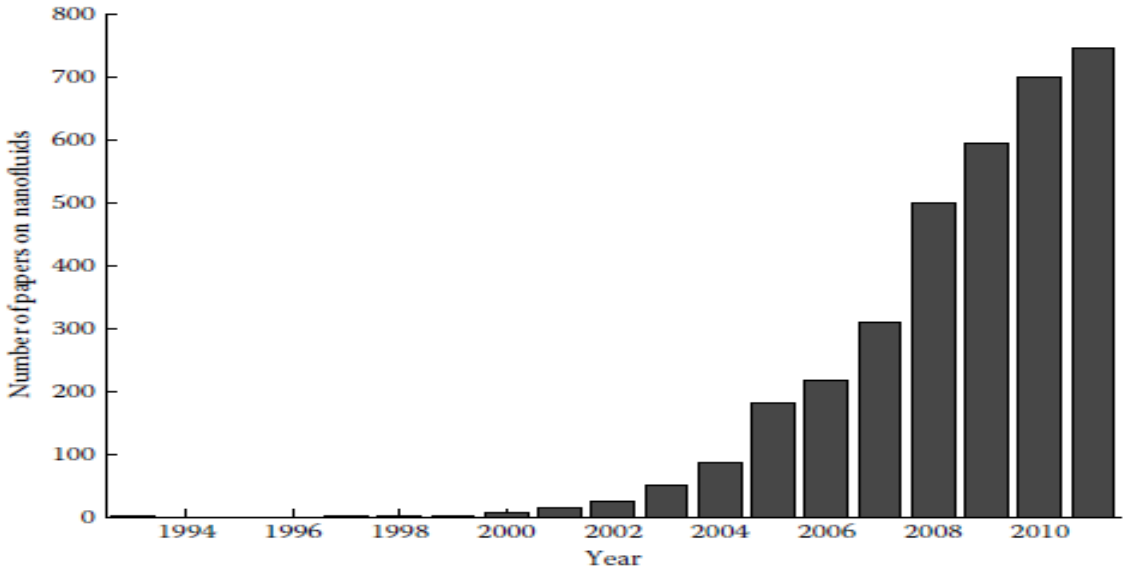

Figure 1 Increase in articles on nanofluids over the years [7]

With the advent of high power computation and extremely fast processing has enables investigators to model and simulate experiments with models that give almost the same results under operating conditions used in experiments and at a much less cost than experimental analysis. CFD is one such tool that has dramatically changed the outlook of current research in fluid dynamics and heat transfer. In the field of nanofluids too there has been considerable usage of numerical softwares including many CFD codes. The most common method discrete solver has been the finite volume method (FVM). Different geometries have been used in the past for conducting nanofluid heat transfer simulation. The most common have been single pipe and double pipe flow and there are now so called

well established correlations and analysis results available in lierature. Laminar flow regime has been studied in detail and the effect of nanofluids on heat transfer and other aspects have been explored. This is because despite extensive theoretical research in this area the practical solution is made complex due to effect of local diffusion, local eddies, and natural convection. Some of the earlier laminar studies of the past decade include those of L. Qiang et al. and G. Roy [8-9]. Much work has been done using metal oxides nanofluids like Al_2O_3-water and CuO-water. Convective heat transfer is an important part in any energy or industrial process. Therefore, it has been researched considerably in both experimental and numerical domains. [10-14]. As nanofluid are fluids, different phase models are required to correctly capture the physics involved in fluid flow and heat transfer. Usually single phase models and mutiphase models are used in numerical research. The single phase models treat the fluid as a single fluid with nanoparticles in a continuum with the base fluid whereas multiphase models involve the treatment of nanoparticles as a single fluid phase and base fluid as another.

In this study a CFD based numerical analysis in the transitional region of a circular pipe has been perfomed using two different types of metal oxide nanofluids i.e. Al_2O_3-water and CuO-water. This research focuses on combined entry length problem due to the fact of getting higher heat transfer in the entrance region of conduits. The objective of this work is to understand the effect of flow geometry, inlet temperature (20-80 °C), nanoparticle concentration (1-5 %), nanoparticle diameter (20-100 nm), and Re number (400-2000) on performance factors of HTC and pressure drop in a short pipe of length 1 m and diameter 20 mm. A constant wall heat flux boundary condition and laminar flow regime is employed. Single phase modeling approach is employed. The results presented are based on average values of inlet temperature of 60°C, nanoparticle concentration of 3%, diameter of 60 nm, and Re number of 1200 respectively. A comparative analysis is made based on equal Re number criteria.

2. Pre Analysis

Nanofluid flow in a circular single heat pipe is studied. The following correlations for flow in a pipe would be validated along with nanofluid model specific benchmarks and correlations. The flow would be fully hydrodynamically developed for a Re number of 500 after reaching hydrodynamic entrance length defined as

$$L_e = 0.05ReD = 0.5\ m \tag{7}$$

As indicated by the constant 0.05, the shear stress on the wall would be within 1.4% of the value at z=∞ with a higher constant indicating accuracy.

The nature of the model is a combined entry length i.e. hydrodynamically and thermally developing flow or simultaneously developing flow as the velocity at the inlet is not a fully developed parabolic profile as well as the heat flux starts from the inlet. Due to this the heat transfer in the entrance region is more sensitive to the Pr number defined as the ratio of momentum diffusivity (kinematic viscosity or viscous diffusion rate) to thermal diffusivity (thermal diffusion rate) [15].

$$Pr = \frac{\nu}{\alpha} = \frac{c_p \mu}{k} \tag{8}$$

where

c_p is the specific heat capacity at constant pressure,

μ is the dynamic viscosity, and

k is the thermal conductivity
Consequently the thermal entrance length is defined as

$$L_t = 0.05DRePr = \frac{0.05VD^2}{\alpha} = 2.452 \text{ m} \quad (9)$$

The normalized wall shear or skin friction coefficient (C_f) is another factor to check associated with the entrance length [15].

$$C_f = \frac{\tau_w}{0.5\rho V^2} = \frac{16}{Re} = 0.032 \quad (10)$$

where τ_w is the wall shear equal to $\mu \frac{\partial w}{\partial y}|_w$,
w is the axial centerline velocity, and
V is the average freestream velocity.
In the fully developed region w will approach twice that of the average velocity according to the analytical solution of parabolic velocity profile [15].

$$\frac{w}{V} = 2(1 - (\frac{y}{Y})^2) \quad (11)$$

The Nu number is defined as

$$Nu = \frac{hD}{k} \quad (12)$$

where h is the heat transfer coefficient equal to $\frac{q}{T_w - Average\ Bulk\ Temperature}$
For fully thermally developed flow Nu=4.364
Lastly, flow in a laminar regime complicates the calculation of heat transfer due to close interaction of energy and momentum exchange.

3. Geometry and Mesh

The code used for simulating the model is ANSYS 16. Computational domain is a geometry of pipe of diameter 10 mm and length 1 m. All of this is done in DesignModeler, a sub-component of ANSYS. The domain is a key input for the mathematical model (governing equations plus boundary conditions) to be solved over it. Grid generation is carried out in ICEM CFD, another sub-component of ANSYS and doesn't affect the mathematical model but only affects the numerical method. Moreover, an O-grid is created in ICEM CFD to improve block corner angles because of the nature of cylindrical geometry.

3.1 Mesh Quality

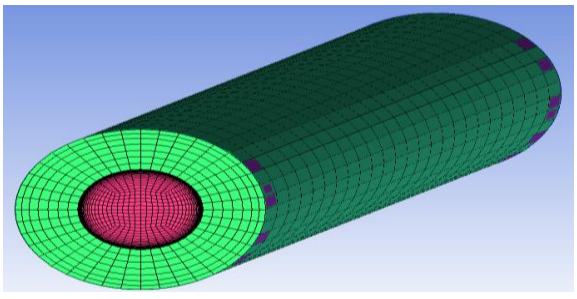

Figure 2 (a) Double O-grid in ICEM CFD

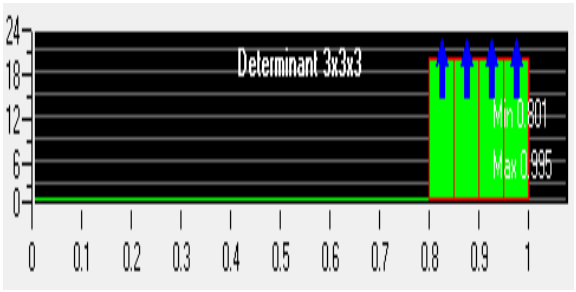

Figure 2 (b) Quality metrics

4. Model Setup

4.1 Pre-Processor

Boundary conditions, fluid properties, and governing equations are assigned in CFX-Pre. The analysis type is steady state and the physical model is laminar model. Full second order discretzation scheme has been employed to minimize discretization errors and ensure accuracy. Treatment of nanofluid as a single phase or multiphase determines what type of heat transfer correlations can be formed and used.

4.1.1 Single Phase

In order to simulate, the following conservation form of governing equations were solved.

Continuity Equation or Mass Equation [16]:

$$\frac{\partial \rho}{\partial t} + \nabla . \rho \boldsymbol{u} = 0 \quad (13)$$

For incompressible flows (as it is in this case), the equation reduces to

$$\nabla . \boldsymbol{u} = 0 \quad (14)$$

Momentum Equation [16]:

$$\rho \frac{Du_i}{Dt} = -\gamma \nabla h - \nabla P + \nabla . \tau_{ji} + F_i \quad (15)$$

where $\frac{D}{Dt} = \frac{\partial u_i}{\partial t} + \nabla . u_i u_j$ is the material derivative,

$\gamma = \rho g$ is the specific weight,

h=distance opposite to the direction of body force (e.g. weight),

P=static pressure,

$\tau_{ji} = \left[\mu \left(\frac{\partial u_j}{\partial x_i} + \frac{\partial u_i}{\partial x_j}\right) \delta_{ji}\right] - \frac{2}{3}\mu \frac{\partial u_m}{\partial x_m} \delta_{ji}$ is the stress tensor,

δ_{ji}=1 if j=i and δ_{ji}=0 if j≠i and is the Kronecker delta. It is a second order tensor, and

F_i=body forces

Energy Equation [16]:

$$\frac{\partial T}{\partial t} + \nabla . \boldsymbol{u} T = \nabla . \left(\alpha_f \nabla T\right) \quad (16)$$

In laminar flow energy transfer is acieved by diffusion i.e. molecular interactions. At high Re number within the laminar regime, energy transfer can also takes place due to viscous shear stresses.

Density and specific heat capacity can be calculated as mass averaged quantities and usually are not measured. The first density correlation was given by Albert Einstein [17].

Later B. C. Pak and Y. I. Cho developed density and specific heat models [18] (Eq. (17)) followed by Xuan and Roetzel [14] (Eq. (18)).

$$\rho_{nf} = (1 - \emptyset)\rho_f + \emptyset\rho_p \quad (17)$$

$$\left(\rho c_p\right)_{nf} = (1 - \emptyset)\left(\rho c_p\right)_f + \emptyset\left(\rho c_p\right)_s \quad (18)$$

The second correlation was used in this study.

Classical effective medium theory (EMT) was used to define thermal conductivity below to model static effect. It is static because particles are fully dispersed in base fluid and hence a static mechanism [19].

$$(k_{eff})_{nf} = k_f\left(\frac{k_p + 2k_f + 2\emptyset\left(k_p - k_f\right)}{k_p + 2k_f - \emptyset\left(k_p - k_f\right)}\right) \quad (19)$$

4.2 Boundary Conditions

The following boundary conditions were applied to the boundaries of the problem.

Region or Zone	Boundary Type	Value
INLET	Inlet	0.0223 m/s (Velocity Inlet)
OUTLET	Outlet	0 Pa (Pressure Outlet)
WALL	Wall	10000 Wm^{-2} (Constant Wall Heat Flux)

Table 1. Boundary conditions

4.3 Assumptions and Simplifications

There are no bouyancy effects, domain motion, thermal dispersion effects or mesh deformation in fluid domain modeling. Heat transfer and turbulence models of thermal energy and laminar are selected in fluid domain physical models. Scalable wall function are used as the boundary layer. Non sphericity of particles is not taken into account. Only sphere particles are considered.

4.4 Grid Independency

In order to remove dependency of results on the grid a refinements was carried out to accurately account for effects of boundary layer and near wall gradients. As a consequence, the following grid independency was applied at a Re number of 500 with Nu number, maximum temperature, and maximum velocity as the comparison criteria.

Number	Grid elements	Nusselt Number	Maximum temperature (°C)	Maximum velocity (m/s)
1	13500	4.471	104.3	0.0448
2	72800	4.523	103.5	0.0447
3	448800	4.532	103.3	0.0447
4	3070400	4.436	103.3	0.0447

Table 2. Grid independency

An extensive mesh refinement was applied to decrease disretization error and improve accuracy. As a tradeoff between mesh improvement and iterations exist (which is

responsible for decreasing linearization errors) a grid of 72800 elements was chosen with 19, 20, and 50 elements in the radial, azimuthal (tangential) and axial directions. Further mesh improvement in any direction did not further resolve physics features and a stable maximum temperature of 103.5°C, Nu number value of 4.523, and velocity of 0.0447 m/s was reached at the outlet length of 1 m at a Re number of 500.

5. Numerical Method

The methods used to solve the mathematical model depend upon on the terms solved in the governing equations. For resolving the advection terms a "high resolution" advection scheme is employed together with a convergence control of 1000 iterations to ensure that the solution is sufficiently converged and minimize the linearization errors. Timescale control is chosen to be "physical timescale" as the internal laminar pipe flow is an advection dominated flow requiring relaxation of non-linearities and a value of 2 s is chosen to get a steady state solution. As bouyancy is not considered the physical timescale is not changed. The solver output gives a maximum Re number in laminar regime validating the model. All residuals converge to a value below 10^{-6}. Previous setting of 10^{-3} didn't even give qualitatively the correct results. The residual-an aggregate imbalance should be less than a specified tolerance and defined as [20].

$$R = \frac{\Sigma |R_i|}{Scaling\ Factor} \tag{20}$$

In order to set guess values at all cell centers, the domain is globally initialized with the gauge pressure equal to 0 and velocity equal to the average inlet velocity. This is checked by displaying cell center values at longitudinal traverse contour of the complete pipe. The nodal values go from a value of the inlet velocity to a value of 0 near the pipe wall, also placing a check on the boundary condition. The effect of boundary conditions on cell center values is checked by first running one iteration and checking the contour again. The value at the wall decrease with respect to inlet velocity that shows the effect of the wall boundary condition. The mass imbalances in solver output are scaled by a factor of 10^6 as compared with the contours and agree. Increasing the number of iterations to first 100 and then a 1000 guarantee the convergence of the governing variables.

6. Results and Discussions

6.1 Base Fluid

The base fluid chosen for this investigation is water. The reason for selecting this particular liquid lies in the many unique properties that are favorable for nanoparticles suspensions. from both an experimental and simulation point of view. These include abundance in nature, medium density, good working temperature for single phase analysis (boiling point of 100°C), high specific heat, and well established correlations that can be extended to nanofluids. Properties of water are shown in Table 3.

Density (kg/m^3)	Specific Heat (J/kgK)	Thermal Conductivity (W/mK)	Viscosity (kg/ms or Pas)
997	4181.7	0.6069	8.899×10^{-4}

Table 3. Thermophysical properties of base fluid water

6.1.1 Velocity and Pressure Distribution

The results were validated by comparing them with theoretical calculations and axial centerline velocity increases along the length of the pipe becoming twice that of the average free stream inlet velocity i.e. 0.0446 m/s in fully developed region. The profile consequently becomes parabolic as the boundary layer subtly develops along the wall slows down the fluid there due to viscous effects and pushes the fluid towards the center. Pressure linearly decreases along the length of the pipe to 0 Pa confirming our check on the outlet boundary condition as the pressure difference forces the fluid along the length of the pipe.

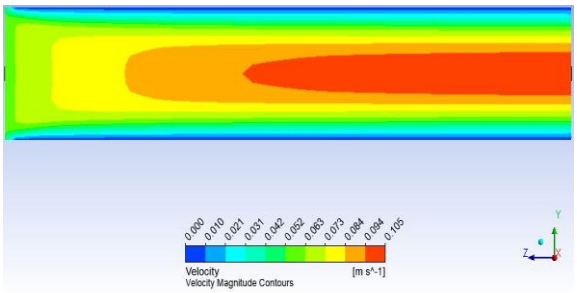

Figure 3 Velocity distribution along length of the pipe at an average Re number of 1200

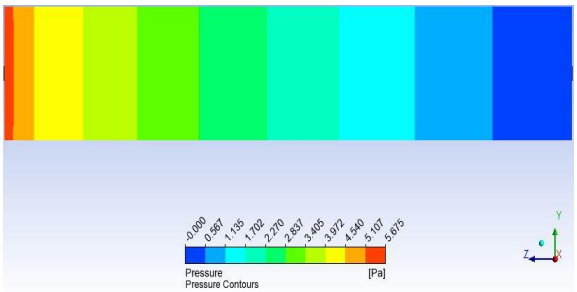

Figure 4 Pressure distribution along length of the pipe at an average Re number of 1200

6.1.2 Heat Transfer

Usually h_{avg} is associated with an average bulk mean temperature The h_{avg} in ANSYS is defined as

$$h_{avg} = \frac{q}{T_w - Adjacent\ Wall\ Temperature} \tag{21}$$

This accounts for user. In this case Adjacent Wall Temperature was defined by setting expert parameter "tbulk for htc". This sets a locally defined bulk temperature for h and consequently Nu calculation. The h_{avg} can also be defined as

$$h_{avg} = \frac{1}{L}\int_0^L h(z)dz \tag{22}$$

There is excellent agreement of Nu number with empirical correlation (Eqs. (23), (24), and (25)) of Shah and London [21] as shown in Fig. 5. The correlation defined below was chosen because of its application in constant wall heat flux laminar forced convection in relatively big diameter (~1-20 mm) pipes.

$$Nu = 3.302(x_*)^{-\frac{1}{3}} - 1 \text{ if } x_* \leq 0.00005 \tag{23}$$

$$Nu = 1.302(x_*)^{-\frac{1}{3}} - 0.5 \text{ if } 0.00005 < \text{x} * < 0.0015 \tag{24}$$

$$Nu = 4.264 + 8.68(10^3 x_*)^{-0.506} e^{-41x_*} \text{ if } x_* > 0.001 \quad (25)$$

where $x^* = \frac{x}{DRePr}$

Averaging over the length of pipe the correlation for average Nu number for entrance region is defined as

$$Nu_{average} = 1.953 * (L_*)^{-\frac{1}{3}} \text{ if } L_* \leq 0.03 \quad (26)$$

$$Nu_{average} = 4.364 + 0.0722 * (L_*)^{-1} \text{ if } L_* > 0.03 \quad (27)$$

where $L^* = \frac{L}{DRePr}$

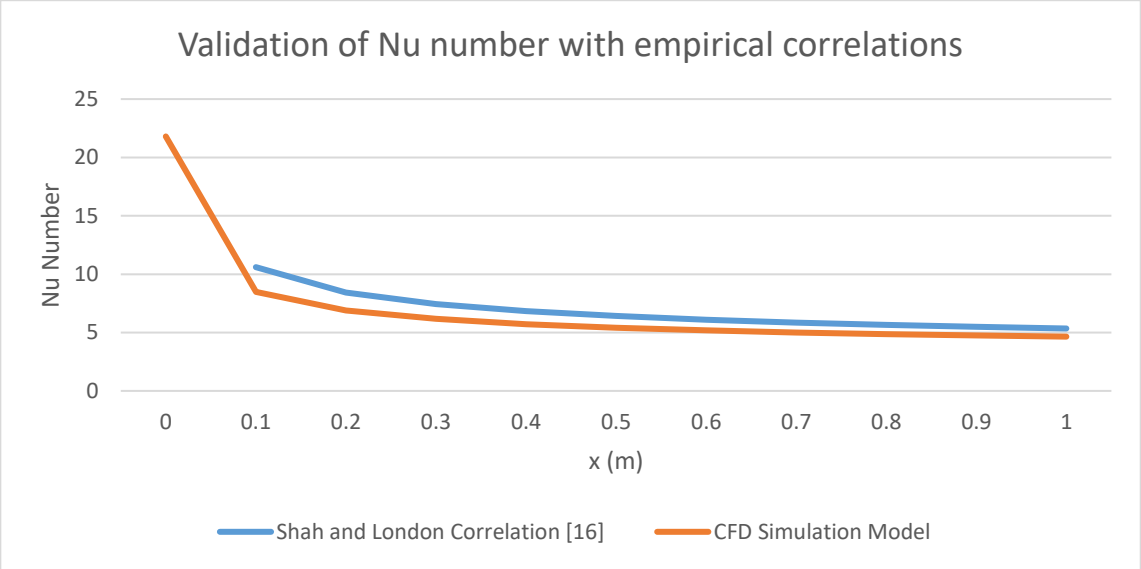

Figure 5 CFD model and corrleation comparison of Nu number versus length of pipe at Re number 500

6.1.3 Temperature Distribution

The temperature varies along the radial direction in a way that maximum temperature occurs along the wall due to impingement of heat flux. The thermal boundary layer is more subtle as compared to velocity due to the nature of terms in the energy equation of governing equations. Maximum heat transfer takes place at the end of the pipe where a maximum wall temperature of 77.8°C occurs at the wall.

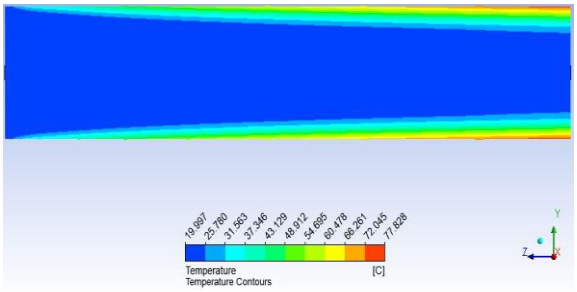

Figure 6 Temperature distribution along length of the pipe at an average Re number of 1200

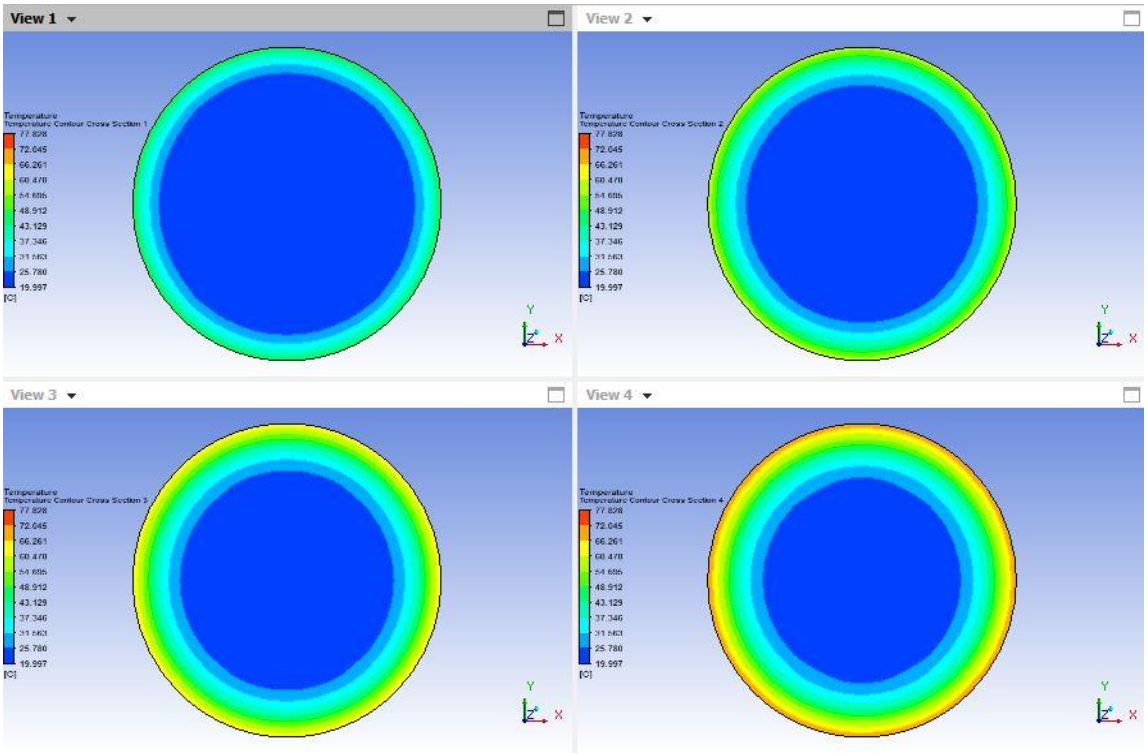

Figure 7 Cross section temperatures of water at an average Re number of 1200 at distances of 0.2 m (top left), 0.4 m (top right), 0.6 m (bottom left), and 0.8 m (bottom right) from inlet

6.2 Alumina Nanofluid

6.2.1 Velocity and Pressure Distribution

As the fluid enters the pipe the boundary layer in the entrance region pushes the fluid towards the centeral position. With no other choice the fluid is forced to increase its velocity and consequently try to develop a uniform velocity at the center as a result of conservation of flow and mass. The velocity is marginally decreased due to presence of nanoparticles as density and viscosity is increased by a very small amount. Parabolic velocity profile with centerline velocity of Al_2O_3-water nanofluid is shown in Fig. 8.

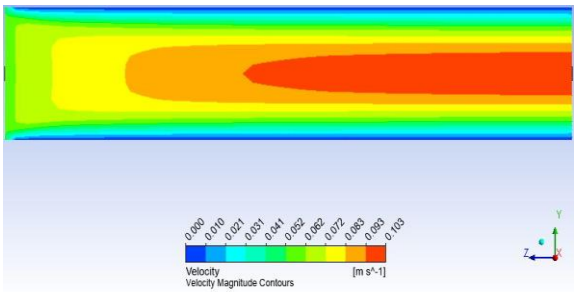

Figure 8 Velocity distribution of Al_2O_3-water nanofluid along length of the pipe at an average concentration of 3% and an average Re number of 1200

Unlike sharp velocity gradients at the wall the pressure remains almost constant throughout different sections of the pipe respectively. Despite this characteristic the

pressure of a nanofluid is distinct as compared to base fluid in Fig. 4 and the pressure is 6.132% higher at the inlet. Moreover, throughout a cross section the pressure remain constant as well along a certain length of the pipe which inreases with distance along the pipe as shown in Fig. 9. As a result inertial momentum helps the fluid to move easily.

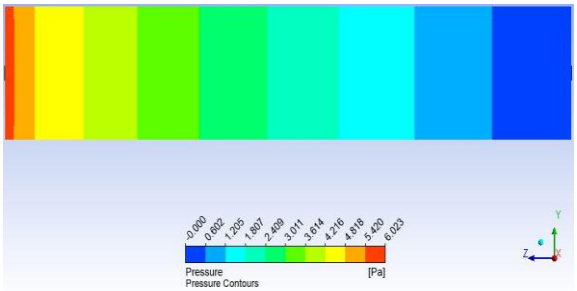

Figure 9 Pressure distribution of Al_2O_3-water nanofluid along length of the pipe at an average concentration of 3% and an average Re number of 1200

6.2.2 Heat Transfer and Temperature Distribution

With the introduction of nanofluid in base fluid the Nu number decreases in the laminar flow regime. Nu number approaches 4.364 as the grid is refined at the end of the pipe validating hand calculations. Fig. 10 shows that the wall temperature decreases when the fluid is changed from base fluid to nanfofluid. This is a consequence of the combnation of constant wall heat flux boundary condition and higher thermal conductivity of nanoparticle. Especially interesting is the fact that the temperature gradients at the wall continuously change along the length of the pipe once again confirming the combined entrance transitional length of the problem. For any cross section the nanofluid temperature increases from the center to the wall. The highest temperature increases along the axial length unlike the velocity profile which becomes fully developed approximatly at the mid of the pipe at a value of 0.5 m. As the velocities have been kept the same for both the base fluid and nanofluid there is a slight increase of around 2.5°C.

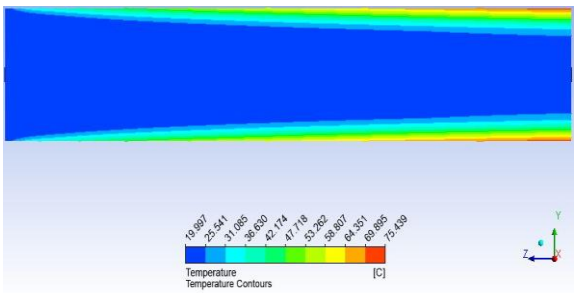

Figure 10 Temperature distribution of Al_2O_3-water along length of the pipe at an average concentration of 3% and an average Re number of 1200

Increasing the concentration to 3% the boundary layer development is more pronounced as more volume of the fluid has been heated. This leads to a lower wall temperature as more heat has been transferred leading to a higher h value. This is also the reason why most heat transfer occurs early near the inlet. This is evident in a comparison of Fig. 6 (bottom right) and Fig. 11 (bottom right).

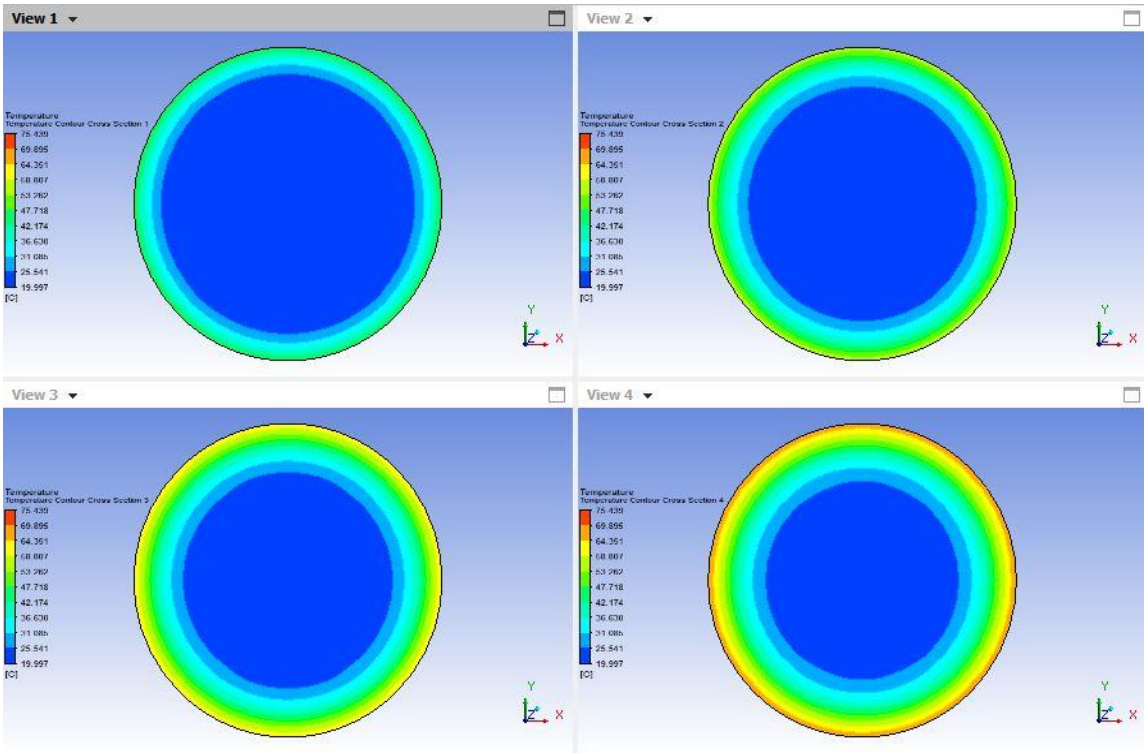

Figure 11 Cross section temperatures of Al_2O_3-water nanofluid at an average concentration of 3% and an average Re number of 1200 at distances of 0.2 m (top left), 0.4 m (top right), 0.6 m (bottom left), and 0.8 m (bottom right) from inlet

6.2.3 Effect of Axial Length

The performance parameter evaluated here is local HTC. Increasing the axial length causes the HTC to decrease as shown in Fig. 12 as fluid moves along length because most heat is convectively transferred in the entrance where most of the heat transfer occurs.

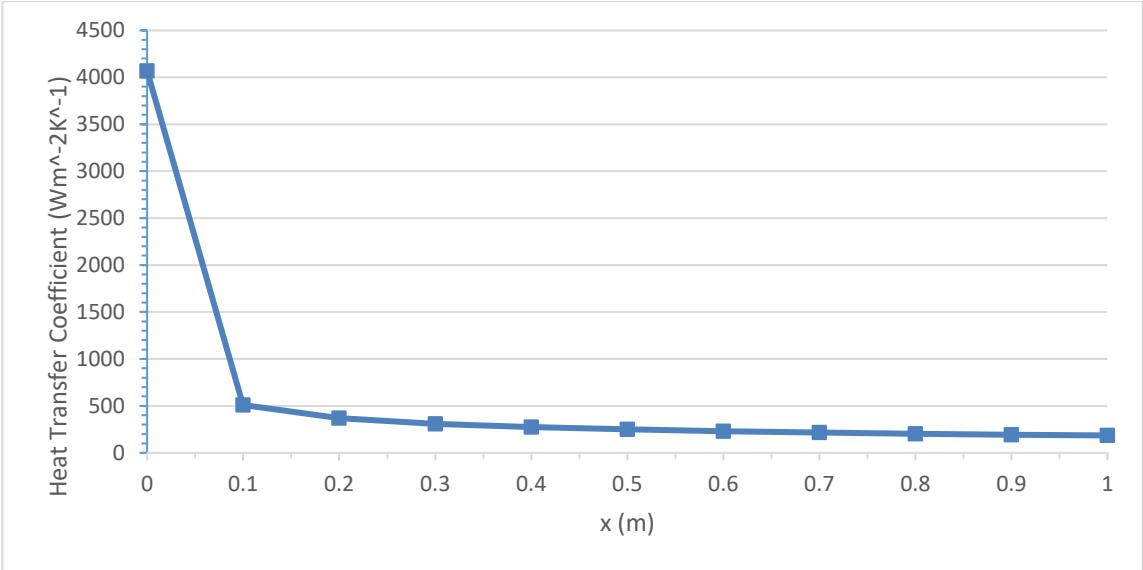

Figure 12 Effect of axial length on local HTC of Al_2O_3-water nanofluid at an average concentration of 3% and an average Re number of 1200

6.2.4 Effect of Concentration of Nanoparticle

At concentration of 1% or 0.01, h_{avg} enhancement is 1.354% whereas theoretical calculation gives enhancement of 1.644% (Shah averaged correlation) compared to base fluid. It increases with concentration with enhancement of 6.871% and theoretical enhancement of 8.444% at 5% concentration. This is in agreement with Eq. (13).

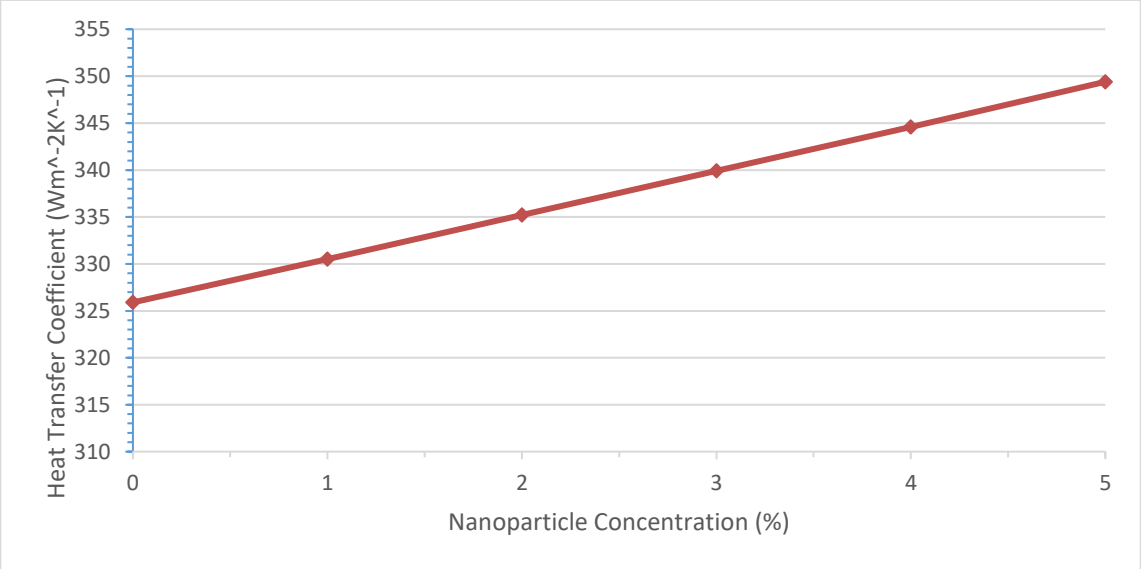

Figure 13 Effect of concentration on average HTC of Al_2O_3-water nanofluid at an average Re number of 1200

6.2.5 Effect of Diameter of Nanoparticle

Increasing diameter of particle decreases h by correlation od Khanafer and Vafai [22].

$$(k_{eff})_{nf} = (1 + 1.0112\emptyset + 2.4375\emptyset\left(\frac{47}{d}\right) - 0.0248(\frac{k_p}{0.613}))k_f \quad (28)$$

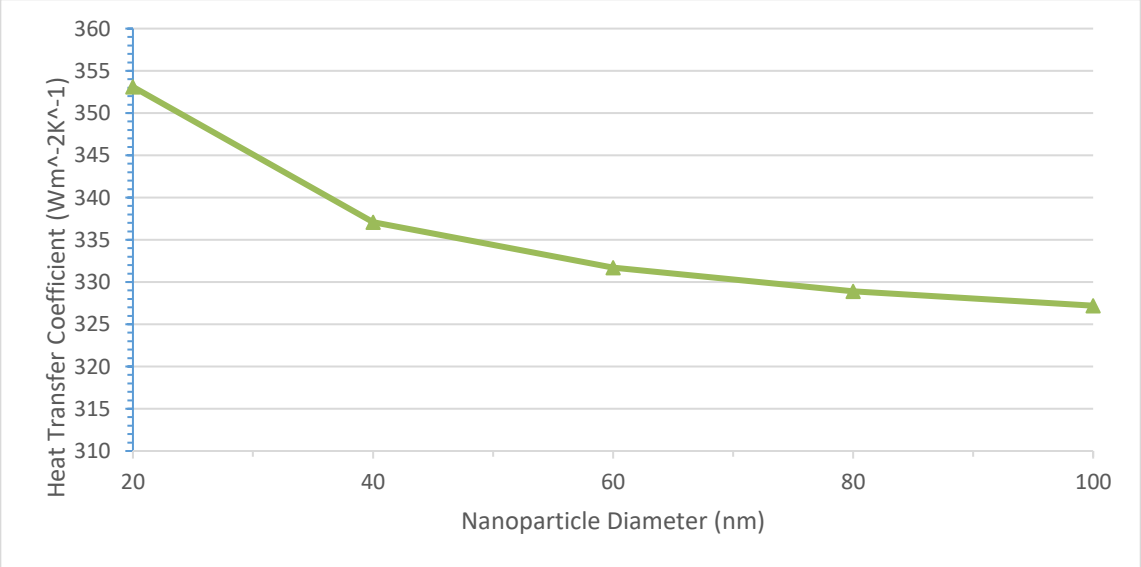

Figure 14 Effect of nanoparticle diameter on average HTC of Al_2O_3-water nanofluid at an average concentration of 3% and an average Re number of 1200

6.2.6 Effect of Re Number

Increasing Re number increases heat transfer from the wall to the bulk of the nanofluid with higher Re number having a higher heat HTC and is a manifestation of an increase in velocity and possible increase of wall temperatures. The effect is highligted in Fig. 15. Increasing Re number increases the turbulence effects in fluid enabling better mixing.

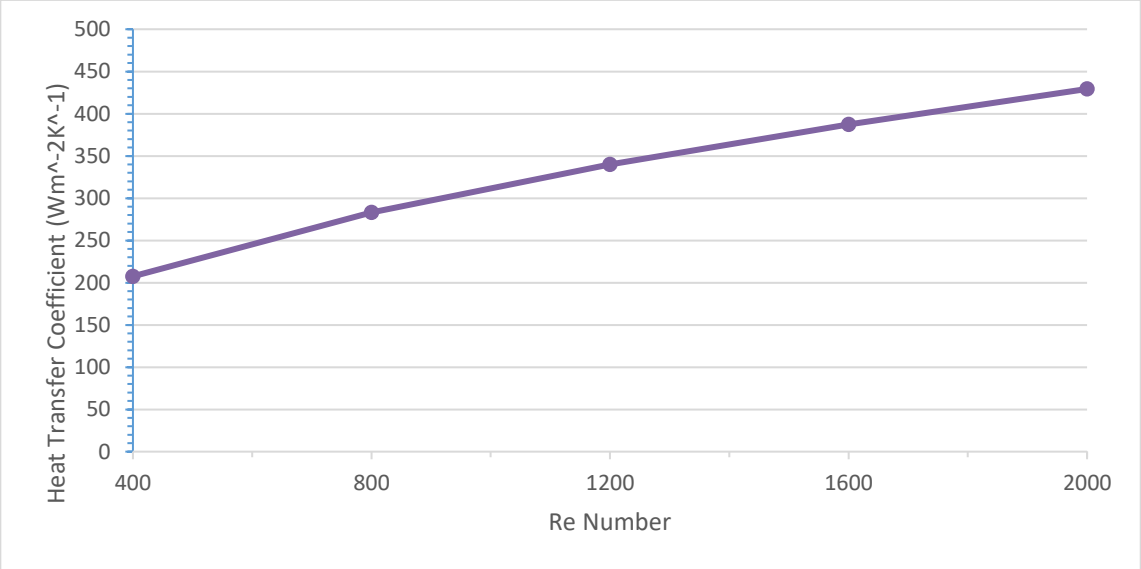

Figure 15 Effect of Re number on average HTC of Al_2O_3-water nanofluid at an average concentration of 3%

6.2.7 Effect of Inlet Temperature

Amount of heat transferred from wall to bulk fluid in pipe depends on boundary conditions. With wall boundary condition constant increasing inlet temperature decreases HTC as difference between wall and bulk temperature increases. This is shown in Fig. 16.

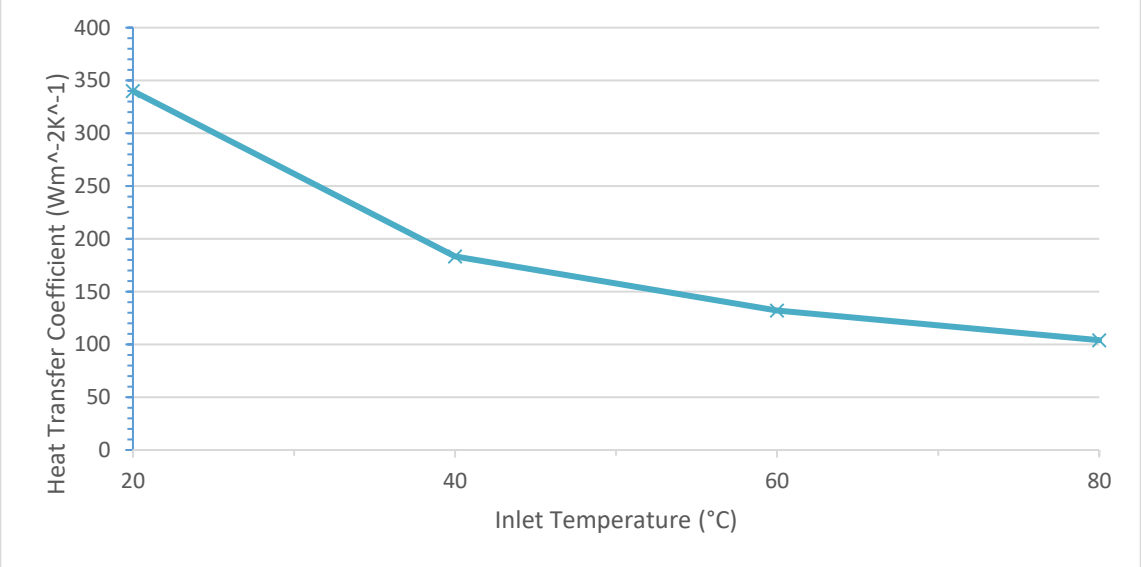

Figure 16 Effect of inlet temperature on average heat HTC of Al_2O_3-water nanofluid at an average concentration of 3% and an average Re number of 1200

6.3 Copper Oxide Nanofluid

6.3.1 Velocity and Pressure Distribution

The velocity and pressure distribution of CuO-water nanofluid is similar to that of Al_2O_3-water nanofluid. Higher density of CuO hinders development of velocity boundary layers and as a result a lower centerline velocity of 0.097 m/s is achieved at the outlet. This decrease is minor as compared to the other nanofluid but may be signficiant at higher concentration and Re number. Pressure difference is relatively higher because of direct influence of concentration and density. This is evident at the inlet where the pressure of Al_2O_3-water nanofluid is 6.526% higher than CuO-water nanofluid. Viscosity of the nanofluids can cause a change in the pressure drop of nanofluids but as the viscosity correlation used is not dependent on temperature there is not much of a difference between the two nanofluids at the same inlet temperature and Re number. Thus, the major factor remains the density. The velocity and pressure maps of CuO-water nanofluid are shown in Fig. 17 and Fig. 18.

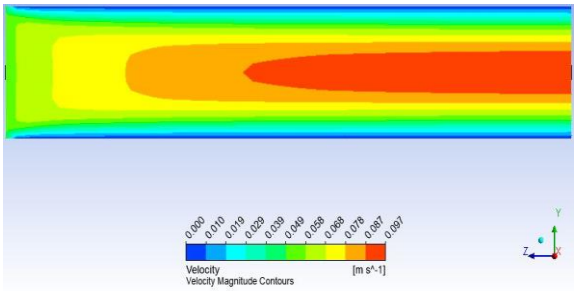

Figure 17 Velocity distribution of CuO-water nanofluid along length of the pipe at an average concentration of 3% and an average Re number of 1200

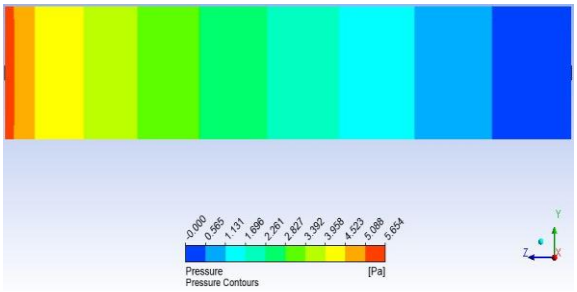

Figure 18 Pressure distribution of CuO-water nanofluid along length of the pipe at an average concentration of 3% and an average Re number of 1200

6.3.2 Heat Transfer and Temperature Distribution

Figure 19 shows the longitudinal and cross section temperature profiles for CuO-water nanofluids. As noted previously increasing concentration at low concentrations but at a high concentration of 3% the wall temperature decreases. For CuO-water nanofluid the decrease in wall temperature leads to an increase in bulk temperature of about 1.5°C. The cross sectional temperatures are shown in Fig. 20.

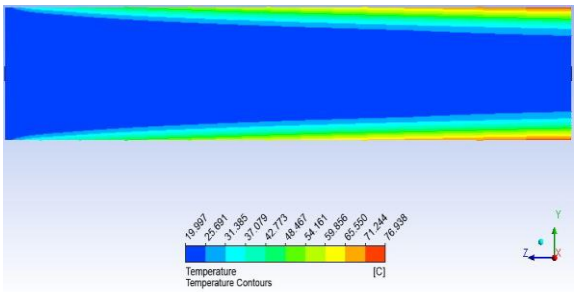

Figure 19 Temperature distribution of CuO-water nanofluid along length of the pipe at an average concentration of 3% and an average Re number of 1200

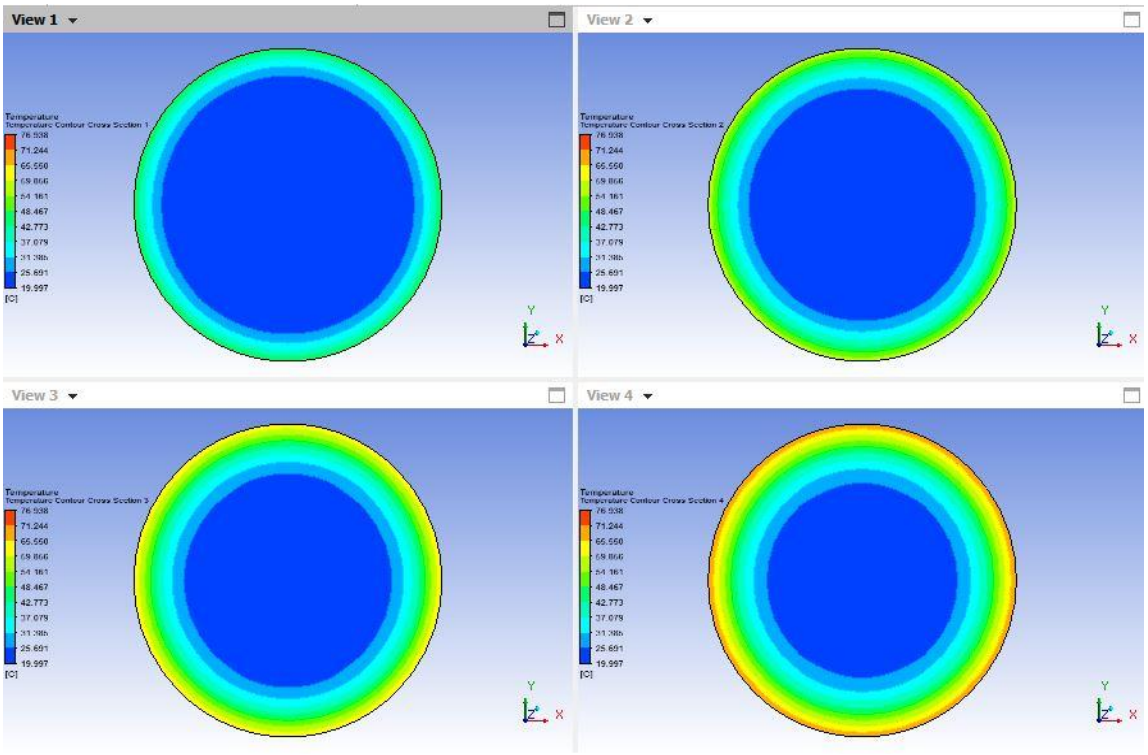

Figure 20 Cross section temperatures of CuO-water nanofluid at an average concentration of 3% and an average Re number of 1200 at distances of 0.2 m (top left), 0.4 m (top right), 0.6 m (bottom left), and 0.8 m (bottom right) from inlet

6.3.3 Effect of Axial Length

Similar trend is observed for local HTC of CuO-water nanofluids with axial length as that of Al_2O_3-water nanofluids. Despite having lower thermal conductivity and higher density, the local h doesn't change much. It has been demonstrated from past researches that heat transfer enhancement may occur due to boundary layer development, particle migration, particle mixing, and particle rearrangement but the major region for lower CuO-water h is disturbance of thermal boundary layers.

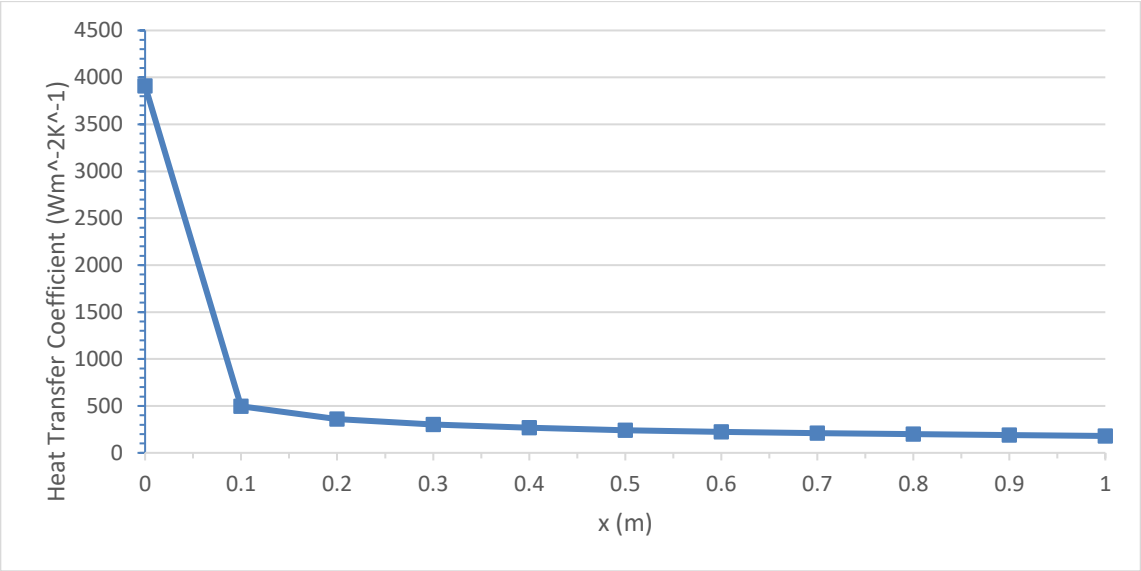

Figure 21 Effect of axial length on local HTC of CuO-water nanofluid at an average concentration of 3% and an average Re number of 1200

6.3.4 Effect of Concentration of Nanoparticle

A change of nanoparticle to CuO reduces heat transfer and at a concentration of 1% or 0.01 and Re number of 400, h_{avg} enhancement of 0.3511% whereas theoretical calculation gives enhancement of .8406% (Shah averaged correlation) compared to base fluid. This enhancement increases with increase in concentration of nanoparticle with an enhancement of 2.257% and theoretical enhancement of 4.613% at a concentration of 5%.

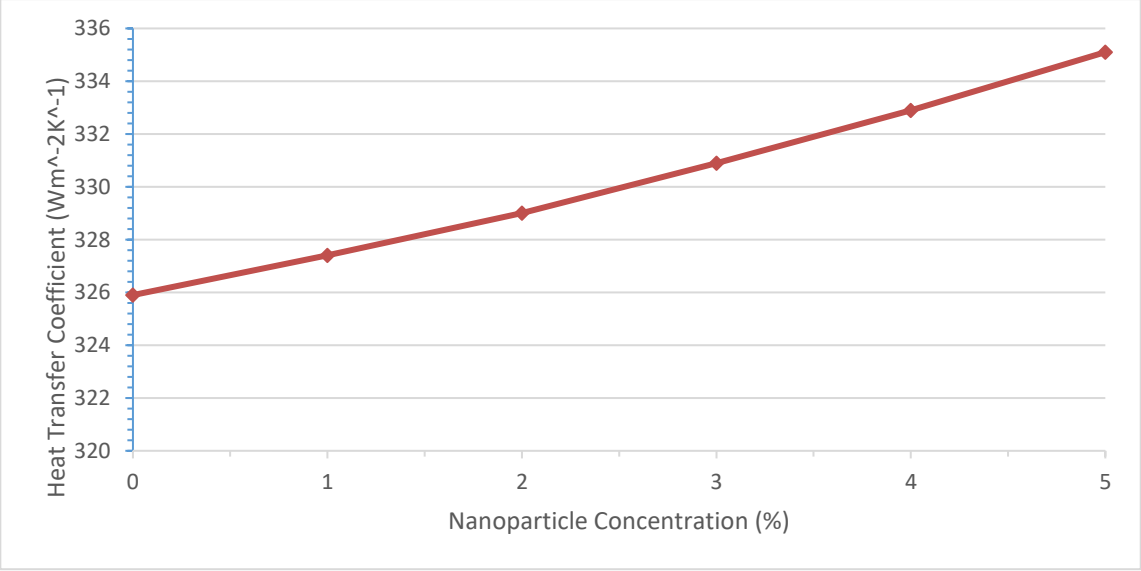

Figure 22 Effect of concentration on average HTC of CuO-water nanofluid at an average Re number of 1200

6.3.5 Effect of Diameter of Nanoparticle

For the same size of nanoparticles, CuO-water nanofluids has a distinctively less impact on h_{avg} as compared to Al_2O_3-water nanofluids even though it has a lower thermal

conductivity which should give a relatively high value of h_{avg}. This is because decrease of h_{avg} because of increase in d outweighs impact of lower thermal conductivity. There is a h_{avg} decrease of 8.076% for a d value from 20 nm to 100 nm as shown in Fig. 23.

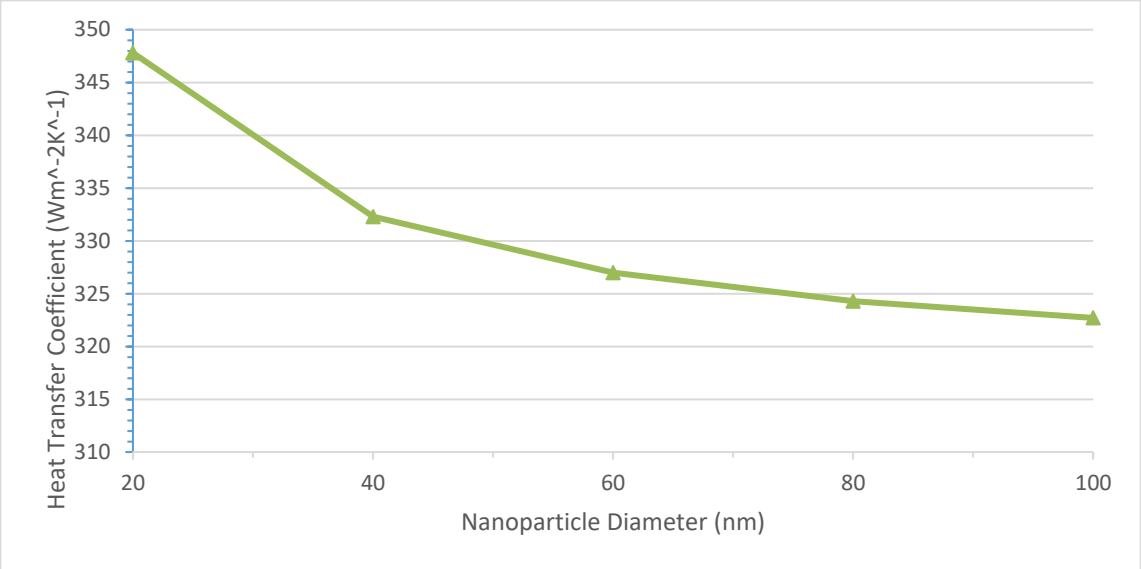

Figure 23 Effect of nanoparticle diameter on average HTC of CuO-water nanofluid at an average concentration of 3% and an average Re number of 1200

6.3.6 Effect of Re Number

The increase of Re number has the highest increasing effect on HTC in nanofluids. In fact inclusion of d underpredicts h_{avg} at the same inlet temperature. The effect of Re number for CuO-water nanofluids increases. Higher wall temperature of around 76.94°C is achieved for CuO-water as compared to 75.44°C for Al_2O_3-water due to lower thermal conductivity and cause h_{avg} to be lower than Al_2O_3-water nanofluids as shown in Fig. 24.

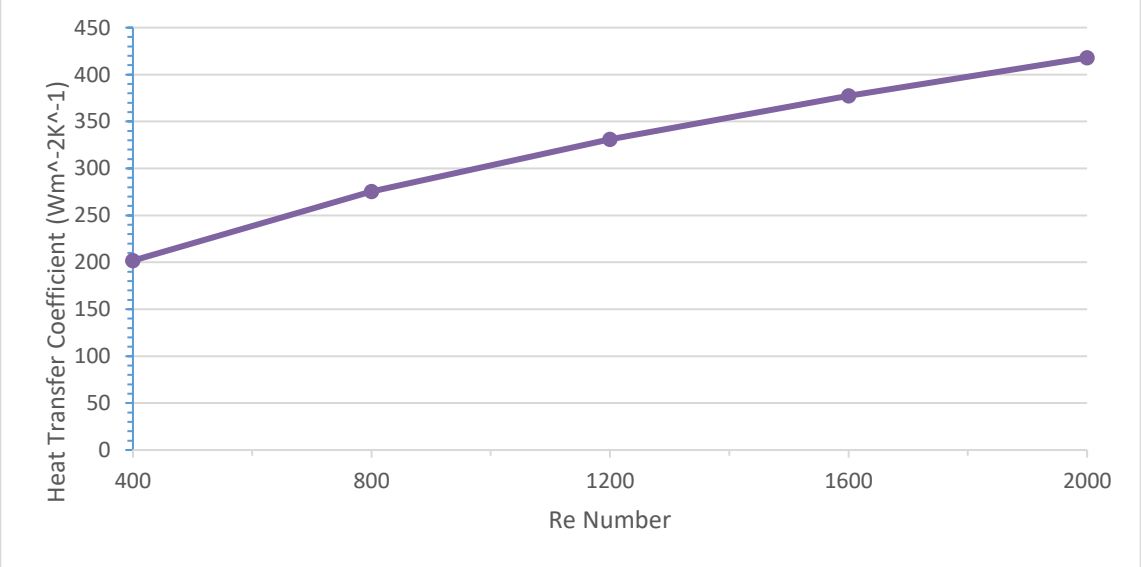

Figure 24 Effect of Re number on average HTC of CuO-water nanofluid at an average concentration of 3% and an average Re number of 1200

6.3.7 Effect of Inlet Temperature

The effect of inlet temperature on CuO-water nanofluids is similar to Al_2O_3-water and there isn't much of a difference between the two effects. This is shown in Fig. 25.

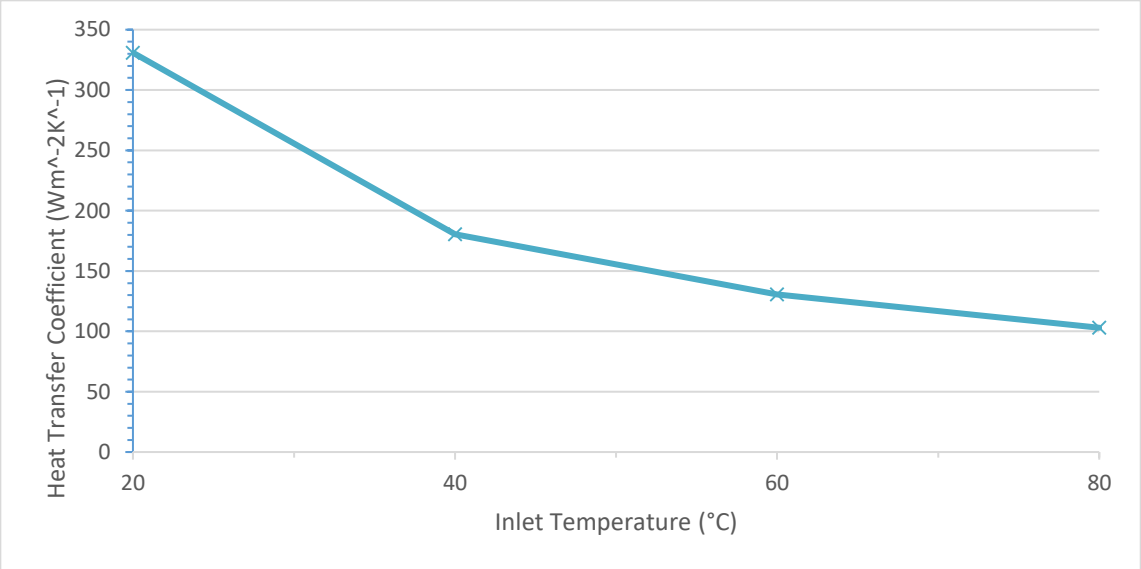

Figure 25 Effect of inlet temperature on average HTC of CuO-water nanofluid at an concentration of 3% and an average Re number of 1200

6.4 Comparative Analysis of Different Types of Nanofluids

6.4.1 Effect of Axial Length

Along the length of the pipe the local HTC remains almost the same for the two nanofluids because local HTC is dependent only on local wall temperature and local bulk temperature. As wall temperature increases so does bulk temperature but wall temperature increases sharply than bulk temperature at entrance and thus HTC decreases. Beyond the entrance region it remains constant along the length of the pipe. This is shown in Fig. 26.

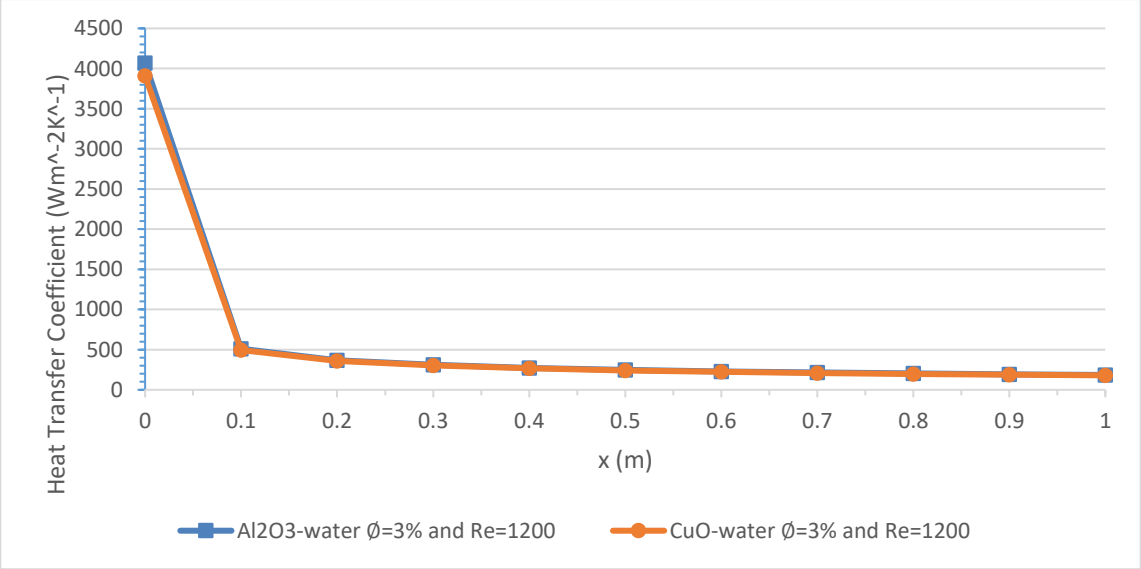

Figure 26 Equal axial length comparison of nanofluids

6.4.2 Effect of Concentration

At same concentration Al_2O_3-water nanofluid exhibits a higher value of h_{avg} than CuO-water nanofluid. This difference increases explicitly for higher values of concentration. There is a linear increase in h because thermal conductivity linearly increase with concentration in static model of Maxwell. Again higher thermal conductivity of Al_2O_3 is attributed for considerably high values. Effect is shown in Fig. 27.

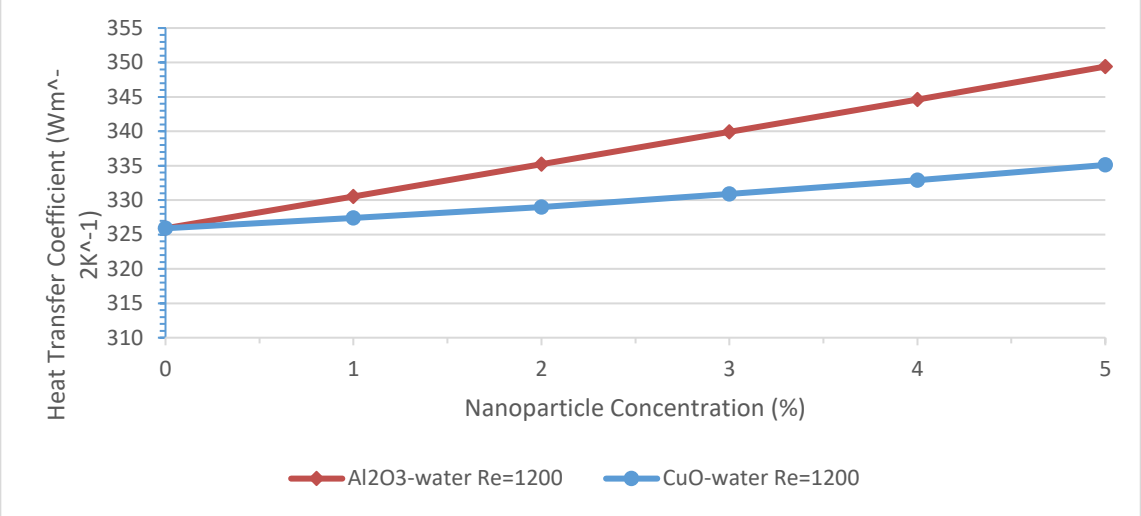

Figure 27 Equal concentration comparsion of nanofluids

6.4.3 Effect of Diameter

Comparing the two nanofluids, the effect of diameter is shown in Fig. 28. Increases the size of particle decreases temperature that is more for CuO-water nanofluid. This decrease is due to high density and lower thermal conductivity of CuO which decreases heat transfer. Interstingly both nanofluids have the same trend and consequently the same difference with Al_2O_3-water nanofluids having 1.724% higher values as shown in Fig. 28.

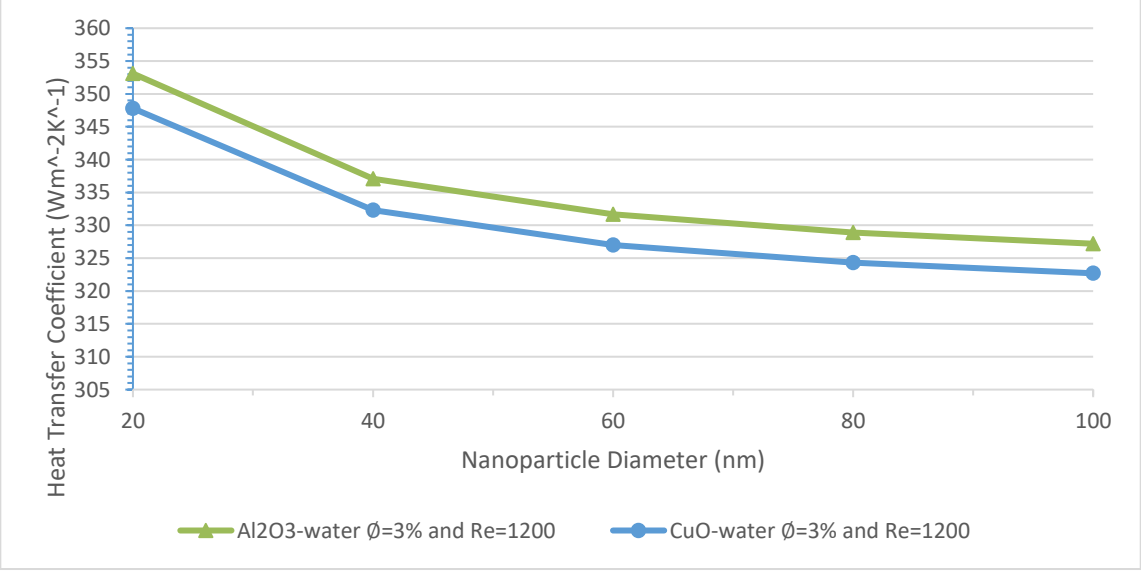

Figure 28 Equal diameter comparsion of nanofluids

6.4.4 Effect of Re Number

The comparison criteria chosen for the analysis of Al_2O_3-water and CuO-water nanofluids is Re number. At the same Re numbers the velocities are chosen to be the same. This gives different heat transfer enhancements ratios for the two fluids. As seen in Fig. 28 Al_2O_3-water nanofluid has a higher heat transfer enhancement than CuO-water because of higher thermal conductivity and lower specific heat capacity compared to CuO-water nanofluid.

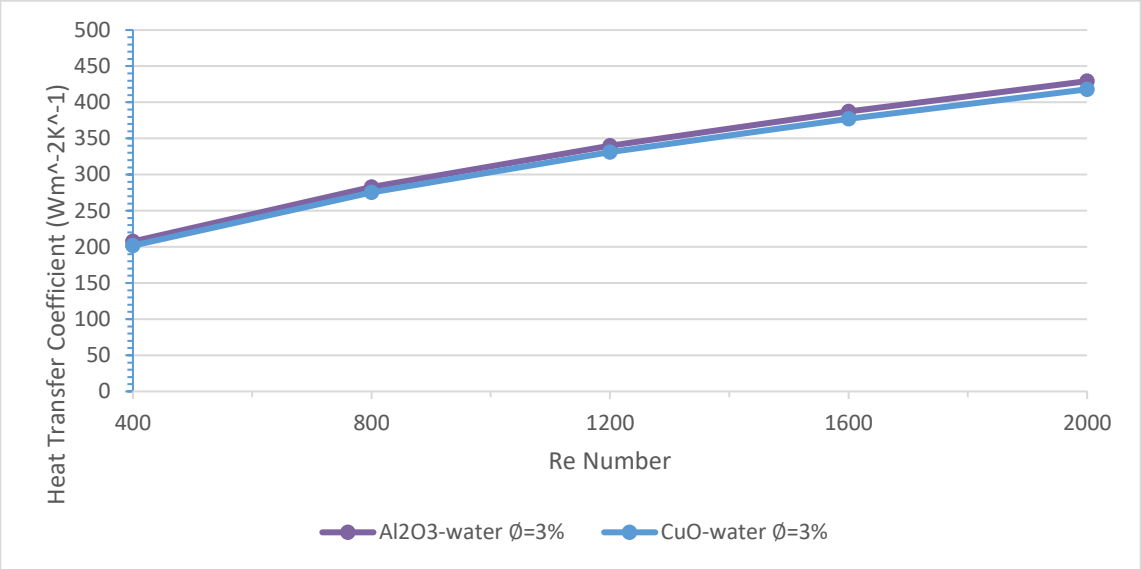

Figure 28 Equal Re number comparison of nanofluids

7. Conclusions

The following conclusions were drawned on the basis of these research simulations.

- The difference in h enhancement between the simulation and theoretical results is most probably due to non-inclusion of viscosity Batchelor model of nanofluid which directly affects the pressure drop for forced convection in pipes.
- Heat transfer coefficient of nanofluid decreases along the axial length of the pipe. The trend is almost the same for both nanofluids. Highest heat transfer occurs at the entrance of the tube due to largest difference between bulk temperature and wall temperature.
- Increasing concentration increases average HTC with values of 4.296% and 1.534% for Al_2O_3-water and CuO-water in laminar flow at an average concentration of 3% and Re number of 1200 respectively. The inrease is more for Al_2O_3-water as compared to CuO-water.
- Diameter has an inverse effect on average HTC. For lower sizes h is higher due to higher mobility of nanoparticles within base fluid. This cause better heat transfer between the partlces and the fluid layers around it which then convect the heat throughout the fluid.
- For CuO-water nanofluid the pressure is a little higher at the beginning due to high density of CuO as compared to Al_2O_3.
- Heat transfer is more for Al_2O_3-water nanofluid compared to CuO. This is due to the lower thermal conductivity and higher density of CuO.

- For practial applications like tubular heat exchanger it is observed that a lower value of concentration and inlet temperature along with a higher Re number may optimize a system. This can counter the adverse affects of higher pressure drops at higher concentrations.

8. Acknowledgements

The authors express thanks to guidance and examination committee (GEC) members Dr. Muhammad Zubair, and Dr. Emad Ud Din for their guidance and support throughout this research which was supported by Thermal Energy laboratory, U.S.-Pakistan Center for Advanced Studies in Energy (USPCAS-E), National University of Sciences and Technology (NUST), Islamabad, Pakistan.

References

[1-2] V. Bianco et al., “Heat Transfer Enhancement with Nanofluids,” pp. vii, 2015.
[3] S. U. S. Choi and J. A. Eastman, “Enhancing thermal conductivity of fluids with nanoparticles,” Proceedings of the 1995 ASME International Mechanical Engineering Congress and Exposition, vol. 231. ASME, San Francisco, California, USA, pp. 99–105, 1995.
[4] R. Saidur et al., “A review on applications and challenges of nanofluids,” Renewable and Sustainable Energy Reviews, vol. 15, no. 3, pp. 1646–1668, 2011.
[5] C. Mangrulkar and V. Kriplani, “Nanofluid Heat Transfer-A Review,” International Journal of Engineering and Technology, vol. 3, no. 1, pp. 136–142, 2013.
[6] R. Saidur et al., “A review on applications and challenges of nanofluids,” Renewable and Sustainable Energy Reviews, vol. 15, issue 3, pp. 1646–1668, 2011.
[7] G. Puliti et al., “Nanofluids and their properties,” Applied Mechanics Review, vol. 64, issue 3, pp. 030803-1–030803-23, 2012.
[8] Li Qiang and X. Yimin, “Convective heat transfer and flow characteristics of Cu-water nanofluid,” Science in China Series E: Technolgical Science, vol. 45, issue 4, pp. 408–416, 2002.
[9] G. Roy et al., “Numerical investigation of laminar flow and heat transfer in a radial flow cooling system with the use of nanofluids,” Superlattices and microstructures, vol. 35, issue 3-6, pp. 497–511, 2004.
[10] Y. Xuan and Q. Li, “Investigation on convective heat transfer and flow features of nanofluids,” ASME Journal of Heat Transfer, vol. 125, pp. 151–155, 2003.
[11] Y. Yang et al., “Heat transfer properties of nanoparticle in fluid dispersions in laminar flow,” International Journal of Heat and Mass Transfer, vol. 48, issue 6, pp. 1107–1116, 2005.
[12] S. Z. Heris et al., “Experimental investigation of oxide nanofluid laminar flow convective heat transfer, in circular tube,” International Communication in Heat and Mass Transfer, vol. 33, issue 4, pp. 529–533, 2006.
[13] S. Z. Heris et al., “Experimental investigation of convective heat transfer of Al2O3/Water nanofluid in circular tube,” International Journal of Heat and Fluid Flow, vol. 28, issue 2, pp. 203–210, 2007.
[14] S. E. B. Maiga et al., “Heat transfer behavior of nanofluids in a uniformly heated tube,” Superlattices and Microstructures, vol. 35, issue , pp. 543–557, 2004.
[15] M. Massoud, Engineering Thermofluids Thermodynamics, Fluid Mechanics, and Heat Transfer, first edition, Springer, Berlin Heidelberg New York, 2005.
[16] H. K. Versteeg and W. Malalasekera, “An introduction to computational fluid dynamics: the finite volume method,” John Wiley and Sons Inc., New York, 1995.
[17] A. Einstein, “A determination of molecular dimensions,” Ann. Physics, vol. 324, issue 2, pp. 289–306, 1906.
[18] B. C. Pak and Y. I. Cho, “Hydrodynamic and heat transfer study of dispersed fluids with submicron metallic oxide particles,” Experimental Heat Transfer, vol. 11, issue 2, pp. 151–170, 1998.
[19] W. Duangthongsuk and S. Wongwises, “Comparison of the effects of measured and computed thermophysical properties of nanofluids on heat transfer performance,” Experimental Thermal and Fluid Science, vol. 34, issue 5, pp. 616–624, 2010.
[20] ANSYS® ANSYS CFX, Release 15.0, Help System, ANSYS Documentation CFX Reference Guide, ANSYS, Inc.

[21] R. K. Shah and A. L. London, “Laminar flow forced convection in ducts,” Advances in Heat Transfer, Academic Press, New York, 1978.
[22] K. Khanafer and K. Vafai, “A critical synthesis of thermophysical characteristics of nanofluids,” International Journal of Heat and Mass Transfer, vol. 54, issues 19-20, pp. 441, 2011.